

Response to Referee #1 for comments on “Investigation of the global methane budget over 1980-2017 using GFDL-AM4.1” by He et al.

We thank the reviewer for the insightful comments and suggestions on our manuscript. Below, our responses in bold text follow the reviewer’s comments shown in plain text.

5

General comments:

The work describes CH₄ budget using an atmospheric chemistry-transport model that is developed at the GFDL. The authors have taken in to account all possible causes of variabilities in CH₄ budget, such as the emissions and loss due to tropospheric hydroxyl (OH). As shown in the manuscript, OH variability is of as much importance as the emissions in explaining the CH₄ growth rate variabilities in different decades in the period of 1980s to 2010s. The manuscript is generally well written. However, I felt toward the end of the manuscript is a bit of stretch and could be reduced (I have made some suggestions in my specific comments). The manuscript can be accepted after a major revision.

Reply:
We thank the reviewer for the positive comments. As suggested by the reviewer, we have shortened Section 3 and revised the manuscript carefully. Below are our point-by-point responses.

Specific comments:

Line 49 & 62ff: can the growth rate discussions in the introduction be made concise and put together at one place.

Reply:
As suggested by the reviewer, we have removed the sentence highlighting past studies on drivers of methane trend and variability avoid redundancy. However, we keep the sentence on the observed changes in growth rate to motivate the study.

Line 80ff: I think there are other prominent inverse modelling results trying to explain the recent regrowth of CH₄ concentrations.

Reply:
We have revised this sentence and included additional references in the revised manuscript as below:

“The observed renewed growth since 2007 has been explained alternatively through increases in tropical emissions (Houweling et al., 2014; Nisbet et al., 2016) such as agricultural emissions (Schaefer et al., 2016; Patra et al., 2016) and tropical wetland emissions (Bousquet et al., 2011; Maasackers et al., 2019), increases in fossil fuel emissions (Rice et al., 2016; Worden et al., 2017), decreases in sources compensated by decreases in sinks due to OH levels (Turner et al., 2017; Rigby et al, 2017), or a combination of changes in different sources such as increases in fossil, agriculture, and waste emissions with decreases in biomass burning emissions (Saunois et al., 2017).”

Line 135-137: This is a quite strange statement. After reading the whole manuscript I do not believe you have tried to address these couple of issues to a great extent. May be remove?

Reply:
We have removed these sentences as suggested by the reviewer.

40

Line 156: Not from wetchart? I mean does wetchart not have IAV?

Reply:

We use WETCHARTs version 1.0 (Bloom et al., 2017) for wetland emissions. The seasonality and spatial distributions are based on ensemble mean. We then repeated the emissions every year. There is also an extend
45 ensemble version of WETCHARTs with interannual variability of wetland emissions only for 2001-2015. We did a sensitivity test with this version to compare with climatological wetland emissions. The results are shown in Figures S2 and S3 in the Supplement. We find a better model performance with climatological wetland emissions. Besides, with the optimization on wetland emissions, the signal of the initial interannual variability of wetland emissions would be lost anyway. Therefore, we keep this version (i.e., climatological wetland emissions) as the starting point for
50 wetland emission optimization.

Line 206: Not clear if this is after LNO_x scaling? please make this statement precise (e.g., Control).

Reply:

This magnitude is for standard AM4.1 without scaling. We have revised the sentences in the revised manuscript to
55 make it clearer as below.

*“The climatological global mean LNO_x emission simulated by standard AM4.1 is about 3.6 TgN yr⁻¹, within the range of 2-8 TgN yr⁻¹ estimated by previous studies (e.g., Schumann and Huntrieser, 2007). We additionally apply scaling factors (e.g., 0.5 and 2.0) to LNO_x emissions, producing LNO_x at the lower and upper limits of the estimated range for sensitivity
60 simulations described below. ”*

Line 249ff: "The meridional curve" needed some clarifications here, e.g., selected sites within a latitude band to get the mean CH₄ at 5 different latitude bands or something like that.

Reply:

We have included detailed description in Section 2.2 in the revised manuscript as below:

*“The global estimates are based on spatial and temporal smoothing of CH₄ measurements from 45 surface marine boundary layer (MBL) sites. Locations of MBL sites are shown in Figure S1, and information for each MBL site is listed in Table S1 in the Supplement. First, the average trend and seasonal cycle are approximated for each sampling site by
70 fitting a second-order polynomial and four harmonics to the data. We characterize deviations from this average behaviour by transforming the residuals to frequency domain, then multiplying by a low pass filter (Thoning et al., 1989; Thoning, 2019). Zonal and global averages are determined by extracting values at synchronized times steps from the smoothed fits to the data, then fitting another curve as a function of latitude (Tans et al., 1989). We divide these fits into sine (latitude) = 0.05 intervals, which define a matrix of zonally averaged CH₄ as a function of time and latitude.”*

75 Line 296: Sometimes the sites like Key Biscayne are sampled by moving the model grids to the ocean side. You might check that out.

Reply:

We thank the reviewer for the suggestion. Moving the model grid to the ocean side reduces the model bias. Similar issue also exists at Mace Head site.

80

Line 315ff: The tropical bias in all HIPPO is a bit strange! Not OH but transport (or emissions)? I am suspecting this because the bias due to OH would appear at all altitudes (timescale ~1yr), because the bias is in the lower troposphere, if the vertical transport is slow, you would find more CH₄ is accumulated in the lower troposphere (timescale~week)

Reply:

85 **We agree with the reviewer that the bias could be due to transport or emissions, which we already mentioned in the manuscript at lines 251-253. Also, OH is much higher over tropics than higher latitudes. It is possible that OH over tropics are overestimated in the model. Unfortunately, without observations, we are not able to rule out any possibilities.**

90 Line 326: do you run CH₃CCl₃ & SF₆?, say within the CCM framework?

Reply:

We do not run with CH₃CCl₃ & SF₆.

95 Line 346ff: suggesting too much emissions in the NH, where most of Anthro emissions are...May be you can test this better by site-level comparisons.

Reply:

100 **We have updated all the plots in the revised manuscript due to a bug fix in the scripts for model evaluation. As shown in Figure 4 in the main text, the model is able to capture methane trend very well over high latitudes, with R = 1.0 and RMSE < 10 ppb in the Northern Hemisphere and RMSE ~ 11 ppb in the Southern Hemisphere. For site-level comparisons, which are shown in Figures S4-5, over Northern Hemisphere, the model is able to reproduce methane DMFs at most of sites with RMSE < 25 ppb and R > 0.9 although there are some overestimations at certain sites possibly due to overestimations in the local sources. Site-level comparisons are presented at lines 298-319 in the revised manuscript.**

105 Line 353ff: I cannot find this 1 year mismatch (please be clear), instead I find a persistent offset during 1984-1991 (how the major and minor ticks marked in Fig. 5; the labeled ticks only should be major?

Reply:

110 **We have updated all the plots in the revised manuscript due to a bug fix in the scripts for model evaluation. As shown in Figure 4, the model fails to reproduce methane growth rates during 1984-1991, especially over tropics. This could be due in part to the fewer available observations used for emission optimization during this time period. The plots of methane growth rates are also updated with same major and minor ticks as shown for methane trend plots in Figure 4.**

115 Line 369: How can you say that? I thought your optimization was not good for this period, because the number of observation sites may not have covered the global reasonably well. I mean biased high toward the NH. Could you check how many SH sites you have data before 1988.

Reply:

120 **We agree with the reviewer that we have fewer observations available before 1988 used for emission optimization. Over Southern Hemisphere, there are only six sites (i.e., SPO, HBA, PSA, CGO, ASC, and SMO) as shown in Figure S5 that at least have one-year data available before 1988, which are much fewer than the number of sites over Northern Hemisphere.**

Line 374: Most likely due to an overestimation of China emissions (e.g., Saeki and Patra, GOSL, 2017, and references therein) (regional inversion is needed for adjusting such regional emission biases)

125 **Reply:**

We thank the reviewer for the references. We have included them in the revised manuscript as below:

“The overestimates are likely due to overestimation of emissions over Southeast Asia (e.g., Saeki and Patra, 2017, Patra et al., 2016, and Thompson et al., 2015), which could affect these remote sites through transport.”

130 Line 378: "...which is also a remote site" and remote from China emissions

Reply:

We agree with the reviewer’s comment. This again suggests an overestimation in the emissions over Southeast Asia. We have included this in the revised manuscript as below:

135 *“However, the model predicts surface methane DMF relatively well at Ascension Island (ASC, 8°S, 14.4°W, 85 m), which is also a remote site without impacts from East Asia.”*

140 Lines 394ff: I am not very sure if the comparison with GOSAT/SCIA are adding any values to this work. Better be kept aside for a full paper, unless the reasons for the mean offsets are figured out and discussed. For instance you could compare your results with the ACE-FTS data to find out if there is any bias in the stratospheric CH₄ as there is no significant offsets in the tropospheric CH₄ is seen in comparison with surface data and HIPPO.

Reply:

We have moved the model evaluation against satellite observations to the Supplement.

145 Line 426ff: The emission increase in the 1990s is apparently linked to OH increase in AM; which sector can provide this extra emissions. I think this result is very different from what I have seen in the literature, and thus needing some explanation. Surprisingly, the emission increase rate in the 1990s is greater than the recent regrowth period.

Reply:

150 **In S0Wopt, the total emission growth during the 1980s is mainly from emission growth from agriculture (0.7 Tg yr⁻¹), energy (0.3 Tg yr⁻¹), waste (1.0 Tg yr⁻¹), and wetland (1.8 Tg yr⁻¹), while the total emission growth during the 1990s is mainly from waste (0.8 Tg yr⁻¹) and wetland (3.7 Tg yr⁻¹). Therefore, these extra emissions in the 1990s are mainly from wetland in S0Wopt scenario.**

155 **In S0Aopt, the total emission growth during the 1980s is mainly from emission growth from agriculture (1.4 Tg yr⁻¹), energy (0.9 Tg yr⁻¹), and waste (1.4 Tg yr⁻¹), while the total emission growth during the 1990s is mainly from agriculture (1.3 Tg yr⁻¹), energy (1.1 Tg yr⁻¹), waste (1.6 Tg yr⁻¹), and biomass burning (0.4 Tg yr⁻¹). Therefore, these extra emissions in the 1990s are mainly from energy, waste, and biomass burning sectors in S0Aopt scenario.**

160 **The emission increase rate in the 1990s is greater than the recent growth period because OH decreases in the recent growth period. When we optimize emissions, we consider the impacts of OH trends. In the recent growth period, OH is decreasing, and therefore methane lifetime increases. This amplifies the responses of methane concentrations to the changes in the emissions. Therefore, a smaller increase in the emissions during this period can lead to larger increases in methane concentrations compared to that in the 1990s.**

165 Lines 484ff: The discussions using Fig 9-11 aren’t that interesting as presented. I would recommend the authors to move these plots to the supplement or show 1-2 panels in the main text; for example all the 4 panels in Fig 9 & 10 are essentially showing very similar distributions. The S0Aopt and S0Wopt are also showing similar behaviour. This is mainly because the

emission (E)-a priori emissions are the same in both the simulations, and the correction emissions Del-E following Anthropogenic or Wetland emission patterns only play minor role. I am actually curious if you could use some of the continental sites, e.g., NWR, LEF, SGP or TAP, and use the model-measurement comparisons to say whether the S0Aopt or S0Wopt are more realistic.

170 **Reply:**

We thank the reviewer for these suggestions. We have moved Figures 9-11 to Figures S7-10 in the Supplement. We also include site-level comparisons in the revised manuscript at lines 286-309. Despite the differences in the relative contributions of individual sources in S0Aopt and S0Wopt, due to the mixed-source effect and transport, the performance by S0Wopt and S0Aopt are very similar at most of sites. It is difficult to tell which one is more realistic in general. However, we do see general higher CH₄ concentrations in S0Aopt than S0Wopt over the Northern Hemisphere.

175

As shown in the Supplement Figure S4-5, over tropics, S0Wopt is in general better with smaller biases at KUM, POCN20, POCN25, and MID, which suggests overestimations in the Southeast Asian emissions. Also, anthropogenic emissions may be underestimated in S0Wopt at WLG and NWR and overestimated at TAP site based on the comparisons of S0Aopt and S0Wopt, whereas wetland emissions may be overestimated in S0Wopt at LEF site.

180

Line 519: Such high correlations are a bit surprising, if I see the lines in Fig. 12. For example AGR show -ve trend, yet show positive correlation. How is that possible?

Reply:

185

The high correlation is mainly for periods of 1983-1998 and 2007-2014. In Figure 12 (now Figure 7 in the revised manuscript), the negative trend for AGR during 1999-2006 is very weak (i.e., -0.2 ppb/yr), almost no significant trend. The correlation here is more dominated by the interannual variability than linear trend. The positive correlation therefore suggests the interannual variability of CH₄AGR agrees with that of total CH₄.

190

Line 633: This is similar to the essential conclusion in some other publications as well, where ENE and Animals were made responsible for the post-2006 CH₄ growth rate. I guess it is extremely difficult to separate emissions from Animals and Wetlands by 13C signature in CH₄.

Reply:

195

We agree with the reviewer's comments that rely on methane ¹³C signatures only is not able to distinguish emissions from animals and wetlands.

Lines 638ff: I am curious if inconsistency between the tropospheric OH and CH₄-loss by OH are arising from the spin-up. Did you spun-up the simulations using different OH from the 1970s?

Reply:

200

In our spin-up simulations, we drive the model with 1979 emissions for 50 spin-up years. During spin-up, OH changes every year based on the simulated chemistry. We used the spun-up atmospheric conditions for all the production runs, including low-OH and high-OH cases. In other words, we use the same initial conditions for low and high OH cases. As OH is short-lived species, the initial condition of OH has little impact on OH concentrations and trends. Based on our model tests, we find a very close relationship between tropospheric OH and lightning NO_x. The changes in CH₄-OH loss are not only affected by changes in OH but also CH₄. Decreases in OH levels during 2008-2015 does necessary lead to decreases in CH₄-OH loss as CH₄ is increasing during this time period.

205

Response to Referee #2 for comments on “Investigation of the global methane budget over 1980-2017 using GFDL-AM4.1” by He et al.

We thank the reviewer for the insightful comments and suggestions on our manuscript. Below, our responses in bold text follow the reviewer’s comments shown in plain text.

The author presents an analysis of the methane global budget using an atmospheric chemistry model over almost 4 decades (1980-2017) and considering changes in both emissions and sinks. As conclusion, they provide likely scenarios of changes in sources and sinks of methane explaining the methane growth different periods of these past decades.

GENERAL COMMENT

The manuscript is well written and organize, and quite easy to follow. The methodology and different steps are well explained. Understanding the methane budget and particularly its changes is crucial to establish pathways for emission reduction. As a result, this study contributes significantly to the debate.

Reply:

We thank the reviewer for the positive comments.

However part of the result section is quite lengthy and may be shortened and more straightforward– see specific comments below. The comparisons to the observation (surface and satellite) as done here, do not really help in discriminating better scenarios.

Reply:

We thank the reviewer for the suggestions. We have revised the manuscript and shortened the result section.

Regarding the abstract and conclusion of the paper: there might not be a single driver of the recent methane growth, but a combination of different increasing/decreasing sources/sinks (Saunois et al., 2017). Different studies (as cited) may appear in disagreement as only the major driver (one source) is highlighted (in the abstract, title or conclusion) but considering the uncertainty of the estimates, this could be a combination – with high uncertainty on the relative contributions; but this does not mean that there are no agreement between studies. One of the objective is to “investigate the possible drivers” of the methane changes. So why keeping a single source as a driver? Why not considering the combination and trying to estimate the relative contribution? Also, testing different initial emissions would further strengthen the resulting range.

Reply:

We agree with the reviewer that it is more likely a combination of different drivers instead of one single driver that lead to recent methane growth, which is also indicated by the model results discussed in the manuscript. The more important question is the relative contributions from these drivers, which, as mentioned by the reviewer, is highly uncertain. We have included additional discussions in the revised manuscript regarding the relative contributions. However, as mentioned in the manuscript, we need additional observational constraints (e.g., methane isotopes, ethane) to better quantify the relative contributions, which is the next step of the work.

With different initial emissions, the optimized methane emissions totals would be similar but spatial distribution and seasonality could be different. We did one sensitivity test with time-varying wetland emissions (i.e., S0Origswet) as shown in Figures S2 and S3 in the Supplement. Using time-varying wetland emissions does not alter our results much. Based on the results comparison in Figures S2 and S3, which suggest better performance by climatological wetland emissions (i.e., S0Orig), we decide to start with this wetland emission.

As this manuscript is more focused on global totals, even with different initial emissions (e.g., different wetland emissions), after the emission optimization, the impacts would be very small on global averages, but could be large on regional scales. Also, the relative contributions would be different. However, the Aopt and Wopt sensitivities conducted in this work provide extreme scenarios for the contributions from anthropogenic sources and wetland sources. As mentioned earlier, additional observational constraints could be applied to refine the resulting ranges.

Finally, I would recommend publication in ACP after major revisions addressing the general and specific comments highlighted in this review.

Reply:

260 **We thank the reviewer for the suggestions. We have revised the manuscript and addressed the comments point by point below.**

SPECIFIC COMMENTS

Section 1 – Introduction

265 Lines 38 to 42. Removes those lines: it's stated later and better near the end of the section.

Reply:

We have removed these lines in the revised manuscript.

270 Line 43- 47. Add a general reference here (e.g. Sauniois et al. (2016)).

Reply:

We have added the reference in the revised manuscript.

275 Line 60-67. There have been other studies that tried to highlight some more likely scenarios combining changes from individual sources. E.g., Sauniois et al., (2017) suggested a combination (with relative contributions) of changes from the different methane sources contributing to the renewed growth (increasing from fossil, agriculture and waste emissions, decrease of biomass burning, . . .).

280 **Reply:**

We have included the statement of combined changes in sources with the reference in the revised manuscript as below:

285 *“The observed renewed growth since 2007 has been explained alternatively through increases in tropical emissions (Houweling et al., 2014; Nisbet et al., 2016) such as agricultural emissions (Schaefer et al., 2016; Patra et al., 2016) and tropical wetland emissions (Bousquet et al., 2011; Maasakkers et al., 2019), increases in fossil fuel emissions (Rice et al., 2016; Worden et al., 2017), decreases in sources compensated by decreases in sinks due to OH levels (Turner et al., 2017; Rigby et al, 2017), or a combination of changes in different sources such as increases in fossil, agriculture, and waste emissions with decreases in biomass burning emissions (Sauniois et al., 2017).”*

290

Section 2 – Methodology and data

Line 125. “BMB emissions contribute to IAV”. . . because wetland emissions are considered constant in the study. Wetland emissions contribute a lot to methane emission IAV (Kirschke et al., 2013).

295 **Reply:**

We have clarified this statement in the revised manuscript as below:

300 *“Although wetlands are in reality a major contributor to interannual variability in methane emissions (Bousquet et al., 2006; Kirschke et al., 2013), our use of climatological wetland emissions causes the interannual variability in our methane emissions to be dominated by BMB emissions.”*

Line 151. “. . . largely underestimate. . .”. What is largely here? Please quantify.

Reply:

305 **We have evaluated the model results with initial emission inventories, which is shown in Figure S2 in the Supplement. The simulated methane DMF is about 126 ppb lower than observed CH₄ DMF from NOAA GMD surface observations (with RMSE = 120 ppb).**

310 Line 153. “optimization simulations”? The optimization approach is described later (from line 169), but this description should directly follow the first mentioning of “optimization approach”. Which observations are used for this “optimization”? surface marine boundary layer – described after? Please specify and put Section 2.3 Observation before Section Simulation Design.

315 **Reply:**
Thank you for the suggestion. We have reordered the sections such that the section on Observations appears before Simulation Design.

320 Line 174. The relative contributions from the different sectors are also kept as in the initial emission set up, and depend on it. As a result this highly depend on the initial set of emissions. Testing other set of initial emissions would really be valuable to assess the uncertainty related to the set up and strengthen the results. EDGARv4.3.2 instead of CEDS for example. Other wetland emissions including IAV. . .

325 **Reply:**
We agree that our results depend on the individual contributions in the initial emission inventories. Using different initial emission inventories may help assess the associated uncertainties of individual sector contributions to a certain degree, but to better quantify the individual contributions and assess the uncertainties, we could apply additional observational constraints, which is our next step of the study.

330 **Methane anthropogenic emissions from EDGARv4.3.2 are about 5-9% lower than CEDS anthropogenic emissions, mainly due to lower emissions from energy sector (Janssens-Maenhout et al., 2019). The share of ENE to total anthropogenic emissions in EDGARv4.3.2 (i.e., 33%) are also lower than those in CEDS (i.e., 38%), but both increase after 2006. We are unable to test EDGARv4.3.2 emissions in this work but will consider it for future work.**

335 **To address the reviewer’s point about wetland emissions with IAV, we performed a test simulation with wetland emissions including IAV for 2001–2015 (i.e., S0Origswet) based on an extended ensemble version of WetCharts (Bloom et al., 2017) as shown in Figures S2 and S3. The results from this simulation are very similar to those from climatological wetland emissions (i.e., S0Orig). We expect that optimization of wetland emissions will cause the original IAV in emissions to be lost.**

340 Line 180. DeltaE include IAV missing from the initial emissions. In the case of SAopt, this is attributed to anthropogenic emissions, is that realistic?

345 **Reply:**
The IAV of methane emissions are mainly dominated by that from wetland and biomass burning. However, IAV could also exist in anthropogenic emissions due to the dependence of microbial methane sources, such as rice paddies, on soil temperature and precipitation (e.g., Knox et al., 2016). The optimization to match observations resulted in higher IAV in total emissions than in the initial emissions. Because the purpose of S0Aopt is to investigate the role of changes in total anthropogenic emissions (anthro plus BB) rather than individual sectors, we applied this IAV to all sectors which we acknowledge introduces some unrealistic IAV in the anthropogenic emissions. We chose this
350 **experimental construct to limit the number of sensitivity simulations.**

Line 184. The reader would probably want to have fast access to FigS2. . Indeed all the discussion is on emissions from SAopt and SWopt and not on the initial emissions. That would be better to combine Fig1 and Fig S2

355

Reply:

We have combined these figures as new Fig 1 in the revised manuscript.

360

Line 200. At which frequency are the observations considered? Frequency of the sampling of the model? Monthly?

Reply:

Since the frequency of the model output is monthly, the observations are also monthly-based.

365

Section 3 Results and discussions.

Line 241. Testing different wetland emission data sets – with different seasonality may help to quantify the influence of wetland emission seasonality on the observed bias. OH influence could be seen in simulation S2 with higher OH: is S2 performing better?

370

Reply:

We agree that different wetland emission datasets can help assess the impacts of wetland emission seasonality on the observed bias. We did a sensitive test with time-varying wetland emissions (i.e., S0Origswet) for 2001-2015 as shown in Figures S2 and S3 in the Supplement. In terms of seasonality, we did not find much difference between S0Orig and S0Origswet. In a future study, we plan to simulate wetland emissions in the land model (LM4.1) coupled to AM4.1 to better capture the spatial and temporal variability of wetland emissions than prescribed emissions.

375

The S2 performance is similar to S0 as we re-optimized methane emissions based on higher OH case. Higher OH case does not change the spatial and temporal variability of OH but only the magnitude of OH levels.

380

Line 244. Is it reasonable to state that SWopt perform a bit better than SAopt? So far no comparison is made between the two simulations.

Reply:

As we optimize the global total emissions instead of spatial distribution, globally, the performance of Wopt and Aopt is very similar to each other, however there are regional differences because of the differences in the spatial distribution of emissions. For example, in the Southern Hemisphere, Wopt performance is very similar to Aopt. In the Northern Hemisphere, Wopt performs better than Aopt at KUM, POCN20, ASK, and TAP sites, while it performs worse at KEY, WIS, and UTA. It is really site-specific. We have included site-specific comparisons between S0Wopt and S0Aopt in the revised manuscript as below:

390

“S0Aopt and S0Wopt simulate very similar surface methane DMF and their comparison with NOAA-GMD observations at individual sites show both simulations to be biased low over Southern Hemisphere sites, but the low bias decreases northward (Figure S5 in the Supplement). The simulations are biased moderately high (with RMSEs up to ~ 40 ppb) over tropical regions (e.g., POCS15, POCS10, SMO, POCS05, POCN00, CHR, and POCN05). These sites are mainly remote sites and surface methane DMF represents background methane levels. The overestimates are likely due to overestimation of emissions over Southeast Asia (e.g., Saeki and Patra, 2017, Patra et al., 2016, and Thompson et al., 2015), which could affect these remote sites through transport. However, the model predicts surface methane DMF relatively well at Ascension Island (ASC, 8°S, 14.4°W, 85 m), which is also a remote site without impacts from East Asia. The high biases over the tropics suggest a need to improve regional emissions (e.g., Southeast Asia). Moderate overestimates also occur at Mahe Island (SEY, 4.7°S, 55.5°E), a location that could be affected by air masses from polluted areas over the tropics and Northern Hemisphere. Over middle and high latitudes of the Northern Hemisphere, both S0Aopt and S0Wopt simulate surface methane DMF relatively well at most sites, except at Key Biscayne (KEY, 25.7°N, 80.2°W), Tae-ahn Peninsula (TAP, 36.7°N, 126.1°W), Park Falls (LEF, 45.9°N, 113.7°W), and Mace Head (MHD, 53.3°N, 9.9°W). KEY, MHD, and TAP are sampled under onshore winds, whereas LEF are affected by local sources and model transport. The high biases at these sites could be due in part to model sampling bias (e.g., model grid

400

405 *box overlapping land while samples are collected at coast with onshore winds) and uncertainties in local emissions (e.g., possible overestimation in the emissions over East Asia). On the other hand, both S0Wopt and S0Aopt are able to capture monthly variations in methane at most of the sites except at LEF, where $R = 0.4$ for S0Wopt and 0.5 for S0Aopt, respectively. In general, both S0Wopt and S0Aopt are able to reproduce the surface methane DMF and capture the trend at most sites (e.g., with R greater than 0.5 at 98% of total sites and with RMSE less than 30 ppb at 74% of total sites). As shown in Figure S5, S0Aopt in general better estimates methane trends and growth over low latitudes of the Southern Hemisphere (e.g., SMO) and middle/high latitudes of the Northern Hemisphere (e.g., ASK, KEY, WIS, UTA, NWR, UUA, LEF, CBA, STM, and ALT) than S0Wopt. Based on the site-level comparisons between S0Wopt and S0Aopt, anthropogenic emissions over Southeast Asia are likely overestimated in both S0Aopt and S0Wopt, while they could be underestimated at WLG and NWR in S0Wopt but be reasonably well represented in S0Aopt.”*

415 Line 253: The reasons of the biases compared to HIPPO are exactly the same as those seen with surface observations. See comment for line 241.

420 **Reply:**
Please see reply to comment for line 241.

Line 255. 2% difference with the updated GFDL-AM4.1, using optimized emissions. How much was the difference when using initial emissions? How much better is it compared to the previous version of GFDL-AM4.1?

425 **Reply:**
With initial emissions, the simulated methane profiles are about 12% lower than HIPPO measurements. For the standard version of GFDL-AM4.1, which uses prescribed methane concentrations, the simulated methane profiles are about 5% higher than HIPPO measurements in the Southern Hemisphere and 4% lower in the Northern Hemisphere.

430 Line 264. Isn't it by construction? As total emissions are optimized using surface marine boundary layer observations. . .

435 **Reply:**
The match of global means is certainly by design, but not that for latitude bands. As shown in Figure 4 in the main text, the model is still able to capture methane trends and variability at different latitude bands. We have revised the sentences as below:

440 *“S0Wopt and S0Aopt are also able to reproduce global annual mean surface methane DMF (with root-mean-square-error (RMSE) = 10.4 ppb in S0Wopt and 11.6 ppb in S0Aopt) over 1983-2017, which is expected from emission optimization. Meanwhile, both simulations are able to reproduce the methane timeseries very well (with $R = 1.0$ in both S0Wopt and S0Aopt) over different latitude bands as shown in Figure 4.”*

Line 274. Not clear about the 1-year mismatch. There is not always a 1-year delay between spikes. . .

445 **Reply:**
We corrected a bug in the scripts for model evaluation and updated all the relevant plots. We then updated results and discussions in the revised manuscript as below:

450 *“Table 3 summarizes methane growth rates during 1984-1991, 1992-1998, 1999-2006, and 2007-2017. S0Aopt and S0Wopt simulate very similar methane growth rates as their emission totals are the same. During 1984-1991, both S0Aopt and S0Wopt slightly overestimate methane growth rates by ~ 2 ppb yr^{-1} , possibly due to fewer available observations used for emission optimization during this time period than afterwards. After 1991, the simulated methane growth rates are in general comparable to the observations (with annual mean difference within ± 1 ppb yr^{-1}). The major discrepancies in the simulated methane growth rates and observations occur over the tropics and high northern latitudes as shown in Figure 4. Over the tropics, both S0Aopt and S0Wopt overestimate methane growth rates (by about 5-10 ppb yr^{-1}) during 1984-*

455 *1990 when there were limited observations available, but are able to reproduce methane growth rates relatively well afterwards. Agreement of the methane growth rate is worse in the Northern Hemisphere than in the Southern Hemisphere, especially at high northern latitudes, mainly due to the large bias during 1984-1988 and a slight shift in peak growth (or peak decrease) during 1997-2005. The number of observational MBL sites does not provide adequate coverage of the globe, especially in the 1980s, which could have different impacts on the Northern and Southern*
460 *Hemisphere when optimizing global total emissions. In general, S0Aopt estimates slightly better methane growth rates than S0Wopt, especially over 30-90° N. The biases in methane growth rates also suggest a need to refine regional emissions.”*

465 Line 275-281. Are those numbers necessary in the text? What is the point? That could be summarize in a Table for the full numbers and in the text summarize to “SWopt performs better over this period while SAopt performs better over that period”. The differences in growth rate are much lower than their own range of uncertainty.

Reply:

470 **As suggested by the reviewer, we have summarized the growth rates in the table and revised these sentences in the revised manuscript (see reply to comment line 274).**

Line 283. Does it imply that the results (following results on the emissions changes) are less robust for this region? This is unfortunate as most of the methane emissions occur in the NH.

475 **Reply:**

We corrected a bug in the scripts for model evaluation and updated all the relevant plots. After the correction, both Aopt and Wopt are able to reproduce methane growth rates despite there is a slight mismatch (~1-2 years) during 1998-2008. But compared to other regions, the correlation is slightly worse over 30-90° N. This suggests a need to improve/optimize regional emissions.

480 Line 286. Indeed. Related to wetland emissions? Is it related to the missing IAV in wetland initial emissions?

Reply:

485 **Many reasons could lead to such biases over 30-90N. Uncertainties in the IAV of both wetland and anthropogenic emissions could lead to such bias. The biases also suggest a need to improve/optimize regional emissions.**

Line 301. Could the bias model sampling be overcome/reduced? Does the bias change with the grid box choice for coastal sites?

490 **Reply:**

Yes. If we move the grid box to the ocean side, the bias is reduced significantly. For example, at KEY and MHD sites, the RMSEs are reduced from ~90 ppb to 33 ppb and from ~50 ppb to 20 ppb, respectively.

495 Line 306-319. The model observation comparison using GOSAT and SCHIAMACHY is not really helpful. As the model is optimized against surface observations, it's saying that surface observation and satellite data see similar trends (but are offset by latitudinal biases), that biases exist in the satellite data (latitudinal biases), and that uncertainties in the transport model (especially in the stratosphere but not only) can explain the difference between model and satellite columns. Nothing new for an atmospheric model assessment, and this comparison does not discriminate one simulation from the other. This part may be removed and put in the supplementary material.

500 **Reply:**

As suggested by the reviewer, we have moved this part to the Supplement.

Line 325. By construction?

505

Reply:

Yes. Both simulations reproduce the global growth rates by design. But the model with optimized emissions is still able to reproduce the growth rates at different latitude bands.

510 Line 332-333. This sentence should be removed and put in Section2.

Reply:

As suggested by the reviewer, we have moved this sentence to Section2.

515 Line335_336. This sentence could be removed with causes of interannual variability put in sentence of line 329-330.

Reply:

As suggested by the reviewer, we have combined these sentences as below:

520 *“As shown in Figure 5, the optimized emissions in general increase during 1980-2017, with an annual mean of 580 ± 34 Tg yr⁻¹ (mean \pm standard deviation) and show much larger interannual variability during 1991-1993 and 1997-2000, which is likely due to the strong El Niño events during 1991-1992 and 1997-1998 as well as the Mt Pinatubo eruption in 1991 (Dlugokencky et al., 1996; Bousquet et al., 2006; Bândă et al., 2016).”*

525 Also 1991-1992 high IAV is also related to Mt Pinatubo eruption (decrease in CH₄) (ref. e.g., Banda et al., 2016, <https://www.atmos-chemphys.net/16/195/2016/>; Dlugokencky, E. J. et al. Changes in CH₄ and CO growth rates after the eruption of Mt Pinatubo and their link with changes in tropical tropospheric UV flux. Geophys. Res. Lett. 23, 2761–2764 (1996); 21. Bousquet, P. et al. Contribution of anthropogenic and natural sources to atmospheric methane variability. Nature 443, 439–443 (2006)).

530

Reply:

We thank the reviewer for providing the references. We have included these references into the revised manuscript.

Line 343. Is it possible to overplot Naus et al. OH level on Figure 8?

535

Reply:

We have included OH anomaly from Naus et al. (2019) in the Figure 6 in the revised manuscript.

540 Table 3. Single values are provided for the emission estimates while several simulations were performed. The authors compare their initial emission to the literature – which could have been done in Section2. However they stated that there initial emission were underestimate and then all the paper is on the optimized emissions. So Table 3 should compare their optimized emissions with the literature!

Reply:

545 **Table 3 includes numbers for optimized emissions as reflected in rows of ΔE and sum of sources. Also, for ΔE and sum of sources, we include estimated ranges based on different OH levels as well. To address the reviewer’s comment, we have included estimated ranges for individual sectors based on the Aopt and Wopt under different OH levels, which is now shown in Table 4 in the revised manuscript.**

550 Line 351-353. Total natural emissions from bottom-up estimates are much lower than top-down because there are not constrained and just an “addition” from independent individual source estimates, knowing the large uncertainty of each natural source. . . The initial emissions should be much comparable to top-down estimates, as the large source from freshwater is not included in the initial emissions (about 100Tg in the bottom up methane budget).

555 **Reply:**
We thank the reviewer for the explanation. We have included this discussion in the revised manuscript as below:

560 *“Since there is no observational constraint on bottom-up estimates, total natural emissions are simply summed over independent individual sources, which could be overestimated in the bottom-up approach considering the relatively large uncertainties in each individual source. In addition, in the bottom-up estimate from Kirschke et al. (2013) and Saunio et al. (2016), some other natural sources, such as freshwater, are not included in the initial emission inventories in this work; however, they are likely double counted in the bottom-up estimates (e.g., high-latitude inland waters are likely also considered as wetland areas) as pointed out in Saunio et al. (2019).”*

565 Line 353-354. Not really, see comment above. The difference between the initial emission of this study and the bottom-up estimate from Kirschke et al and Saunio et al., is mainly driven by source not included in the initial emission set up (freshwater), and probably double counted in the bottom-up budget. Estimates for other natural sources from Kirschke et al., 2013 and Saunio et al., 2016 should be added. This is also due to the use of a climatological value for wetland emissions from the 2000s applied to the whole period. As IAV and trends are missing in the initial emissions, some signal is lost compared to estimates reported by Kirschke et al. and Saunio et al.

570 **Reply:**
We thank the reviewer for the explanation. We have included this discussion in the revised manuscript (see reply above) .

575 Line 356. Remove Saunio et al., 2016 as the study starts in 2000.

580 **Reply:**
Removed.

585 Line 358 and following. Well, that would be better to show the range of total anthropogenic and wetland optimized emissions and to compare these ones with the literature. Table 3. It also presents values for the more recent period. These values may be compared with the updated global methane budget recently released in ESSDD Saunio et al., 2019 (<https://www.earth-syst-sci-data-discuss.net/essd-2019-128/>)

590 **Reply:**
We have updated Table 3 (now Table 4) with values from Saunio et al. (2019).

595 Section 3.3.1. These results are quite expected knowing the distribution of anthropogenic emissions and wetland emissions. There are interesting but could be more when compared against observations. If the surface methane DMF and growth rate observed values at each sites are over plotted on these spatial distributions, does it help in discriminating which optimized emissions fit the best?

600 **Reply:**
The overlay plots have been generated as shown in Figure S7 and Figure S9 in the Supplement. But S0Aopt and S0Wopt gives very similar methane DMF and growth rates. We included site-level comparisons in Section 3.1. As also suggested by the other reviewer, we have removed this part into the Supplement.

605 Line 400-401. By construction?

610 **Reply:**
For global trends, the match of model simulations with observations are by design.

615 Line 406. . . are KEPT constant. . .

605

Reply:

We have corrected this in the revised manuscript as below:

610

“Since wetland emissions and other natural emissions are kept constant every year in S0Aopt, with increases in OH levels during 1983-1998, all tagged natural tracers show a weak decreasing trend.”

Line 432 and line 437. How can we explain higher sink?

Reply:

615

Although concentrations of tracer CH4WET decrease, with the increases in OH levels during 1999-2006, CH4WET sinks also increase, which could be higher than wetland emissions. Also, during this time period, CH4WET decreasing trend is very weak (e.g., -0.6 ppb/yr). During 2007-2017, wetland emissions are lower compared to 1999-2006 (see Figure 1) while OH levels are higher. Therefore, the decreasing trend (e.g., -4.6 ppb/yr) is much larger compared to 1999-2006.

620

Line 453. Indeed. . .Is testing a different initial inventory an option? It would help, confirming or infirming some results. . .

Reply:

See reply to General comments above.

625

Line 454. Other sectors (than wetland?)

Reply:

630

Yes. For S0Wopt, except wetland, which is optimized, all other sources are based on the initial emission inventories.

Section3.3.2: could this section be shortened? It’s quite hard to follow. . . Instead of describing each simulation in detail (with numbers etc.), would it be shorter to conclude for each period, which sector(s) drive the changes (increase. . .) and if the two simulations agree or not? And keep the details and numbers for the supplementary. . .

635

Reply:

We thank the reviewer for the suggestion. We have shortened and revised this section as Section 3.3 in the revised manuscript.

640

Line 457 and following. The two sensitivity tests may be presented in Section 2 as well. And included in the above discussion..

Reply:

As suggested by the reviewer, we have included two sensitivity tests in Section 2 as well as in Section3.3.

645

Section 3.4 Sensitivity to OH.

How does the model compare with the other CCMI models? (see Zhao et al., 2019 Fig 4 and 7. <https://www.atmos-chem-physdiscuss.net/acp-2019-281/acp-2019-281.pdf>)

650

Reply:

In general, our OH trend is within the range of OH trends in Zhao et al. (2019). From 1980 to 2000, OH in AM4.1 increases by 4.7%, comparable to 4.6±2.4% in Zhao et al. (2019). During 2000-2010, OH anomaly varies from -0.29 mole cm⁻³ to 0.34 molec cm⁻³.

TECHNICAL COMMENTS Line 87. 1980-2017 instead of 1980-2014

655

Reply:
Thanks, corrected.

660

References:

Bloom, A. A., Bowman, K. W., Lee, M., Turner, A. J., Schroeder, R., Worden, J. R., Weidner, R., McDonald, K. C., and Jacob, D. J.: A global wetland methane emissions and uncertainty dataset for atmospheric chemical transport models (WetCHARTs version 1.0), *Geosci. Model Dev.*, 10, 2141-2156, <https://doi.org/10.5194/gmd-10-2141-2017>, 2017.

665

Knox, S. H., Matthes, J. H., Sturtevant, C., Oikawa, P. Y., Verfaillie, J., and Baldocchi, D.: Biophysical controls on interannual variability in ecosystem-scale CO₂ and CH₄ exchange in a California rice paddy, *J. Geophys. Res. Biogeosci.*, 121, 978–1001, doi:10.1002/2015JG003247, 2016.

670

Janssens-Maenhout, G., Crippa, M., Guizzardi, D., Muntean, M., Schaaf, E., Dentener, F., Bergamaschi, P., Pagliari, V., Olivier, J. G. J., Peters, J. A. H. W., van Aardenne, J. A., Monni, S., Doering, U., Petrescu, A. M. R., Solazzo, E., and Oreggioni, G. D.: EDGAR v4.3.2 Global Atlas of the three major greenhouse gas emissions for the period 1970–2012, *Earth Syst. Sci. Data*, 11, 959–1002, <https://doi.org/10.5194/essd-11-959-2019>, 2019.

675

Investigation of the global methane budget over 1980-2017 using GFDL-AM4.1

Jian He^{1,2}, Vaishali Naik², Larry W. Horowitz², Ed Dlugokencky³, and Kirk Thoning³

680 ¹Program in Atmospheric and Oceanic Sciences, Princeton University, Princeton, New Jersey, USA

²NOAA Geophysical Fluid Dynamics Laboratory, Princeton, New Jersey, USA

³NOAA Earth System Research Laboratory, Boulder, Colorado, USA

Correspondence to: Jian He (jian.he@noaa.gov)

Abstract. Changes in atmospheric methane abundance have implications for both chemistry and climate as methane is both a
685 strong greenhouse gas and an important precursor for tropospheric ozone. A better understanding of the drivers of trends and
variability in methane abundance over the recent past is therefore critical for building confidence in projections of future
methane levels. In this work, the representation of methane in the atmospheric chemistry model AM4.1 is improved by
optimizing total methane emissions (to an annual mean of 580±34 ~~576±32~~ Tg yr⁻¹) to match surface observations over 1980-
2017. The simulations with optimized global emissions are in general able to capture the observed global trend, variability,
690 seasonal cycle, and latitudinal gradient of methane. Simulations with different emission adjustments suggest that increases in
methane sources (mainly from energy and waste sectors) balanced by increases in methane sinks (mainly due to increases in
OH levels) lead to methane stabilization (with an imbalance of 5 Tg yr⁻¹) during 1999-2006, and that increases in methane
sources (mainly from agriculture, energy, and waste sectors) combined with little change in sinks (despite small decreases in
OH levels) during 2007-2012 lead to renewed methane growth (with an imbalance of 14 Tg yr⁻¹ for 2007-2017). Compared to
695 1999-2006, both methane emissions and sinks are greater (by 31 Tg yr⁻¹ and 22 Tg yr⁻¹, respectively) during 2007-2017. Our
tagged tracer analysis indicates that anthropogenic sources (such as agriculture, energy, and waste sectors) are more likely
major contributors to the renewed growth in methane after 2006. A sharp increase in wetland emissions (a likely scenario)
with concomitant sharp decrease in anthropogenic emissions (a less likely scenario), would be required starting in 2006 to
drive the methane growth by wetland tracer. Our results also indicate that the energy sector is more likely a major contributor
700 to the methane renewed growth after 2006 than wetland, as increases in wetland emissions alone are not able to explain the
renewed methane growth with constant anthropogenic emissions. In addition, a significant increase in wetland emissions would
be required starting in 2006, if anthropogenic emissions declined, for wetland emissions to drive renewed growth in methane,
which is a less likely scenario. Simulations with varying OH levels indicate that 1% change in OH levels could lead to an
annual mean of ~4 Tg yr⁻¹ difference in the optimized emissions and 0.08 year difference in the estimated tropospheric methane
705 lifetime. Continued increases in methane emissions along with decreases in tropospheric OH concentrations during 2008-2015
prolong methane lifetime and therefore amplify the response of methane concentrations to emission changes. Uncertainties
still exist in the partitioning of emissions among individual sources and regions.

1 Introduction

Atmospheric methane (CH₄) is the second most important anthropogenic greenhouse gas with a global warming potential 28-34 times that of carbon dioxide (CO₂) over a 100-year time horizon (Myhre et al., 2013). Methane is also a precursor for tropospheric ozone (O₃) - both an air pollutant and greenhouse gas - influencing ozone background levels (Fiore et al., 2002). Controlling methane has been shown to be a win-win for both climate and air quality (Shindell et al., 2012). From a preindustrial level of 722±25 ppb (Etheridge et al., 1998; Dlugokencky et al., 2005), methane has increased by a factor of ~2.5 to a value of 1857±1 ppb in 2018 ~~1850±1 ppb in 2017~~ (Dlugokencky et al., 2018), mostly due to anthropogenic activities (Dlugokencky et al., 2011). The global network of surface observations over the past 3-4 decades indicates that methane went through a period of rapid growth from the 1980s to 1990s, nearly stabilized from 1999 to 2006, and then renewed its rapid growth. ~~Studies of the drivers of observed changes in methane trends and variability have focused on the contributions from changes in methane sources and sinks.~~ Here, we ~~apply a prototype of the new generation NOAA Geophysical Fluid Dynamics Laboratory chemistry climate model, GFDL-AM4.1 (Zhao et al., 2018a, b; Horowitz et al., manuscript in preparation) with an improved representation of methane, to~~ estimate methane budget during 1980-2017 and explore the contributions of methane sources and sinks to its observed trends and variability during 1980-2017.

Methane is emitted into the atmosphere from both anthropogenic activities (e.g., agriculture, energy, industry, transportation, waste management, and biomass burning) and natural processes (e.g., wetland, termites, oceanic and geological processes, and volcanoes), and is removed from the atmosphere mainly by reaction with hydroxyl radical (OH) in the troposphere, with less contributions to destruction by reactions with excited atomic oxygen (O(¹D)) and atomic chlorine (Cl) in the stratosphere and uptake by soils (Saunois et al., 2016). Measurements of the global distribution of surface methane beginning in 1983 have revealed that atmospheric methane approached steady state during 1983-2006 and renewed its growth since then. During 1983-2006, methane growth rates decreased from 12 ppb yr⁻¹ during 1984-1991 to 5 ppb yr⁻¹ during 1992-1998 (Nisbet et al., 2014; Dlugokencky et al., 2018) and to 0.7±0.6 ppb yr⁻¹ during 1999-2006 (Dlugokencky et al., 2018). After 2006, ~~renewed~~ methane started increasing again ~~growth started~~ with a growth rate of 5.7±1.2 ppb yr⁻¹ in 2007-2013 and reached 12.6 ± 0.5 ppb yr⁻¹ in 2014 and 10.0 ± 0.7 ppb yr⁻¹ in 2015 (Nisbet et al., 2016; Dlugokencky et al., 2018). Investigations of the drivers of the observed methane trend and interannual variability have mainly focused on the changes in the global methane budget. While anthropogenic activities are widely considered responsible for the long-term methane increase since pre-industrial times (Dlugokencky et al., 2011), there is no consensus on the drivers for the methane stabilization during 1999-2006 and renewed growth since 2007. Previous studies have attributed the stabilization during 1999-2006 to the combined effects of alternatively increased anthropogenic emissions with decreased wetland emissions (Bousquet et al., 2006a), decreased fossil fuel emissions (Dlugokencky et al., 2003; Simpson et al., 2012; Schaefer et al., 2016) or rice paddies emissions (Kai et al., 2011), stable emissions from microbial and fossil fuel sources (Levin et al., 2012), or variations of methane sinks (Rigby et al., 2008; Montzka et al., 2011; Schaefer et al., 2016). The observed renewed growth since 2007 has been explained alternatively through ~~increases in wetland emissions (Dlugokencky et al., 2009; Bousquet et al., 2011; Nisbet et al., 2016),~~ increases in tropical

emissions (Houweling et al., 2014; Nisbet et al., 2016), such as agricultural emissions (Schaefer et al., 2016; Patra et al., 2016) and tropical wetland emissions (Bousquet et al., 2011; Maasakkers et al., 2019), increases in fossil fuel emissions (Rice et al., 2016; Worden et al., 2017), and decreases in sources compensated by decreases in sinks due to OH levels (Turner et al., 2017; Rigby et al., 2017), or a combination of changes in different sources such as increases in fossil, agriculture, and waste emissions with decreases in biomass burning emissions (Saunio et al., 2017). These different explanations reflect limitations in our understanding of recent changes in methane and its budget.

Previous work has generally combined observations of methane and its isotopic composition ($\delta^{13}\text{C}_{\text{CH}_4}$) $\delta^{13}\text{C}$ with isotopic source signatures weighted by their emissions with inverse models (top-down), process-based models (bottom-up), or box models to estimate methane emissions and sinks and their variability (Bousquet et al., 2006a; Monteil et al., 2011; Rigby et al., 2012; Bloom et al., 2012; Kirschke et al., 2013; Ghosh et al., 2015; Schwietzke et al., 2016; Schaefer et al., 2016; Nisbet et al., 2014, 2016; Dalsøren et al., 2016; Turner et al., 2017; Rigby et al., 2017). Inverse models use observations to derive emissions, but usually prescribe climatological OH, O(¹D), and Cl levels or loss rates (e.g., Rice et al., 2016; Tsuruta et al., 2017). Box models, on the other hand, use methane observations together with those of other proxy chemicals (e.g., ¹³C/¹²C ratio, ethane, carbon monoxide, methyl chloroform) to provide information on the global methane budget (e.g., Schaefer et al., 2016; Turner et al., 2017), but lack information on spatial variability or regional characteristics. With process-based models (e.g., wetlands) and inventories representing different source types (e.g., fossil fuel emissions) to drive chemistry transport chemical transport models, the bottom-up approach is able to estimate the methane budget for all individual sources and sinks. However, without observational constraints, there is considerable uncertainty in the total methane emissions derived from a combination of independent bottom-up estimates (Saunio et al., 2016).

Bottom-up global Earth System Models (ESMs) that realistically simulate the physical, chemical, and biogeochemical processes, as well as interactions and feedbacks among these processes, are useful tools to characterize the global methane cycle and quantify the global methane budget and impacts on composition and climate. Dalsøren et al. (2016) investigated the evolution of atmospheric methane by driving a chemistry transport chemical transport model with bottom-up emissions. While their model results are able to match the observed time evolution of methane without emission adjustments, surface methane is largely underpredicted in their study. Ghosh et al. (2015) optimized bottom-up emissions data to investigate methane trends; however, OH trends and interannual variability were not considered in their chemistry transport chemical transport model. Here, we apply a prototype of the full-chemistry version of the Geophysical Fluid Dynamics Laboratory (GFDL) new-generation Atmospheric Model, version 4.1 (AM4.1, Zhao et al., 2018a, b; Horowitz et al., manuscript in preparation) to investigate the evolution of methane over 1980-~~2014~~2017. Our main objectives are to improve the representation of methane in GFDL-AM4.1, to comprehensively evaluate the model performance of methane predictions with an improved representation of methane budget, and to investigate possible drivers of the methane trends and variability. This paper is structured as follows: Section 2 describes the modeling approach, emission inventories, and observations used for model evaluation. Results of the model evaluation, global methane budget analysis, and model sensitivities are presented in Section 3. Finally, Section 4 summarizes the results and discusses the implication of these results.

775 2 Methodology and data

2.1 Model description and initialization

We use a prototype version of the new generation ~~NOAA Geophysical Fluid Dynamics Laboratory GFDL~~ chemistry-climate model, GFDL-AM4.1 (Zhao et al., 2018a, b; Horowitz et al., manuscript in preparation). A detailed description of the physics and dynamics in AM4.1 is provided by Zhao et al. (2018a, b). The version of AM4.1 with full interactive chemistry used in
780 this work is described by Schnell et al. (2018). In its standard form, this model setup consists of a cubed sphere finite-volume dynamical core with a horizontal resolution of ~100 km with 49 vertical levels extending from the surface up to ~80 km. The model's lowermost level is approximately 30 m thick. The chemistry and aerosol physics in this model have been updated from the previous version (GFDL-AM3; Naik et al., 2013), as described by Mao et al. (2013a, b) and Paulot et al. (2016). There are a total of 102 advected gas tracers and 18 aerosol tracers, 44 photolysis ~~reactions~~, and 205 ~~kinetic-gas-phase~~ reactions
785 included in the chemical mechanism in this version of AM4.1 to represent tropospheric and stratospheric chemistry.

The standard AM4.1 configuration uses global annual-mean methane concentrations as a lower boundary condition to simulate the atmospheric distribution of methane. ~~Although the model simulates reasonable global mean methane abundances, large biases exist in the simulated latitudinal distribution and seasonal cycle.~~ This modeling framework ~~also~~ does not allow for the full characterization of the drivers of methane trends and variability. To overcome this issue, we updated AM4.1 to be driven
790 by methane emissions. Table 1 provides information on the methane emission datasets used in this work. Surface emissions from anthropogenic sources - including agriculture (AGR), energy production (ENE), industry (IND), road transportation (TRA), residential, commercial, and other sectors (RCO), waste (WST), and international shipping (SHP)- are from the Community Emissions Data System (CEDS, version 2017-05-18, Hoesly et al., 2018) developed in support of the Coupled Model Intercomparison Project Phase 6 (CMIP6) for 1980-2014. Emissions for 2015-2017 are from a middle-of-the-road
795 scenario of Shared Socioeconomic Pathways targeting a forcing level of 4.5 W m⁻² (SSP2-4.5), developed in support of the ScenarioMIP experiment within CMIP6 (Gidden et al., 2018). Biomass burning (BMB) emissions are from van Marle et al. (2017) for 1980-2014 and from SSP2-4.5 for 2015-2017, and are vertically distributed over seven ecosystem-dependent altitude levels between the surface and 6 km above the surface, following the methodology of Dentener et al. (2006). Anthropogenic and biomass burning emissions are represented by monthly gridded emissions including seasonal and
800 interannual variability. Natural emissions include wetland (WET) emissions from the WetCHARTs version 1.0 inventory (Bloom et al., 2017), ocean (OCN) emissions from Brasseur et al. (1998) with near-shore methane fluxes from Lambert and Schmidt (1993) and Patra et al. (2011), termites (TMI) from Fung et al. (1991), and mud volcanoes (VOL) from Etiope and Milkov (2004) and Patra et al. (2011). Wetland emissions and ocean emissions are climatological monthly means without interannual variability. The remaining natural emissions are based on a climatological annual mean (repeated every month
805 without seasonal variability). Trends in the total emissions and emissions from major sectors over 1980 to 2017 are shown in Figure 1. Trends in total emissions are primarily driven by trends in ENE, AGR, and WST emissions. ~~while Despite Although wetlands are the dominant driver of emissions could contribute a lot to the interannual variability of methane emissions~~

(Bousquet et al., 2006[VN1]; Kirschke et al., 2013). ~~due to the climatological wetland emissions used in this work, the interannual variability in our of methane emissions dataset is primarily driven by BMB emissions because we use climatological mean wetland emissions in the initial methane inventories contribute to interannual variability.~~ Anthropogenic and biomass burning emissions of other short-lived species also follow CEDS and SSP2-4.5 inventories. Natural emissions of other short-lived species are from Naik et al. (2013). Biogenic isoprene emissions are calculated interactively following Guenther et al. (2006).

The methane sinks considered in AM4.1 include oxidation by OH radicals, Cl, and O(¹D), and dry deposition. ~~Since the~~ The model does ~~not represent tropospheric halogen chemistry, it does not~~ consider removal of methane by Cl in the troposphere, ~~a sink that remains poorly constrained which has been shown to be extremely minor~~ (Hossaini et al., 2016[VN2]; Gromov et al., 2018; Wang et al., 2019[VN3]). The dry deposition flux of methane is ~~calculated~~ estimated based on a monthly climatology of deposition velocities (Horowitz et al, 2003) calculated by a resistance-in-series scheme (Wesely, 1989; Hess et al., 2000) and used to mimic methane loss by soil uptake, which accounts for about 5% of the total methane sink (Kirschke et al., 2013; Saunois et al., 2016).

In this work, we included 12 additional methane tracers tagged by source sector to attribute methane from agriculture (CH₄AGR), energy (CH₄ENE), industry (CH₄IND), transportation (CH₄TRA), residents (CH₄RCO), waste (CH₄WST), shipping (CH₄SHP), biomass burning (CH₄BMB), ocean (CH₄OCN), wetland (CH₄WET), termites (CH₄TMI), and mud volcanoes (CH₄VOL). The tracers are emitted from corresponding sources, and undergo the same chemical pathways and dynamics as the full CH₄ tracer. For analysis, we combine CH₄IND, CH₄TRA, CH₄RCO, and CH₄SHP as other anthropogenic tracers (i.e., CH₄OAT), and combine CH₄OCN, CH₄TMI, and CH₄VOL as other natural tracers (i.e., CH₄ONA).

Initially the model was spun up in a 50-year run with repetitive 1979 emissions until stable atmospheric burdens of methane and tagged tracers were obtained. After the spin-up, several sets of simulations were conducted for 1980-2017 to quantify the methane budget and investigate the impacts of changes in methane sources and sinks on methane abundance (see Section 2.23). All model simulations are forced with interannually-varying sea surface temperatures and sea ice from Taylor et al. (2000), prepared in support of the CMIP6 Atmospheric Model Intercomparison Project (AMIP) simulations. Horizontal winds are nudged to the National Centers for Environmental Prediction (NCEP) reanalysis (Kalnay et al., 1996) using a pressure-dependent nudging technique (Lin et al., 2012).

835 2.2 Observations

We evaluate the simulated methane dry-air mole fraction (DMF) against a suite of ground-based and aircraft observations to thoroughly evaluate the model simulated spatial and temporal distribution of methane. To evaluate surface CH₄, we use measurements from a globally distributed network of air sampling sites maintained by the Global Monitoring Division (GMD) of the Earth System Research Laboratory at the National Oceanic and Atmospheric Administration (NOAA) (Dlugokencky et al., 2018). The global estimates derived from surface measurements are based on a number of sites at remote marine sea level

locations with well-mixed marine boundary layer (MBL) to represent background methane. The locations of MBL sites are shown in Figure S1 and the information for each MBL site is listed in Table S1 in the Supplement. A function fit consisting of yearly harmonics and a polynomial trend, with fast fourier transform and low pass filtering of the residuals are applied to the monthly mean methane DMF to approximate the long-term trend and average seasonal cycle at each MBL site (Thoning et al., 1989; Thoning, 2019). We divide the ~~sine (latitude) at 0.05 interval~~^{1°}s and calculate methane DMF at each latitude band based on the selected sites within that latitude band. A meridional curve (Tans et al., 1989) was fitted through these band values to get the latitudinal distribution of methane. The same sampling and processing approach (Thoning et al., 1989; Tans et al., 1989) is applied to the simulated monthly mean methane DMF to calculate global and zonal averages to facilitate consistent model-observation comparison. Besides ~~the comparison with global estimates from MBL sites~~, we also evaluate the model performance at various individual GMD sites to investigate regional emission representations. For site specific evaluation, we sample the model grid cell at the location of the corresponding site and at the model layer with height closest to the altitude of the corresponding site.

To investigate background tropospheric methane variability, we compare the simulated vertical profiles with aircraft measurements from the High-performance Instrumented Airborne Platform for Environmental Research (HIAPER) Pole-to-Pole observation (HIPPO) campaigns from January 2009 to September 2011 (Wofsy et al., 2012). A total of 787 profiles were flown during the 5 campaigns with continuous profiling between approximately 150 m and 8500 m altitudes, but also including many profiles up to 14 km altitude. For each HIPPO mission, we spatially sample the model consistent with the observations and average the model for the months of the campaign to create climatological monthly means.

2.2.3 Simulation design

We conduct several sets of hindcast simulations for 1980-2017, as listed in Table 2, to quantify the methane budget and investigate the contributions of sources and sinks to the trend and variability of methane. The model simulation using the initial methane emissions inventory (E_{mit}) described in Section 2.1 was found to largely underestimate the methane ~~burden~~^{DMF by 126 ppb} (see Figures S2 and S3 in the Supplement). Assuming that this mismatch is due to a bias in the simulated methane budget, we can either increase methane sources or decrease methane sinks to match the observations. We perform several optimization simulations that explore the sensitivity of methane to uncertainties in emissions of methane and levels of OH, the dominant sink for methane. Because OH trends and variability depend on a number of factors, including temperature, water vapor, O_3 , and emissions of nitrogen oxide (NO_x), carbon monoxide (CO), and volatile organic compounds (VOCs), it is not straightforward to perturb OH. Previous work has shown that interannual variability of global OH is highly correlated with NO_x from lightning (Fiore et al., 2006; Murray et al., 2013). Therefore, we apply ~~a~~^{scaling factors} to lightning NO_x (LNO_x) emissions to indirectly adjust OH levels without influencing its variability. The LNO_x emissions are calculated interactively based on Horowitz et al. (2003) as a function of subgrid convection parameterized in the model. The climatological global mean LNO_x emission simulated by standard AM4.1 is about 3.6 TgN yr^{-1} , within the range of $2\text{-}8 \text{ TgN yr}^{-1}$ estimated by

previous studies (e.g., Schumann and Huntrieser, 2007). We later additionally apply scaling factors (e.g., 0.5 and 2.0) to LNO_x emissions to be at lower and upper limits of the estimated range for sensitivity simulations described below.

875 Here, we test the sensitivity of simulated methane to three assumptions: 1) standard OH levels simulated by AM4.1 (referred as “S0”); 2) low OH levels via applying a scaling factor of 0.5 to the default LNO_x emission calculations (referred as “S1”); 3) high OH levels via applying a factor of 2 to the default LNO_x emission calculation (referred as “S2”). For each OH option, we begin with initial methane emissions and then optimize global total emissions as described below to match simulated methane with surface observations. Different OH levels could lead to different estimations of the optimized total emissions, which provides a measure of uncertainties in our optimized total methane emissions.

880 The estimations of optimized emissions are based on the comparisons of simulated surface methane with NOAA-GMD MBL surface observations. We apply a simple mass balance approach to optimize global total methane emissions, following the methodology of Ghosh et al. (2015). We calculate an increment ΔE by which global emissions need to be modified for each year. Unlike inverse modeling studies ~~such as~~ (Houweling et al., 2017), we do not optimize emissions for each grid cell. 885 Instead, we uniformly scale emissions for particular sectors (as described below) globally for each year by the rate of the optimized emission total ($E_{opt} = E_{init} + \Delta E$) to the initial emissions (E_{init}). We assume that the spatial distribution of methane emissions from the initial emission inventories are the best available information we have. Considering the large uncertainties in the anthropogenic and wetland emissions, we perform two simulations in which we achieve the optimized emission totals by scaling either anthropogenic and biomass burning sources; ~~including biomass burning sector~~ only (referred to as “Aopt”) 890 or the wetland sector only (referred to as “Wopt”) for the standard (S0) LNO_x scenario. The purpose of conducting these simulations is to investigate the impact of optimizing emissions from different sectors on methane predictions. For the Aopt case, eight anthropogenic sectors (i.e., AGR, ENE, IND, TRA, RCO, WST, SHP, and BMB) are uniformly scaled by the ratio of ΔE to total anthropogenic emissions, keeping the fractions of individual sources unchanged. For the Wopt case, wetland emissions are rescaled to increase this source by ΔE . For S1 and S2 scenarios, we apply ΔE to wetland sector only. The total 895 E_{opt} emissions are the same for both Aopt and Wopt cases. Time series of methane optimized total emissions and emissions from major sectors from S0Aopt and S0Wopt over the 1980 to 2017 period are shown in Figure S2_1 in the Supplement.

Based on evidence from $\delta^{13}\text{C}\text{H}_4$, recent studies suggest increasing wetland emissions may be responsible for the renewed growth of methane (Dlugokencky et al., 2009; Nisbet et al., 2016). We perform two additional sensitivity simulations to test the possibility of wetland emissions driving the renewed methane growth during 2006-2014. One simulation is driven by the 900 ~~emissions with repeating 2006 S0Aopt anthropogenic and biomass burning emissions for 2006-2014 but adjusting wetland emissions to ensure that the total methane emissions are the same as in S0Wopt (or S0Aopt), which would imply that the increases in methane emissions are only due to the increases in wetland emissions. This sensitivity simulation is referred to as “S0A06”. Another sensitivity simulation is driven by the emissions combined of a combination of emissions for S0Aopt and S0Wopt as follows: S0Aopt emissions for 1980-2005 and S0Wopt emissions for 2006-2014. This simulation is referred to as “S0Comb”.~~ 905 “S0Comb”.

2.3 Observations

We evaluate the simulated methane dry air mole fraction (DMF) against a suite of ground-based and aircraft observations and satellite retrievals of column-averaged CH_4 to thoroughly evaluate the model-simulated spatial and temporal distribution of methane. To evaluate surface CH_4 , we use measurements from a globally distributed network of air sampling sites maintained by the Global Monitoring Division (GMD) of the Earth System Research Laboratory at the National Oceanic and Atmospheric Administration (NOAA) (Dlugokeneky et al., 2018). The global estimates derived from surface measurements are based on a number of sites at remote marine sea-level locations with well-mixed marine boundary layer (MBL) to represent background methane. The locations of MBL sites are shown in Figure S1 and the information for each MBL site is listed in Table S1 in the Supplement. A function fit consisting of yearly harmonics and a polynomial trend, with fast Fourier transform and low-pass filtering of the residuals are applied to the monthly mean methane DMF to approximate the long-term trend and average seasonal cycle at each MBL site (Thoning et al., 1989; Thoning, 2019). A meridional curve (Tans et al., 1989) was fitted through these site values to get the latitudinal distribution of methane. The same sampling and processing approach (Thoning et al., 1989; Tans et al., 1989) is applied to the simulated monthly mean methane DMF to calculate global and zonal averages to facilitate consistent model-observation comparison. Besides the comparison with global estimates from MBL sites, we also evaluate the model performance at various GMD sites to investigate the contributions from local sources. For site-specific evaluation, we sample the model grid cell at the location of the corresponding site and at the model layer with height closest to the altitude of the corresponding site.

Due to the sparseness of the ground-based observational sites, especially over continental regions, we also evaluate simulated methane against satellite retrievals to reveal information on regional characteristics. Total column-averaged methane DMFs are evaluated against satellite retrievals from the Scanning Imaging Absorption Spectrometer for Atmospheric Chartography (SCIAMACHY) instrument on board the European Space Agency's environmental research satellite ENVISAT (Frankenberg et al., 2011) for January 2003 to April 2012 and the Thermal And Near Infrared Sensor for carbon Observations—Fourier Transform Spectrometer (TANSO-FTS) instrument onboard the Japanese Greenhouse gases Observing SATellite (GOSAT) (Kuze et al., 2016) for April 2009 to December 2016. We compare monthly mean satellite retrievals with simulated monthly mean methane. Retrieval-specific averaging kernels are also applied to simulated monthly mean methane to calculate simulated column-averaged methane DMF.

To investigate background tropospheric methane variability, we compare the simulated vertical profiles with aircraft measurements from the High-performance Instrumented Airborne Platform for Environmental Research (HIAPER) Pole-to-Pole observation (HIPPO) campaigns from January 2009 to September 2011 (Wofsy et al., 2012). A total of 787 profiles were flown during the 5 campaigns with continuous profiling between approximately 150 m and 8500 m altitudes, but also including many profiles up to 14 km altitude. For each HIPPO mission, we spatially sample the model consistent with the observations and average the model for the months of the campaign to create climatological monthly means.

3 Results and discussions

3.1 ~~Observations~~Model evaluation

940 The detailed model evaluation for S0Aopt and S0Wopt are discussed below. We first evaluate the mean climatological spatial distribution and seasonal variability simulated by the model and then evaluate the trends and variability.

3.1.1 Climatological evaluation

Figure 2 shows the model bias and correlation coefficient of simulated climatological mean surface methane DMF against NOAA GMD surface observations (Dlugokencky et al., 2018) for ~~the~~ 1983-2017. The mean seasonal cycle at individual GMD sites is shown in Figure ~~S3-S4~~ in the Supplement. GMD sites with at least 20 years of observational records are selected for model climatological evaluation. The information of these sites is shown in Table S2 in the Supplement. As shown in Figure 2a, simulations with optimization of either anthropogenic (S0Aopt) or wetland (S0Wopt) emissions are generally able to reproduce surface methane DMF with model biases within ± 30 ppb at most sites. Both S0Wopt and S0Aopt simulate methane DMF relatively well over the Southern Hemisphere. Going from south to north, the low bias in methane DMF decreases and becomes a high bias over the tropics. Simulated methane in both S0Aopt and S0Wopt are moderately high biased over the tropical Pacific Ocean (by up to ~ 40 ppb), indicating possible overestimation of methane emissions over the tropics and possible underestimations in tropical OH levels. Large positive biases occur at Key Biscayne (KEY, 25.7 N, 80.2 W) and Mace Head (MHD, 53.3 N, 9.9 W) for both S0Wopt and S0Aopt, likely due to a model sampling bias, with model grid box overlapping land while samples are collected with onshore winds. Over middle and high latitudes of Northern Hemisphere, the simulated surface methane DMF shows low and high biases at individual sites, possibly due in part to uncertainties in the local emissions. As shown in Figure 2b, both S0Aopt and S0Wopt are able to capture the methane seasonal cycle at most sites (with a correlation coefficient (R) larger than 0.5 for about 80% of sites). Both S0Aopt and S0Wopt are able to reproduce the methane seasonal cycle over the Southern Hemisphere. However, both S0Aopt and S0Wopt show poor performance in the seasonal cycle over the Southern tropical Pacific Ocean, with $R < 0.5$ (e.g., POCS10 and POCS15 in Figure ~~S3-S4~~ in the Supplement), but show good performance in the seasonal cycle over the Northern tropical Pacific Ocean, with $R = 0.9$ (e.g., POCN05, POCN10, and POCN15 in Figure ~~S3-S4~~ in the Supplement). Poor performance also exists at a few sites in middle and high northern latitudes (e.g., AZR, UUM, LEF, MHD, and ICE shown in Figure ~~S3-S4~~ in the ~~supplement~~Supplement), mainly due to overestimates of methane during summer. The major differences in simulated methane seasonal cycles between S0Aopt and S0Wopt occur over Northern Hemisphere, with slightly better performance by S0Wopt over Pacific Ocean and by S0Aopt over continental sites (e.g., UUM, WLG, UTA, and NWR). Uncertainties in the seasonality of methane emissions, OH abundances, and long-range transport could lead to biases in the seasonal cycle. In general, both S0Aopt and S0Wopt are able to capture the methane latitudinal gradient (e.g., $R = 0.9$). This suggests that the spatial distribution of methane in emissions is reasonable on the large scale despite uncertainties in representing local sources.

To investigate background tropospheric methane variability, Figure 3 shows the bias in the simulated vertical distribution of methane with respect to HIPPO observations for the S0Aopt and S0Wopt simulations. S0Aopt and S0Wopt simulations produce very similar methane profiles. Both S0Aopt and S0Wopt match observed methane profiles very well over Southern Hemisphere. Compared to HIPPO measurements, methane in both simulations is consistently high over the tropical Pacific Ocean (by up to ~ 50 ppb) from the surface to 700 mb during all HIPPO campaigns. These biases decrease with altitude and decrease with latitude except for summer. In the Northern Hemisphere, both S0Wopt and S0Aopt simulations capture the observed methane from near the surface to 700 mb, but are generally biased low, except in summer when they are biased high, especially at mid-latitudes. Mid-latitude background methane is affected by both high-latitude and low-latitude air masses on synoptic scales. Biases over these regions could result from many processes (e.g., overestimation of the summer emissions, insufficient OH levels, and model transport). In general, the relative differences between the simulated methane profiles and HIPPO measurements are within 2% over most regions, demonstrating the capability of the improved GFDL-AM4.1 for simulating tropospheric methane.

3.1.2 Trend evaluation

As described in Section 2.32, we applied a function fit consisting of yearly harmonics and a polynomial trend, with fast fourier transform and low pass filtering of the residuals to the monthly mean methane DMF (Thoning et al., 1989; Thoning, 2019) to estimate the long-term trend and growth rates discussed below. The comparisons of simulated global mean background surface methane trends and growth rates to NOAA-GMD observations are shown in Figures 4 and 54. Both S0Wopt and S0Aopt predict similar global mean surface methane DMF, trend, and growth rates, since the global methane budget (emissions and sinks) is the same in the two simulations. S0Wopt and S0Aopt are also able to reproduce the global annual mean surface methane DMF (with root-mean-square-error (RMSE) = ~~8.3~~10.4 ppb in S0Wopt and ~~11.68~~9 ppb in S0Aopt) over 1983-2017, which is expected from emission and optimization. Meanwhile, both simulations are able to capture the methane trend very well (with R = 1.0 in both S0Wopt and S0Aopt) over different latitude bands as shown in Figure 4, especially over the Southern Hemisphere. In general, the RMSE for S0Wopt is lower than that for S0Aopt, except over the southern tropics. The major discrepancies in the surface methane DMF between model simulations and observations are mainly over the low northern latitudes (0-30°N), especially the tropics (Figure 4d), where the RMSE is greater than 20 ppb. Over the high northern latitudes, both S0Aopt and S0Wopt reproduce overestimates background methane DMF very well with RMSE less than 10 by about 20-30 ppb during 1984-1998, whereas S0Wopt performs better over this period. After 1998, S0Aopt reproduces the maximum methane DMF very well, while S0Wopt slightly underestimates methane DMF by up to 10 ppb. Over the high southern latitudes, both S0Aopt and S0Wopt underestimate background methane DMF by up to 35 ppb in the 1980s, which could be due in part to the fewer observational sites in the Southern Hemisphere used for emission optimization during this time period. In general, the agreement between the simulated and observed global methane trends increases our confidence in the optimized methane emission trends used in this work.

As shown in Figure 5, both simulations are in general able to reproduce the observed global methane growth rate (with $R = 0.8$ in both S0Wopt and S0Aopt), despite a slight mismatch (-1 year) during 1997-2007. Table 3 summarizes methane growth rates during 1984-1991, 1992-1998, 1999-2006, and 2007-2017. S0Aopt and S0Wopt simulate very similar methane growth rates as their emission totals are the same. During 1984-1991, both S0Aopt and S0Wopt slightly overestimate methane growth rates by ~ 2 ppb yr⁻¹, possibly due to fewer available observations used for emission optimization during this time period than afterwards. After 1991, the simulated methane growth rates are in general comparable to the observations (with annual mean difference within ± 1 ppb yr⁻¹). Global methane simulated by S0Aopt shows rapid growth during 1984-1991 (13.5 ± 2.1 ppb yr⁻¹; annual mean \pm standard deviation), slower growth during 1992-1998 (4.8 ± 2.6 ppb yr⁻¹), a relative stabilization during 1999-2006 (1.2 ± 4.7 ppb yr⁻¹), and renewed growth during 2007-2017 (6.1 ± 2.8 ppb yr⁻¹). The simulated global methane growth rates by S0Wopt show similar trends (13.5 ± 2.1 ppb yr⁻¹ during 1984-1991, 4.7 ± 3.3 ppb yr⁻¹ during 1992-1998, 1.3 ± 4.8 ppb yr⁻¹ during 1999-2006, and 6.1 ± 2.8 ppb yr⁻¹ during 2007-2017). The simulated growth rates during 1984-1991 are slightly higher than the NOAA-GMD estimates (11.6 ± 1.3 ppb yr⁻¹), while the simulated growth rates during 1992-1998, 1999-2006, and 2007-2017 are within the ranges of NOAA-GMD estimates (5.6 ± 3.5 ppb yr⁻¹, 0.7 ± 3.1 ppb yr⁻¹, 6.9 ± 2.6 ppb yr⁻¹, respectively). The major discrepancies in the simulated methane growth rates and observations occur over the tropics and high northern latitudes as shown in Figure 4. Over the tropics, both S0Aopt and S0Wopt overestimate methane growth rates (by about 5-10 ppb yr⁻¹) during 1984-1990 when there were limited observations available, but are able to reproduce methane growth rates relatively well afterwards. Agreement of the methane growth rate is worse in the Northern Hemisphere than in the Southern Hemisphere, especially at the high northern latitudes, where R is smaller than 0.5. Over 30-90°N, mainly due to the large bias during 1984-1988 and a slight shift in peak growth (or peak decrease) during 1997-2005. The number of observational MBL sites does not cover the globe reasonably well, especially in the 1980s, which could have different impacts on the Northern and Southern Hemisphere when optimizing global total emissions. In general, S0Aopt estimates slightly better methane growth rates than S0Wopt, especially over 30-90° N. The biases in methane growth rates also suggest a need to refine regional emissions.

~~neither S0Aopt nor S0Wopt is able to reproduce methane growth rates during 1984-1989 and there is a slight mismatch ($-1-2$ years) in methane growth rates afterwards. These biases indicate larger uncertainties in the methane emissions at high Northern Hemisphere than in other regions.~~

~~S0Aopt and S0Wopt simulate very similar surface methane DMF and their cComparisons of simulated surface methane DMF to with NOAA-GMD observations at individual sites are show both simulations to be biased low over Southern Hemisphere sites, but the low bias decreases northward (shown in Figure S4-S5 in the supplementSupplement). S0Aopt and S0Wopt simulated very similar methane DMF. Both simulations tend to be biased low over Southern Hemisphere sites, but the low bias decreases northward. The simulations are moderately high biased (with RMSEs up to ~ 40 ppb) over tropical regions (e.g., POCS15, POCS10, SMO, POCS05, POCN00, CHR, and POCN05). These sites are mainly remote sites and surface methane DMF represents background methane levels. The overestimations are likely due to an overestimation in the emissions over Southeast Asia (e.g., Saeki and Patra, 2017, Patra et al., 2016, and Thompson et al., 2015), which could affect these remote~~

035 sites through transport. However, the model predicts surface methane DMF relatively well at Ascension Island (ASC, 8°S,
14.4°W, 85 m), which is also a remote site without impacts from East Asia. The high biases over tropics suggest a need to
improve regional emissions (e.g., Southeast Asia). The ASC is at higher altitude than other remote sites. This indicates that
the model tends to overestimate background methane DMF at the surface, but is able to capture background methane at higher
levels. Moderate overestimates also occur at Mahe Island (SEY, 4.7°S, 55.5°E), a location that could be affected by airmasses
040 from polluted areas over the tropics and Northern Hemisphere. Over middle and high latitude Northern Hemisphere, both
S0Aopt and S0Wopt simulate surface methane DMF relatively well at most sites, except at Key Biscayne (KEY, 25.7°N,
80.2°W), Tae-ahn Peninsula (TAP, 36.7°N, 126.1°W), Park Falls (LEF, 45.9°N, 113.7°W), and Mace Head (MHD, 53.3°N,
9.9°W). KEY and MHD are remote sites and sampled under onshore winds, whereas TAP and LEF are affected by local
sources and model transport. The high biases at these sites could be due in part to model sampling bias (e.g., model grid box
045 overlapping land while samples are collected at coast with onshore winds) and uncertainties in local emissions (e.g., possible
overestimation in the emissions over East Asia). On the other hand, both S0Wopt and S0Aopt are able to capture monthly
variations in methane at most of the sites except at LEF, where R = 0.4 for S0Wopt and 0.5 for S0Aopt, respectively. In general,
both S0Wopt and S0Aopt are able to reproduce the surface methane DMF and capture the trend at most sites (e.g., with R
greater than 0.5 at 98% of total sites and with RMSE less than 30 ppb at 74% of total sites). As shown in Figure S5, S0Aopt
050 in general estimates better methane trends and growth over low latitudes of the Southern Hemisphere (e.g., SMO) and
middle/high latitudes of the Northern Hemisphere (e.g., ASK, KEY, WIS, UTA, NWR, UUA, LEF, CBA, STM, and ALT)
than S0Wopt. Based on the site-level comparisons between S0Wopt and S0Aopt, the anthropogenic emissions over Southeast
Asia are likely overestimated in both S0Aopt and S0Wopt, while they could be underestimated at WLG and NWR sites in
S0Wopt but be reasonably well represented in S0Aopt.

055 ~~Unlike the evaluation of global mean surface methane DMF, which is based on observations from a number of sites with well-~~
~~mixed MBLs, the evaluation of global mean column-averaged methane DMF against satellite retrievals mainly covers~~
~~continents, considering the impacts from polluted areas and the contributions from the troposphere and the stratosphere.~~
~~Simulated monthly mean column-averaged methane DMF are compared with satellite retrievals (e.g., SCIAMACHY and~~
~~GOSAT) in Figure 6. The averaging kernels of SCIAMACHY and GOSAT are individually applied to the model to calculate~~
060 ~~column-averaged methane abundances. Both simulations are able to capture the monthly variation of methane with R greater~~
~~than 0.9, but underestimate column-averaged methane, with RMSE of about 21 ppb and 29 ppb when compared to~~
~~SCIAMACHY and GOSAT retrievals, respectively. The biases increase poleward in both SCIAMACHY and GOSAT~~
~~comparisons; large uncertainty exists in the satellite retrievals over high latitudes (e.g., >70°) due to large solar zenith angles~~
~~and potential high cloud cover. The underestimates are mainly due to biases in the middle/upper troposphere and stratosphere~~
065 ~~(as shown in Figure 3). The differences in the column-averaged methane abundances between satellite retrievals and model~~
~~simulations are mostly within 2% except in polar regions where there are large uncertainties in the satellite retrievals. Both~~
~~simulations are also able to capture the latitudinal distribution of the column-averaged methane DMF with R close to 1.~~

3.2 Global methane budget

Figure 7-5 shows time series of optimized total emissions, global sink, and global burden of methane based on S0Wopt.

070 Since global totals in S0Aopt and S0Wopt simulations are very close to each other, we only show the budget for S0Wopt. As depicted in Figure 7-5, the simulated global methane burden steadily increases from 1980 to 1992, with a growth rate of 39 Tg yr⁻¹. During 1993-1998, the global methane burden growth slows down with a growth rate of 16 Tg yr⁻¹. ~~The growth rates simulated by the model agrees well with the observed growth rates during 1984-1997 as shown in Figure 5a.~~ The simulated growth rate in global methane burden decreases to 4 Tg yr⁻¹ during 1999-2006 while it increases to 16 Tg yr⁻¹ during 2007-2017 and reaches over 20 Tg yr⁻¹ during 2014-2016. The changes in the global burdens are due to the imbalance between methane sources and sinks. As shown in Figure 7-5, the optimized emissions in general increase during 1980-2017, with an annual mean of 576±32 Tg yr⁻¹ (mean±standard deviation) and show much larger interannual variability during 1991-1993 and 1997-2000. ~~The larger interannual variabilities during 1991-1993 and 1997-2000, which are is likely due to the strong El Niño events during 1991-1992 and 1997-1998 as well as Mt Pinatubo eruption in 1991 (Dlugokencky et al., 1996; Bousquet et al., 2006b; Bândă et al., 2016).~~ Although there is an overall increasing trend in total global emissions, growth in annual mean emissions has increased from the 1980s (with an annual emission growth rate of 3.9 Tg yr⁻¹) to the 1990s (4.4 Tg yr⁻¹), but decreased to 0.3 Tg yr⁻¹ during 2000-2006, and increased again to 2.3 Tg yr⁻¹ during 2007-2017. ~~The estimations of optimized emissions are based on the comparisons of simulated surface methane with surface observations. The interannual variability of the optimized emissions is mainly resulted~~ mainly results from the interannual variability of simulated OH levels during emission optimization. Uncertainties in the interannual variability of simulated OH levels and therefore methane sinks could lead to uncertainties in the interannual variability of the optimized emissions. ~~The larger interannual variabilities during 1991-1993 and 1997-2000 are likely due to the strong El Niño events during 1991-1992 and 1997-1998.~~ Unlike methane emissions, the methane sink increases during 1980-2007, with relative stabilization during 2008-2014 but a resumed increase during 2015-2017. The annual mean methane sink during 1980-2017 is 560±44 Tg yr⁻¹ (mean±standard deviation). The trends in methane sink are affected by the changes in both methane and OH levels (assuming that other sinks are minor). Figure 8-6 shows the tropospheric OH anomalies with respect to 1998-2007. An interesting finding is that AM4.1 predicts higher OH levels during 2008-2014 than 1998-2007 by 3.1%, whereas ~~recent~~ previous studies applying multispecies inversion with a box-model framework (e.g., Rigby et al., 2017; Turner et al., 2017) suggest a decline in OH levels after 2007. However, a recent study by Naus et al. (~~2018~~ 2019) found a shift to positive OH trend over 1994-2015 after applying bias corrections based on a 3-D ~~CTM~~ chemical transport model to a similar box model setup. In addition, OH levels simulated by AM4.1 decrease from 2013 to 2015 but increase again afterwards, leading to an increase in methane sinks during 2015-2017. As shown in Figure 7-5, higher methane sources than sinks during 1980-1998 lead to an increase in methane burden. A relative balance between methane sources and sinks during 1999-2006 leads to the methane stabilization. Compared to 1999-2006, both methane sources and sinks are higher during 2007-2017, but methane sources outweigh sinks after 2007 leading to renewed methane growth.

Table 3-4 provides a summary of decadal mean methane budget for 1980-2017. Compared to Kirschke et al. (2013) and Saunio et al. (2016, 2019), the total natural sources from the initial emission inventories (203 Tg yr^{-1}) are at the lower range of top-down estimates during this period, except for the 1990s, when they are slightly higher than top-down estimates but still much lower than the bottom-up estimates. ~~This mainly results from wetland emissions in the initial emission inventories that are slightly higher than top-down estimates but much lower than bottom-up estimates during 1990s. Since there is no observational constraint on bottom-up estimates, the total natural emissions are simply summed over independent individual sources, which could be overestimated in the bottom-up approach considering the uncertainties in each individual source. In addition, in the bottom-up estimate from Kirschke et al. (2013) and Saunio et al. (2019), some other natural sources, such as freshwater, are not included in the initial emission inventories in this work; however, they are likely double counted in the bottom-up estimates. The natural sources estimated in this work (e.g., $203\text{-}297 \text{ Tg yr}^{-1}$) are much comparable to previous top-down estimates (e.g., $150\text{-}273 \text{ Tg yr}^{-1}$), [VN5] which demonstrates the confidence in the natural source estimates.~~

The total anthropogenic sources from the initial emission inventories are overall within the range of top-down or bottom-up estimates, except for 1980-1989, when they are lower than the estimates in Kirschke et al. (2013) and Saunio et al. (2016). The low values in the 1980s result mainly from low estimated sources from agriculture and waste sectors in the CEDS inventory. With the optimized global total emissions, the total sources used in this work and the total sinks estimated by AM4.1 are either in the range of top-down or bottom-up estimates by previous studies. As a result, the imbalance between total sources and total sinks estimated in this work are overall within the range of estimates by previous studies although we find a smaller imbalance than previous estimates for the 2000s and afterwards. The atmospheric growth rates simulated by the model (sampled identically as for observations) are also comparable to the observed atmospheric growth rates.

3.3 ~~Source tagged tracers~~ **Sensitivity to sector optimization**

3.3.1 Spatial distribution

~~As described in Section 2.2, the emission optimization is conducted for anthropogenic sectors (i.e., $S0A_{opt}$) and wetland sector (i.e., $S0W_{opt}$). Although global total methane emissions are the same for $S0A_{opt}$ and $S0W_{opt}$, they have different allocations for anthropogenic and wetland sectors and different spatial distributions as well. Here we analyze the sensitivity of sector optimization on the spatial distribution of simulated methane concentrations. Figures 9 and 10 show the spatial distributions of the differences in the methane emissions and surface methane abundance between $S0A_{opt}$ and $S0W_{opt}$ during the four periods (i.e., 1980-1989, 1990-1999, 2000-2006, and 2007-2017). Surface methane is always lower in A_{opt} than W_{opt} in the tropics (e.g., 15°S - 10°N) during the four periods. This is mainly due to much lower wetland emissions in $S0A_{opt}$ than in $S0W_{opt}$ (Figure 10), which dominates total emissions over these regions (e.g., tropical South America and Central Africa). There is not much difference in surface methane over low and high southern latitudes (e.g., 15°S - 90°S) between the two simulations. This agreement is mainly because larger anthropogenic emissions in $S0A_{opt}$ compensate smaller wetland emissions, producing only small differences in the total emissions, within 0.1 Tg yr^{-1} (Figure 10). Unlike the Southern~~

Hemisphere, surface methane concentrations are in general higher in S0Aopt than S0Wopt in the Northern Hemisphere, especially over the Eastern U.S. and Eurasia, due to much higher anthropogenic emissions in S0Aopt. The lower surface methane values in S0Aopt over northern Canada are due to much lower wetland emissions in S0Aopt.

Figure 11 shows the methane growth rates simulated by Aopt and Wopt during the four time periods. Global mean methane growth rates simulated by Aopt and Wopt are very consistent during the four periods, with growth rates decreasing from 1980s to 1990s, stabilizing during 2000–2006, and increasing after 2007. During the 1980s and 1990s, methane growth rates in both S0Aopt and S0Wopt increase over most of the globe except a decrease over Russia, due to significant decreases in anthropogenic emissions (mainly from the energy sector) in the former Soviet Union, consistent with previous studies (Dlugokenky et al., 2011). During 2000–2006, methane growth rates increase significantly over East Asia in both S0Aopt and S0Wopt while they decrease over tropical South America and Central Africa in S0Wopt but not in Aopt. This is mainly due to decreases in wetland emissions in the S0Wopt case, while wetland emissions are constant for each year in Aopt case. After 2007, both Aopt and Wopt suggest large increases in methane growth rates over East Asia (mainly due to increases in anthropogenic emissions) by up to ~ 38 ppb yr⁻¹ with smaller increases elsewhere (< 7 ppb yr⁻¹), with noticeable increases also over the Arctic (> 7 ppb yr⁻¹). The relatively large methane growth over the Arctic is mainly due to increases in anthropogenic methane from lower latitudes.

As discussed in Sections 3.1 and 3.2, the similarity in S0Aopt and S0Wopt simulation results suggests that for 3-dimensional chemistry transport models, reasonable estimates of total global methane emissions are critical for global methane predictions, despite the uncertainties in the spatial distribution of the emissions and in the estimates of individual sources, which are more important for regional methane predictions. At the same time, accurate estimates of individual sources are necessary to attribute the methane trend and variability into individual sources.

3.3.2 Source tagged tracers

In this section, we apply Mann Kendall (M-K) test to estimate the linear trend (different from long term trend discussed in Section 3.1.2) of global mean source tagged tracers and total methane for 1983–1998, 1999–2006, and 2007–2017 to investigate possible drivers in total methane trends. Figure 12 compares the trends of source tagged tracers and total methane from S0Aopt and S0Wopt during 1983–1998, 1999–2006, and 2007–2017. As shown in Figure 12, both S0Aopt and S0Wopt are in general able to capture the methane trends during different time periods. For S0Aopt, globally, total methane shows an increasing trend of 10.5 ppb yr⁻¹ during 1983–1998, slightly greater than observations (8.8 ppb yr⁻¹), but correlated very well with the observations ($R = 1.0$). The tagged anthropogenic tracers all show increasing trends during 1983–1998 despite the increases in OH levels, with larger increasing trends by AGR (3.6 ppb yr⁻¹) and WST (3.6 ppb yr⁻¹) consistent with emission trends. Major anthropogenic tracers (e.g., CH4AGR, CH4ENE, and CH4WST) correlate very well with total methane, with R varying between 0.9 to 1.0 over this time period. Since wetland emissions and other natural emissions are constant every year in S0Aopt, with the increases in OH levels during 1983–1998, both CH4WET and CH4ONA decrease by 0.5 ppb yr⁻¹ and 0.1 ppb yr⁻¹, respectively, over this period. During 1999–2006, total methane has a small increasing trend of 1.3 ppb yr⁻¹, still

slightly greater than observations (0.6 ppb yr^{-1}), but correlated relatively well with the observations ($R=0.8$). During this time period, there are increasing trends in CH4ENE (2.6 ppb yr^{-1}) and CH4WST (2.3 ppb yr^{-1}) with slightly decreasing trends in CH4AGR (-0.1 ppb yr^{-1}), CH4BMB (-0.9 ppb yr^{-1}) and CH4OAT (-0.5 ppb yr^{-1}). Anthropogenic tracers such as CH4ENE and CH4WST correlate well with total methane, whereas CH4AGR shows a poor correlation with total methane, and CH4BMB and CH4OAT show an anticorrelation with total methane over this time period. Similarly, with the increases in OH levels during 1999–2006, both CH4WET and CH4ONA decrease, with a linear decreasing trend of -1.8 ppb yr^{-1} and -0.4 ppb yr^{-1} . During 2007–2017, total methane shows a renewed increasing trend of 5.3 ppb yr^{-1} , slightly below observations (6.0 ppb yr^{-1}) but correlated relatively well with the observations ($R=1.0$). During this time, CH4ENE shows a large increasing trend (5.8 ppb yr^{-1}), dominating the total methane trend. Interestingly, although there is a slight decrease in OH levels after 2008, with both CH4WET and CH4ONA still show decreasing trends of -1.1 ppb yr^{-1} and -0.3 ppb yr^{-1} during 2007–2017. Also, all the natural tracers show an anticorrelation with total methane during this period. The results from S0Aopt suggest that globally, anthropogenic tracers dominate total methane trends during the entire simulation period. During the 1980s and 1990s, emissions from agriculture, energy, and waste sectors are the major contributors to the methane increase. During 1999–2006, where methane stabilizes, increases in methane sinks and methane sources alternatively dominate the trend for different tracers and therefore the imbalance between methane sinks and sources dominate the total methane trend. During 2007–2017, the energy sector is the major contributor to the methane renewed growth.

The source tagged tracers behave slightly different in S0Wopt. For S0Wopt, globally, total methane shows a similar increasing trend as S0Aopt (as discussed in section 3.1.2). The tagged anthropogenic tracers all show increasing trends during 1983–1998 except CH4ENE (-0.3 ppb yr^{-1}). Anthropogenic tracers (except CH4OAT) in general correlate well with total methane. CH4WET show a significant increasing trend during this period (7.0 ppb yr^{-1}) and correlate relatively well with total methane. During 1999–2006, anthropogenic tracers such as CH4ENE and CH4WST show increasing trends (1.8 ppb yr^{-1} and 1.9 ppb yr^{-1} , respectively) and correlate relatively well with total methane ($R=0.7$ and 0.8 , respectively), whereas all other tracers show decreasing trends and are anticorrelated with total methane. During this time, our wetland tracer (CH4WET) shows a slightly decreasing trend (-0.6 ppb yr^{-1}), mainly due to the slightly higher CH4WET sinks (226 Tg yr^{-1}) than sources (223 Tg yr^{-1}). During 2007–2017, anthropogenic tracers such as CH4AGR, CH4ENE, and CH4WST show significant increasing trends (2.3 ppb yr^{-1} , 6.9 ppb yr^{-1} , and 1.6 ppb yr^{-1} , respectively) and correlate quite well with total methane ($R=1.0$) whereas all other tracers except CH4OAT show decreasing trends and poor correlations with total methane. On the other hand, CH4WET shows a significant decreasing trend during this period (-4.6 ppb yr^{-1}) and an anticorrelation with total methane. The decreasing trend of CH4WET is due to higher CH4WET sinks (217 Tg yr^{-1}) than sources (206 Tg yr^{-1}) during this period. During 1983–1998, wetland emission growth is larger than anthropogenic emission growth due to emission optimization in S0Wopt, leading to the dominance of wetland to drive global methane growth. During 1999–2006, when methane stabilizes, increases in methane emissions from energy and waste sectors dominate the increases in total methane sources as well as their tagged tracers (i.e., CH4ENE and CH4WST), whereas increases in methane sinks dominate all other tracers. Therefore, the imbalance between

total methane sinks and sources dominate the total methane trend, which is also the case in S0Aopt during this time period.

200 During 2007-2017, the energy is the major contributor to the renewed methane growth similar to that in S0Aopt.

In this section, we apply Mann-Kendall (M-K) test to estimate the linear trend (different from long-term trend discussed in Section 3.1.2) of global mean source tagged tracers and total methane for 1983-1998, 1999-2006, and 2007-2017 to investigate possible drivers of total methane trends. Figure 7 compares the trends of source tagged tracers and total methane from S0Aopt and S0Wopt during each time period and Table 5 summarizes the estimated linear trend for each time period along with the

205 dominating tracers. For S0Aopt, total methane shows a strong increasing trend of 10.5 ppb yr⁻¹. The tagged anthropogenic tracers all show increasing trends during 1983-1998 despite the increases in OH levels, with dominant increasing trends by CH4AGR and CH4WST consistent with emission trends. Since wetland emissions and other natural emissions are kept constant every year in S0Aopt, with the increases in OH levels during 1983-1998, all tagged natural tracers show a weak decreasing trend. During 1999-2006, total methane shows a small increasing trend of 1.0 ppb yr⁻¹, due to the increasing trends

210 of CH4ENE and CH4WST compensated by the decreasing trends of other source tagged tracers. The increasing trends of CH4ENE and CH4WST are mainly driven by the increases in the emissions in S0Aopt whereas the decreasing trends of other source tagged tracers are mainly determined by the increases in OH levels. During 2007-2017, total methane shows a renewed increasing trend of 5.3 ppb yr⁻¹, dominated by a strong increasing trend of CH4ENE and smaller increasing trends of CH4AGR and CH4WST. The results from S0Aopt suggest that globally, anthropogenic tracers dominate total methane trends during the

215 entire simulation period. During the 1980s and 1990s, emissions from agriculture, energy, and waste sectors are the major contributors to the methane increase. During 1999-2006, when methane stabilizes, increases in methane sinks and methane sources alternatively dominate the trend for different tracers. During 2007-2017, emissions from agriculture, energy and waste sectors are the major contributors to the methane-renewed growth in methane, with energy sector as the largest contributor.

220 The source tagged tracers behave slightly differently in S0Wopt. For S0Wopt, total methane shows a similar increasing trend as S0Aopt. During 1983-1998, the tagged anthropogenic tracers all show increasing trends except CH4ENE, with overall smaller increasing trends than those in S0Aopt. CH4WET shows a strong increasing trend (7.0 ppb yr⁻¹), dominating the total methane trend. This is mainly because wetland emission growth is larger than anthropogenic emission growth due to the emission optimization in S0Wopt during this period. During 1999-2006, similar to S0Aopt, total methane trend is resulted

225 from the increasing trends of CH4ENE and CH4WST compensated by the decreasing trends of other source tagged tracers. During this time period, CH4WET shows a slightly decreasing trend (-0.8 ppb yr⁻¹), mainly due to the slightly higher CH4WET sinks (226 Tg yr⁻¹) than sources (223 Tg yr⁻¹). During 2007-2017, the total methane trend is dominated by the increasing trends of CH4AGR, CH4ENE, and CH4WST, with CH4ENE as the largest contributor, similar to S0Aopt. On the other hand, CH4WET shows a significant decreasing trend during this period, mainly due to higher CH4WET sinks (217 Tg yr⁻¹) than

230 sources (206 Tg yr⁻¹). Compared to the S0Aopt results, S0Wopt suggest CH4WET as the largest contributor for the methane trends during 1980s and 1990s, mainly due to the emission optimization of different sectors. However, both scenarios suggest CH4AGR, CH4WST, and CH4ENE are the major contributors to the renewed growth, with CH4ENE as the largest contributor.

As shown in Figures 7-5 and 86, OH levels ~~show a slight~~slightly decrease and methane sinks are relatively stable during 2007-2013, but large interannual variability exists during 2013-2017. Decreasing OH levels could lead to increases in methane lifetime and therefore methane build-up. Combined with increases in the emissions, methane starts to increase again during this period. However, it is difficult to separate the contributions from methane emissions and sinks as optimized methane emissions are based on methane mass balance (e.g., changes in the methane loss would act as a feedback on estimates of optimized total emissions). ~~However~~Nevertheless, it is clear that the decrease in OH levels alone (e.g., if emissions are kept constant) would not be enough to reproduce the renewed growth. The remaining question then is which emission sector(s) is (are) the major contributor(s) to the renewed growth over 2007 to 2017. Both S0Wopt and S0Aopt suggest that agriculture, waste and energy sectors ~~is the major sector contributing~~are the major contributors to renewed methane growth. However, both cases depend largely on the initial emission inventory. For example, S0Wopt relies on the emission growth of other sectors from the initial emission inventory, which means if the emission growth of a certain sector is overestimated or underestimated in the initial emission inventory, it would ~~give a different result~~lead to different results. Therefore, we conducted two additional sensitivity simulations (i.e., S0A06 and S0Comb as described in Section 2.3) with different emission growths for anthropogenic and wetland sectors as in S0Aopt and S0Wopt for 2006-2014. Based on evidence from isotopic composition ($\delta^{13}\text{C}_{\text{CH}_4}$), recent studies suggest increasing wetland emissions may be responsible for the renewed growth of methane (Dlugokencky et al., 2009; Nisbet et al., 2016). To test this hypothesis in our modeling framework, we conducted another sensitivity simulation for 2006-2014, by repeating 2006 anthropogenic emissions for all the years but adjusting wetland emissions to ensure that the total methane emissions are the same as in S0Wopt (or S0Aopt), which would imply that the increases in methane emissions are only due to the increases in wetland emissions. This sensitivity simulation is referred to as “S0A06” and the trends for source tagged tracers and total methane by S0A06 and S0Comb are shown in Figure S5 in the supplement4 and Table 5. Interestingly, in S0A06, where anthropogenic and biomass burning emissions are kept constant every year for 2006-2014, anthropogenic tracers still show an increasing trends during 2007-2014, with the dominating increasing trends in by CH4ENE and CH4WST dominating (trend = 3.6 ppb yr⁻¹ and R = 1.0), whereas CH4WET shows a small decreasing trend (trend = -1.0 ppb yr⁻¹ and R = -0.8) despite rising emissions. As OH levels slightly decrease during this time period, with constant emissions except wetland, one might expect possible increasing trends in all tagged tracers except CH4WET. In fact, major anthropogenic tracers such as CH4AGR, CH4ENE, CH4WST, and CH4BMB increase over 2007-2014 in S0A06, but at a slower rate than in S0Wopt (and S0Aopt) due to no emission growth for these tracers. On the other hand, the decreasing OH levels (Figure 8) would lead to less methane sink and therefore higher methane concentrations. Since methane loss is proportional to the product of OH levels and methane concentrations and concentrations of CH4WET are much greater than other source tagged tracers, the loss of CH4WET is also much higher than other tracers. Higher CH4WET loss (224 Tg yr⁻¹) than CH4WET sources (207 Tg yr⁻¹) leads to a decreasing trend in CH4WET. Nevertheless, S0A06 results still suggest that the renewed growth during 2007-2014 is dominated by the increases of CH4ENE and CH4WST, which The results means suggest OH trends play an important role in determining the increasing trend of total methane since emissions of the energy and waste sectors are kept constant in this sensitivity simulation. In addition, increases

in wetland emissions alone are not able to drive increases in CH₄WET over this period, as CH₄WET sinks are equally important for determining the trend in CH₄WET under constant anthropogenic emissions condition. Our analysis also suggests that increases in other microbial sources (e.g., agriculture and waste) would be needed to match the observed negative trend in $\delta^{13}\text{CH}_4$ since 2007 (Nisbet et al., 2019).

~~We perform an additional sensitivity simulation to test the possibility of wetland emissions driving the methane trend during the period of renewed methane growth by combining the emissions of S0Aopt and S0Wopt as follows: S0Aopt emissions for 1980-2005 and S0Wopt emissions for 2006-2014. This simulation is referred to as “S0Comb”; the trends for source tagged tracers and total methane are shown in Figure S6 in the supplement.~~ ~~During 2007-2014, all anthropogenic tracers show decreasing trends except CH₄ENE (2.7-8 ppb yr⁻¹), whereas CH₄WET shows a significant increasing trend (6-35.9 ppb yr⁻¹) and dominates the total methane trend. This is mainly due to lower anthropogenic emissions during this period than previous periods, allowing sinks of anthropogenic methane tracers to start to take over their trends except for CH₄ENE. At the same time, significantly higher wetland emissions during this period than previous periods dominate the increasing trend of CH₄WET. Interestingly, even with the same wetland emissions in S0Wopt and S0Comb for 2006-2014, CH₄WET shows different trends. This is mainly because the CH₄WET concentrations at the beginning of 2006 are much lower in S0Comb than in S0Wopt. Therefore, CH₄WET loss is much lower in S0Comb (190 Tg yr⁻¹) compared to S0Wopt (220 Tg yr⁻¹) over this time period, leading to an increasing CH₄WET trend in S0Comb, but a decreasing trend in S0Wopt. S0Comb results suggest the need for a significant increase in wetland emissions along with decreases in anthropogenic emissions starting in 2006, compared to the stabilization period, for wetland emissions to drive renewed growth in methane. However, this is a less likely scenario as both top-down and bottom-up inventories indicate anthropogenic emissions increasing over 2007-2014. A more likely scenario is that both anthropogenic and wetland emissions increase (i.e., higher during 2007-2014 than 1999-2006). However, in that case, the dominance of wetland emissions in driving the total methane trend would decrease based on our analysis.~~

3.4 Sensitivity to OH levels

As described in Section 2.23, we perform two additional simulations for low and high OH levels (i.e., S1 and S2) for 1980-2017 to investigate the sensitivity of methane predictions to different OH levels. For both OH cases, the interannual variations in OH levels are the same as in S0 because the simulations are driven by the same meteorology. Figures 138(a) and (b) show global tropospheric OH concentrations, methane OH loss, and methane tropospheric lifetime for the three cases (i.e., S0, S1, and S2) in which wetland emissions are optimized (Wopt; Aopt shows a very similar global OH trend as Wopt). Compared to S0, scaling LNO_x production in the model by a factor of 0.5 leads to a reduction in simulated annual global mean OH levels by -6.4 % in S1 over 1980-2017; scaling by a factor of 2 leads to an increase in simulated annual global mean OH by +9.1% in S2-. The global mean OH levels increase from 1980 to 2008 (by 3.6%, with respect to 1980 level), ~~with a linear rate of increase of $4.1 \times 10^3 \text{ molecule cm}^{-3} \text{ yr}^{-1}$, a decrease from 2008 to 2015 (by 2.3%, with respect to 2008 level) with a mean rate~~

300 of $7.1 \times 10^3 \text{ molecule cm}^{-3} \text{ yr}^{-1}$, and an increase from 2015 to 2017 (by 4.6%, with respect to 2015 level) ~~with a mean rate of~~
 ~~$3.2 \times 10^4 \text{ molecule cm}^{-3} \text{ yr}^{-1}$~~ . However, compared to the 1998-2007, OH levels during 2008-2015 and 2015-2017 are still higher
by 2.5% and 1.3%, respectively. Changes in OH levels depend on a number of factors (e.g., temperature, water vapor, O₃,
NO_x, CO, and VOCs). Therefore, OH is influenced by the specific chemistry and forcing data used in the model. Since emission
optimization is also based on methane sinks, the total optimized emissions in S1 are lower than those in S0 by about 4.1%
305 (with an annual mean of ~~-23.724~~ Tg yr⁻¹), and the total optimized emissions in S2 are higher than those in S0 by about 5.8%
(or ~~33.433~~ Tg yr⁻¹). This indicates that a 1% change in OH levels could lead to about 4 Tg yr⁻¹ difference in the optimized
emissions. Increasing methane loss due to OH is simulated for 1980 to 2007 in the three cases due to increases in OH and
methane concentrations (except over the stabilization period when methane was not increasing but OH was increasing). During
2007-2013, the simulated decrease in OH levels combined with increasing methane concentrations leads to relative
310 stabilization in methane OH loss in the three cases. The large interannual variability in OH levels during 2013-2017 dominates
the interannual variability in methane OH loss despite the continued increases in methane.

All three simulations show a similar trend for tropospheric methane lifetime, with a ~~linear decreasing trend~~ from 1980 to 2007
(-0.04 year yr⁻¹ in S0, -0.05 year yr⁻¹ in S1, and -0.03 year yr⁻¹ in S2), a clear increasing trend during 2011-2015 (0.08 year yr⁻¹
in all three simulations), and a decreasing trend during 2015-2017 (-0.2 year yr⁻¹ in all three simulations). The mean
315 tropospheric methane lifetime due to OH loss for 1980-2017 is 9.9 ± 0.4 years in S0Wopt, which is about 0.5 year lower than
S1Wopt (10.4 ± 0.5 years), and about 0.7 year higher than S2Wopt (9.2 ± 0.3 years), due to different OH levels and therefore
methane sinks, but with similar methane burdens. This indicates that a 1% change in OH levels could lead to about 0.08 year
difference in the tropospheric methane lifetime. The mean tropospheric methane lifetimes simulated by the three simulations
~~are is~~ within the uncertainty range of observation-derived estimates for the 2000s (Prather et al., 2012) and model estimates
320 (Voulgarakis et al., 2013; Naik et al., 2013). All simulations show an increase in methane lifetime during 2011-2015, which
could be a signal of the methane feedback on its lifetime (Holmes, 2018) in the model. Continued increases in methane
emissions (Figure 75) during this time period, along with decreases in tropospheric OH concentrations (Figure 138), lengthen
the lifetime of methane and therefore amplify the methane's response to emission changes. If methane emissions continue to
increase, we can expect stronger increases in atmospheric methane due to the amplifying effect of the methane-OH feedback
325 as occurred during in the significant increases in methane growth rates during 2014 and 2015.

4 Conclusions

In this work, we thoroughly evaluate the atmospheric methane budget simulated by the GFDL-AM4.1 and apply the model to
quantify investigate the drivers of changes in global methane over the past four decades. We simulate the DMF of methane
and related tracers for 1980 ~~to~~ 2017 by driving the model with gridded emissions compiled from various sources. In order to
330 match the long-term record of surface methane measurements, we optimize global total methane emissions using a simple
mass-balance approach. Our optimized global total methane emissions are within the range of estimates by previous studies

(both bottom-up and top-down). The GFDL-AM4.1 simulations with emissions following two different optimizations (anthropogenic and wetlands) both reproduce observed global methane trends and variabilities, despite the different contributions from anthropogenic and wetland emissions. This, therefore, suggests that the accurate estimates of global total emissions and of the interannual variability in emissions are critical in predicting the global methane trend and its variability, despite uncertainties in the estimates of individual sources. reproduce observed methane growth rates for the different time periods (e.g., 9.4 ppb yr⁻¹ during 1984-1998, 1.1 ppb yr⁻¹ during 1999-2006, and 6.1 ppb yr⁻¹ during 2007-2017). The simulations In addition, both simulations are in general ~~also~~ able to capture the spatial distribution and seasonal cycle of methane as ~~retrieved by satellites~~ observed by NOAA GMD sites and vertical distribution of methane as measured from aircraft, demonstrating the reasonable spatial and temporal representations of the optimized emissions derived in this work - Both simulations also reproduce observed global methane trends and variabilities, despite the different contributions from anthropogenic and wetland emissions. This therefore suggests that the accurate estimates of global total emissions and of the interannual/seasonal variability in emissions are critical in predicting the global methane trend and its variability, despite uncertainties in the estimates of individual sources.

We then explore the causes of methane trends and variability over 1980-2017 to sources and sinks. The simulation with optimization of anthropogenic emissions shows anthropogenic emissions to be the major contributors to the rapid methane growth during 1980s and 1990s, whereas the simulation with optimization of wetland emissions also shows wetlands to be one of the major contributors during these periods. However, both simulations suggest increases in methane sources (mainly from agriculture, energy and waste sectors), balanced by the increases in methane sinks (mainly due to increases in OH levels), lead to methane stabilization during 1999-2006, and that the agriculture, energy, and waste sectors is/are the major contributors to the renewed growth of methane after 2006, with the largest contribution by energy sector.

Two additional sensitivity simulations further investigate the contributions of wetlands to the methane renewed growth during 2007-2014. The simulation with repeating 2006 emissions for all the sectors except wetland shows a declining contribution of wetland tracer to total methane abundance despite of the increasing contribution of wetland emissions to total emissions, because sinks are equally important for determining the tracer trend. Results from a simulation with combined optimizations (i.e., 1980-2005 optimized anthropogenic emissions and 2006-2014 optimized wetland emissions) suggest that a sharp increase in wetland emissions (a likely scenario) with concomitant sharp decrease in anthropogenic emissions (a less likely scenario), would be required starting in 2006 to drive the methane growth by wetland tracer.

Two additional sensitivity simulations further investigate the contributions of wetlands to the methane renewed growth during 2007-2014. The simulation with repeating 2006 emissions for all the sectors except wetland suggests increases in wetland emissions alone are not able to explain the renewed methane growth because sinks are equally important for determining the trend under constant anthropogenic emissions. Results from a simulation with combined optimizations (i.e., 1980-2005 optimized anthropogenic emissions and 2006-2014 optimized wetland emissions) suggest that a significant increase in wetland emissions along with decreases in anthropogenic emissions starting in 2006 compared to the stabilization period (1999-2006) is required for wetland emissions to drive renewed growth in methane, which is a less likely scenario.

Two additional sensitivity simulations, with low and high OH levels (by scaling LNO_x production in the model by a factor of 0.5 and 2), further investigate methane OH loss and tropospheric lifetime. In general, OH trends dominate methane OH loss trends during different methane growth periods except 2007-2013, when methane OH loss shows little change due to the decrease in OH levels combined with the increase in methane concentrations. The results also indicate that a 1% change in OH levels could lead to about 4 Tg yr⁻¹ difference in the optimized emissions and 0.08 year difference in the estimated tropospheric methane lifetime. The increasing methane lifetime during 2011-2015 in all the OH sensitivity simulations indicate a possible methane feedback on its lifetime in the model. Continued increases in methane emissions along with decreases in tropospheric OH concentrations extend the lifetime of methane and therefore amplify methane's response to emission changes.

Essentially, the global atmospheric methane trend is driven by the competition between its emissions and sinks. Emissions dominate sinks leading to an increasing trend while sinks dominate emissions leading to a decreasing trend. Our model results suggest that the methane stabilization during 1999-2006 is mainly due to increasing emissions balanced by increasing sinks, whereas the methane renewed growth during 2007-2013 is mainly due to increasing sources combined with little change in sinks despite small decreases in OH levels. The significant increases in methane growth during 2014-2015 are mainly due to increasing sources combined with decreasing sinks. Most of the model simulations conducted here suggest that increases in energy sources drive the renewed methane growth, in agreement with previous studies (e.g., Rice et al., 2016; Hausmann et al., 2016; Worden et al., 2017), with second largest contributor from waste sector and third largest contributor from agriculture sector, consistent with the shift in the ratio $\delta^{13}\text{CH}_4$, but in disagreement with other studies that consider emissions from microbial sources as the major contributor (e.g., Nisbet et al., 2016; Schaefer et al., 2016). However, optimization of emissions from anthropogenic sources depends on the "shares" of individual anthropogenic sectors in the initial emission inventories. Uncertainties in these shares could lead to uncertainties in the emission adjustment for each anthropogenic sector. Recent studies using methane isotopic composition suggest that renewed growth in methane is more likely due to the increases in biogenic sources (e.g., Schaefer et al., 2016) as the ratio $\delta^{13}\text{CH}_4\delta^{13}\text{C}$ is shifting to more negative values since 2007. However, it also implies increases in isotopically lighter fossil fuel emissions, or decreases in isotopically heavy sources (e.g., biomass burning), or increases in both microbial and fossil fuel emissions but with increases in microbial emissions stronger than those from fossil fuel sources (Nisbet et al., 2019). It is quite possible that, rather than the energy sector, the increases in the agriculture and waste sectors may drive the renewed methane growth. In that case, it is possible that the growth of agriculture and waste emissions could be underestimated in the optimized emissions, while the growth of energy emissions could be overestimated.

The optimized emission totals estimated in this work represent temporal and spatial distribution of methane total sources reasonably well. However, the emission adjustments are either applied to anthropogenic sectors only or wetland sector only. Uncertainties therefore exist on the distribution of the emission adjustments to individual sectors. Without accurate estimates of emissions from individual sources, it would be difficult to attribute the methane trend and variability to specific sectors. The application of methane isotopes and additional observational constraints (e.g., ethane and $\delta^{13}\text{CH}_4$) could potentially help better partition the emission adjustments to different sectors. In addition, the spatial distribution of optimized emissions depends on

400 the spatial information in the initial emission inventories. Uncertainties in the spatial distribution from the initial emission inventories may remain in the optimized emissions. Our model evaluation suggests that the optimized inventory may overestimate tropical emissions. A process-based emission model (e.g., wetland emissions) coupled with AM4.1 may better represent the spatial and temporal patterns of the emissions than ~~was possible~~prescribed in the present work.

Author contribution

405 Jian He and Vaishali Naik designed the research. Jian He developed the model configuration, performed model simulations, analyzed model results, and prepared the manuscript with contributions from all co-authors. Vaishali Naik provided GFDL-model ready CMIP6 emissions. Larry Horowitz provided meteorological data for nudging. Ed Dlugokencky provided surface observations. Kirk Thoning provided scripts to process observational data. All authors contributed to the discussion of results.

Acknowledgements

410 This work is supported by the Carbon Mitigation Initiative at Princeton University. Atmospheric methane dry air mole fractions are obtained from the NOAA ESRL Carbon Cycle Cooperative Global Air Sampling Network (Dlugokencky et al., 2018, ftp://aftp.cmdl.noaa.gov/data/trace_gases/ch4/flask/surface/). The globally averaged marine surface monthly mean data and annual mean growth rates are obtained from www.esrl.noaa.gov/gmd/ccgg/trends_ch4/. HIPPO data is obtained from Wofsy et al. (2012), Merged 10-second Meteorology, Atmospheric Chemistry, Aerosol Data (R_20121129). ~~Satellite data is obtained~~
415 ~~from <http://www.temis.nl/climate/methane.html>~~. We are grateful to Prabir Patra for providing methane emissions for nearshore exchange and mud volcanoes. We also thank Fabien Paulot for processing sea surface temperatures and sea ice data and the GFDL model development team for developing the AM4.1.

References

- 420 [Bândă, N., Krol, M., van Weele, M., van Noije, T., Le Sager, P., and Röckmann, T.: Can we explain the observed methane variability after the Mount Pinatubo eruption?, Atmos. Chem. Phys., 16, 195–214, <https://doi.org/10.5194/acp-16-195-2016>, 2016.](#)
- Bloom, A. A., Bowman, K. W., Lee, M., Turner, A. J., Schroeder, R., Worden, J. R., Weidner, R., McDonald, K. C., and Jacob, D. J.: A global wetland methane emissions and uncertainty dataset for atmospheric chemical transport models (WetCHARTs version 1.0), Geosci. Model Dev., 10, 2141-2156, <https://doi.org/10.5194/gmd-10-2141-2017>, 2017.
- 425 Bousquet, P., Ciais, P., Miller, J. B., Dlugokencky, E. J., Hauglustaine, D. A., Prigent, C., van der Werf, G. R., Peylin, P., Brunke, E.-G., Carouge, C., Langenfelds, R. L., Lathiere, J., Papa, F., Ramonet, M., Schmidt, M., Steele, L. P., Tyler, S. C.,

- and White, J.: Contribution of anthropogenic and natural sources to atmospheric methane variability, *Nature*, 443, 439–443, doi:10.1038/nature05132, 2006a.
- 430 [Bousquet, P., Ciais, P., Miller, J. B., Dlugokencky, E. J., Hauglustaine, D. A., Prigent, C., Van der Werf, G. R., Peylin, P., Brunke, E. G., Carouge, C., Langenfelds, R. L., Lathiere, J., Papa, F., Ramonet, M., Schmidt, M., Steele, L. P., Tyler, S. C., and White, J.: Contribution of anthropogenic and natural sources to atmospheric methane variability, *Nature*, 443, 439–443, 2006b.](#)
- Bousquet, P., Ringeval, B., Pison, I., Dlugokencky, E. J., Brunke, E.- G., Carouge, C., Chevallier, F., Fortems-Cheiney, A., Frankenberg, C., Hauglustaine, D. A., Krummel, P. B., Langenfelds, R. L., Ramonet, M., Schmidt, M., Steele, L. P., Szopa, 435 S., Yver, C., Viovy, N., and Ciais, P.: Source attribution of the changes in atmospheric methane for 2006–2008, *Atmos. Chem. Phys.*, 11, 3689–3700, doi:10.5194/acp-11-3689-2011, 2011.
- Brasseur, G. P., Hauglustaine, D. A., Walters, S., Rasch, P. J., Muller, J. F., Granier, C., and Tie, X. X.: MOZART, a global chemical transport model for ozone and related chemical tracers, 1. Model description, *J. Geophys. Res. A.*, 103(D21), 28 265–28 289, 1998.
- 440 Dalsøren, S. B., Myhre, C. L., Myhre, G., Gomez-Pelaez, A. J., Søvde, O. A., Isaksen, I. S. A., Weiss, R. F., and Harth, C. M.: Atmospheric methane evolution the last 40 years, *Atmos. Chem. Phys.*, 16, 3099–3126, <https://doi.org/10.5194/acp16-3099-2016>, 2016.
- Dentener, F., Kinne, S., Bond, T., Boucher, O., Cofala, J., Generoso, S., Ginoux, P., Gong, S., Hoelzemann, J. J., Ito, A., Marelli, L., Penner, J. E., Putaud, J.-P., Textor, C., Schulz, M., van der Werf, G. R., and Wilson, J.: Emissions of primary 445 aerosol and precursor gases in the years 2000 and 1750 prescribed data-sets for AeroCom, *Atmos. Chem. Phys.*, 6, 4321–4344, doi:10.5194/acp-6-4321-2006, 2006.
- [Dlugokencky, E. J., Dutton, E. G., Novelli, P. C., and Masarie, K. A.: Changes in CH₄ and CO growth rates after the eruption of Mt. Pinatubo and their link with changes in tropical tropospheric UV flux, *Geophys. Res. Lett.*, 23, 2761–2764, 1996.](#)
- Dlugokencky, E. J., Houweling, S., Bruhwiler, L., Masarie, K., Lang, P., Miller, J., and Tans, P.: Atmospheric methane levels 450 off: Temporary pause or a new steady-state?, *Geophys. Res. Lett.*, 30, 19, doi:10.1029/2003GL018126, 2003.
- Dlugokencky, E. J., Myers, R., Lang, P., Masarie, K., Crotwell, A., Thoning, K., Hall, B., Elkins, J., and Steele, L.: Conversion of NOAA atmospheric dry air CH₄ mole fractions to a gravimetrically prepared standard scale, *J. Geophys. Res.*, 110, D18306, doi:10.1029/2005JD006035, 2005.
- Dlugokencky, E. J., Bruhwiler, L., White, J. W. C., Emmons, L. K., Novelli, P. C., Montzka, S. A., Masarie, K. A., Lang, P. 455 M., Crotwell, A. M., Miller, J. B., and Gatti, L. V.: Observational constraints on recent increases in the atmospheric CH₄ burden, *Geophys. Res. Lett.*, 36, L18803, 10.1029/2009GL039780, 2009.
- Dlugokencky, E. J., Nisbet, E. G., Fisher, R., and Lowry, D.: Global atmospheric methane: budget, changes and dangers, *Philos. T. R. Soc. A*, 369, 2058–2072, 2011.

- Dlugokencky, E. J., Lang, P. M., Crotwell, A. M., Mund, J. W., Crotwell, M. J., and Thoning, K. W.: Atmospheric Methane
1460 Dry Air Mole Fractions from the NOAA ESRL Carbon Cycle Cooperative Global Air Sampling Network, 1983-2017, Version:
2018-08-01, Path: ftp://aftp.cmdl.noaa.gov/data/trace_gases/ch4/flask/surface/, 2018.
- Donner, L. J., Wyman, B. L., Hemler, R. S., Horowitz, L. W., Ming, Y., Zhao, M., Golaz, J.-C., Ginoux, P., Lin, S.-J.,
Schwarzkopf, M. D., Austin, J., Alaka, G., Cooke, W. F., Delworth, T. L., Freidenreich, S. M., Gordon, C. T., Griffies, S. M.,
Held, I. M., Hurlin, W. J., Klein, S. A., Knutson, T. R., Langenhorst, A. R., Lee, H.-C., Lin, Y., Magi, B. I., Malyshev, S. L.,
1465 Milly, P. C. D., Naik, V., Nath, M. J., Pincus, R., Ploshay, J. J., Ramaswamy, V., Seman, C. J., Shevliakova, E., Sirutis, J. J.,
Stern, W. F., Stouffer, R. J., Wilson, R. J., Winton, M., Wittenberg, A. T., and Zeng, F.: The Dynamical Core, Physical
Parameterizations, and Basic Simulation Characteristics of the Atmospheric Component AM3 of the GFDL Global Coupled
Model CM3, *J. Clim.*, 24, 3484– 3519, doi:10.1175/2011JCLI3955.1, 2011.
- Etheridge, D. M., Steele, L. P., Francy, R. J., and Langenfelds, R. L.: Atmospheric methane between 1000 A. D. and present:
1470 Evidence of anthropogenic emissions and climatic variability, *J. Geophys. Res.*, 103, 15 979–15 993, 1998.
- Etioppe, G. and Milkov, A. V.: A new estimate of global methane flux from onshore and shallow submarine mud volcanoes to
the atmosphere, *Environ. Geol.*, 46, 997–1002, doi:10.1007/s00254-004-1085-1, 2004.
- Fiore, A. M., Dentener, F. J., Wild, O., Cuvelier, C., Schultz, M. G., Hess, P., Textor, C., Schulz, M., Doherty, R. M., Horowitz,
L. W., MacKenzie, I. A., Sanderson, M. G., Shindell, D. T., Stevenson, D. S., Szopa, S., van Dingenen, R., Zeng, G., Atherton,
1475 C. S., Bergmann, D. J., Bey, I., Carmichael, G. R., Collins, W. J., Duncan, B. N., Faluvegi, G., Folberth, G. A., Gauss, M.,
Gong, S., Hauglustaine, D., Holloway, T., Isaksen, I. S. A., Jacob, D. J., Jonson, J. E., Kaminski, J. W., Keating, T. J., Lupu,
A., Marmer, E., Montanaro, V., Park, R. J., Pitari, G., Pringle, K. J., Pyle, J. A., Schroeder, S., Vivanco, M. G., Wind, P.,
Wojcik, G., Wu, S., and Zuber, A.: Multimodel estimates of intercontinental source-receptor relationships for ozone pollution,
J. Geophys. Res., 114, D04301, doi:10.1029/2008JD010816, 2009.
- 1480 Fiore, A. M., Horowitz, L. W., Dlugokencky, E. J., and West, J. J.: Impact of meteorology and emissions on methane trends,
1990–2004, *Geophys. Res. Lett.*, 33, L12809, doi:10.1029/2006GL026199, 2006.
- Fiore, A. M., Jacob, D. J., Field, B. D., Streets, D. G., Fernandes, S. D., and Jang, C.: Linking ozone pollution and climate
change: The case for controlling methane, *Geophys. Res. Lett.* 29(19), 1919, doi:10.1029/2002GL015601, 2002.
- ~~Frankenberg, C., Fisher, J. B., Worden, J., Badgley, G., Saatchi, S. S., Lee, J. E., Toon, G. C., Butz, A., Jung, M., Kuze, A.,
1485 and Yokota, T.: New global observations of the terrestrial carbon cycle from GOSAT: patterns of plant fluorescence with gross
primary productivity, *Geophys. Res. Lett.*, 38, 1–6, doi:10.1029/2011GL048738, 2011.~~
- Fung, I., John, J., Lerner, J., Matthews, E., Prather, M., Steele, L. P., and Fraser, P. J.: Three-dimensional model synthesis of
the global methane cycle, *J. Geophys. Res.*, 96, 13033–13065, 1991.
- Ghosh, A., Patra, P. K., Ishijima, K., Umezawa, T., Ito, A., Etheridge, D. M., Sugawara, S., Kawamura, K., Miller, J. B.,
1490 Dlugokencky, E. J., Krummel, P. B., Fraser, P. J., Steele, L. P., Langenfelds, R. L., Trudinger, C. M., White, J. W. C., Vaughn,
B., Saeki, T., Aoki, S., and Nakazawa, T.: Variations in global methane sources and sinks during 1910–2010, *Atmos. Chem.
Phys.*, 15, 2595-2612, <https://doi.org/10.5194/acp-15-2595-2015>, 2015.

- Gidden, M. J., Riahi, K., Smith, S. J., Fujimori, S., Luderer, G., Kriegler, E., van Vuuren, D. P., van den Berg, M., Feng, L., Klein, D., Calvin, K., Doelman, J. C., Frank, S., Fricko, O., Harmsen, M., Hasegawa, T., Havlik, P., Hilaire, J., Hoesly, R., Horing, J., Popp, A., Stehfest, E., and Takahashi, K.: Global emissions pathways under different socioeconomic scenarios for use in CMIP6: a dataset of harmonized emissions trajectories through the end of the century, *Geosci. Model Dev. Discuss.*, <https://doi.org/10.5194/gmd-2018-266>, in review, 2018.
- Gromov, S., Brenninkmeijer, C. A. M., and Jöckel, P.: A very limited role of tropospheric chlorine as a sink of the greenhouse gas methane, *Atmos. Chem. Phys.*, 18, 9831-9843, <https://doi.org/10.5194/acp-18-9831-2018>, 2018.
- Guenther, A., Karl, T., Harley, P., Wiedinmyer, C., Palmer, P. I., and Geron, C.: Estimates of global terrestrial isoprene emissions using MEGAN (Model of Emissions of Gases and Aerosols from Nature), *Atmos. Chem. Phys.*, 6, 3181-3210, <https://doi.org/10.5194/acp-6-3181-2006>, 2006.
- Hausmann, P., Sussmann, R., and Smale, D.: Contribution of oil and natural gas production to renewed increase in atmospheric methane (2007-2014): top-down estimate from ethane and methane column observations, *Atmos. Chem. Phys.*, 16, 3227-3244, <https://doi.org/10.5194/acp-16-3227-2016>, 2016.
- Hess, P. G., Flocke, S., Lamarque, J.-F., Barth, M. C., and Madronich, S.: Episodic modeling of the chemical structure of the troposphere as revealed during the spring MLOPEX intensive, *J. Geophys. Res.*, 105(D22), 26 809-26 839, 2000.
- Hoesly, R. M., Smith, S. J., Feng, L., Klimont, Z., Janssens-Maenhout, G., Pitkanen, T., Seibert, J. J., Vu, L., Andres, R. J., Bolt, R. M., Bond, T. C., Dawidowski, L., Kholod, N., Kurokawa, J.-I., Li, M., Liu, L., Lu, Z., Moura, M. C. P., O'Rourke, P. R., and Zhang, Q.: Historical (1750-2014) anthropogenic emissions of reactive gases and aerosols from the Community Emissions Data System (CEDS), *Geosci. Model Dev.*, 11, 369-408, <https://doi.org/10.5194/gmd-11-369-2018>, 2018.
- Holmes, C. D.: Methane Feedback on Atmospheric Chemistry: Methods, models, and mechanisms, *Journal of Advances in Modeling Earth Systems*, 10, 1087-1099, <https://doi.org/10.1002/2017MS001196>, 2018.
- Horowitz, L. W., Walters, S., Mauzerall, D. L., Emmons, L. K., Rasch, P. J., Granier, C., Tie, X., Lamarque, J.-F., Schultz, M. G., Tyndall, G. S., Orlando, J. J., and Brasseur, G. P.: A global simulation of tropospheric ozone and related tracers: Description and evaluation of MOZART, version 2, *J. Geophys. Res.-Atmos.*, 108, doi:10.1029/2002JD002853, 2003.
- Houweling, S., Bergamaschi, P., Chevallier, F., Heimann, M., Kaminski, T., Krol, M., Michalak, A. M., and Patra, P.: Global inverse modeling of CH₄ sources and sinks: an overview of methods, *Atmos. Chem. Phys.*, 17, 235-256, <https://doi.org/10.5194/acp-17-235-2017>, 2017.
- Houweling, S., Krol, M., Bergamaschi, P., Frankenberg, C., Dlugokencky, E. J., Morino, I., Notholt, J., Sherlock, V., Wunch, D., Beck, V., Gerbig, C., Chen, H., Kort, E. A., Röckmann, T., and Aben, I.: A multi-year methane inversion using SCIAMACHY, accounting for systematic errors using TCCON measurements, *Atmos. Chem. Phys.*, 14, 3991-4012, <https://doi.org/10.5194/acp-14-3991-2014>, 2014.
- Kai, F. M., Tyler, S. C., Randerson, J. T., and Blake, D. R.: Reduced methane growth rate explained by decreased Northern Hemisphere microbial sources, *Nature*, 476, 194-197, 2011.

- Kaylnay, E., Kanamitsu, M., Kistler, R., Collins, W., Deaven, D., Gandin, L., Iredell, M., Saha, S., White, G., Woollen, J., Zhu, Y., Chelliah, M., Ebisuzaki, W., Higgins, W., Janowiak, J., Mo, K. C., Ropelewski, C., Wang, J., Leetmaa, A., Reynolds, R., Jenne, R., and Joseph, D.: The NCEP/NCAR 40-year reanalysis project, *Bull. Amer. Meteorol. Soc.* 77: 437-471, [https://doi.org/10.1175/1520-0477\(1996\)077<0437:TNYRP>2.0.CO;2](https://doi.org/10.1175/1520-0477(1996)077<0437:TNYRP>2.0.CO;2), 1996.
- 530 Kirschke, S., Bousquet, P., Ciais, P., Saunio, M., Canadell, J. G., Dlugokencky, E. J., Bergamaschi, P., Bergmann, D., Blake, D. R., Bruhwiler, L., Cameron-Smith, P., Castaldi, S., Chevallier, F., Feng, L., Fraser, A., Heimann, M., Hodson, E. L., Houweling, S., Josse, B., Fraser, P. J., Krummel, P. B., Lamarque, J.-F., Langenfelds, R. L., Le Quere, C., Naik, V., O'Doherty, S., Palmer, P. I., Pison, I., Plummer, D., Poulter, B., Prinn, R. G., Rigby, M., Ringeval, B., Santini, M., Schmidt, M., Shindell, D. T., Simpson, I. J., Spahni, R., Steele, L. P., Strode, S. A., Sudo, K., Szopa, S., van der Werf, G. R., Voulgarakis, A., van
- 1535 Weele, M., Weiss, R. F., Williams, J. E., and Zeng, G.: Three decades of global methane sources and sinks, *Nat. Geosci.*, 6, 813-823, doi:10.1038/ngeo1955, 2013.
- ~~Kuze, A., Suto, H., Shiomi, K., Kawakami, S., Tanaka, M., Ueda, Y., Deguchi, A., Yoshida, J., Yamamoto, Y., Kataoka, F., Taylor, T. E., and Buijs, H. L.: Update on GOSAT TANSO-FTS performance, operations, and data products after more than 6 years in space, *Atmos. Meas. Tech.*, 9, 2445-2461, doi:10.5194/amt-9-2445-2016, 2016.~~
- 540 Lambert, G. and Schmidt, S.: Reevaluation of the oceanic flux of methane: uncertainties and long term variations, *Chemosph. Global Change Sci.*, 26, 579–589, doi:10.1016/0045-6535(93)90443-9, 1993.
- Levin, I., Veidt, C., Vaughn, B. H., Brailsford, G., Bromley, T., Lowe, R. H. D., Miller, J. B., Poß, C., and White, J. W. C.: No inter-hemispheric $\delta^{13}\text{C}_{\text{CH}_4}$ trend observed, *Nature*, 486, E3–E4, doi:10.1038/nature11175, 2012.
- Lin, M., Fiore, A. M., Horowitz, L. W., Cooper, O. R., Naik, V., Holloway, J., Johnson, B. J., Middlebrook, A. M., Oltmans,
- 1545 S. J., Pollack, I. B., Ryerson, T. B., Warner, J. X., Wiedinmyer, C., Wilson, J., and Wyman, B.: Transport of Asian ozone pollution into surface air over the western United States in spring, *J. Geophys. Res.-Atmos.*, 117, D00V07, doi:10.1029/2011JD016961, 2012.
- ~~Maasackers, J. D., Jacob, D. J., Sulprizio, M. P., Scarpelli, T. R., Nesser, H., Sheng, J.-X., Zhang, Y., Hersher, M., Bloom, A. A., Bowman, K. W., Worden, J. R., Janssens-Maenhout, G., and Parker, R. J.: Global distribution of methane emissions, emission trends, and OH concentrations and trends inferred from an inversion of GOSAT satellite data for 2010–2015, *Atmos. Chem. Phys.*, 19, 7859–7881, <https://doi.org/10.5194/acp-19-7859-2019>, 2019.~~
- 550 Mao, J., Fan, S., Jacob, D. J., and Travis, K. R.: Radical loss in the atmosphere from Cu-Fe redox coupling in aerosols, *Atmos. Chem. Phys.*, 13, 509–519, doi:10.5194/acp-13-509-2013, 2013a.
- Mao, J., Horowitz, L. W., Naik, V., Fan, S., Liu, J., and Fiore, A. M.: Sensitivity of tropospheric oxidants to biomass burning emissions: implications for radiative forcing, *Geophys. Res. Lett.*, 40, 1241–1246, doi:10.1002/grl.50210, 2013b.
- 1555 Monteil, G., Houweling, S., Dlugokencky, E. J., Maenhout, G., Vaughn, B. H., White, J. W. C., and Rockmann, T.: Interpreting methane variations in the past two decades using measurements of CH_4 mixing ratio and isotopic composition, *Atmos. Chem. Phys.*, 11, 9141–9153, doi:10.5194/acp-11-9141-2011, 2011.

- Montzka, S. A., Krol, M., Dlugokencky, E., Hall, B., Jockel, P., and Lelieveld, J.: Small interannual variability of global atmospheric hydroxyl, *Science*, 331, 67–69, doi:10.1126/science.1197640, 2011.
- Murray, L. T., Logan, J. A., and Jacob, D. J.: Interannual variability in tropical tropospheric ozone and OH: the role of lightning, *J. Geophys. Res.*, 118, 1-13, doi:10.1002/jgrd.50857, 2013.
- Myhre, G., Shindell, D., Bréon, F.-M., Collins, W. Fuglestedt, J., Huang, J., Koch, D. Lamarque, J.-F., Lee, D., Mendoza, B., Nakajima, T., Robock, A., Stephens, G. Takemura, T., and Zhang, H.: Anthropogenic and natural radiative forcing, in: *Climate Change 2013: The Physical Science Basis, Fifth Assessment Report of the Intergovernmental Panel on Climate Change*, edited by: Stocker, T. F. et al., Cambridge University Press, Cambridge, UK, New York, NY, USA, 659–740, 2013.
- Naik, V., Horowitz, L. W., Fiore, A. M., Ginoux, P., Mao, J., Aghedo, A. M., and Levy, H.: Impact of preindustrial to presentday changes in short-lived pollutant emissions on atmospheric composition and climate forcing, *J. Geophys. Res.-Atmos.*, 118, 8086–8110, doi:10.1002/jgrd.50608, 2013a.
- Naik, V., Voulgarakis, A., Fiore, A. M., Horowitz, L. W., Lamarque, J.-F., Lin, M., Prather, M. J., Young, P. J., Bergmann, D., Cameron-Smith, P. J., Cionni, I., Collins, W. J., Dalsøren, S. B., Doherty, R., Eyring, V., Faluvegi, G., Folberth, G. A., Josse, B., Lee, Y. H., MacKenzie, I. A., Nagashima, T., van Noije, T. P. C., Plummer, D. A., Righi, M., Rumbold, S. T., Skeie, R., Shindell, D. T., Stevenson, D. S., Strode, S., Sudo, K., Szopa, S., and Zeng, G.: Preindustrial to present-day changes in tropospheric hydroxyl radical and methane lifetime from the Atmospheric Chemistry and Climate Model Intercomparison Project (ACCMIP), *Atmos. Chem. Phys.*, 13, 5277–5298, doi:10.5194/acp-13-5277-2013, 2013b.
- [Naus, S., Montzka, S. A., Pandey, S., Basu, S., Dlugokencky, E. J., and Krol, M.: Constraints and biases in a tropospheric two-box model of OH, *Atmos. Chem. Phys.*, 19, 407–424, https://doi.org/10.5194/acp-19-407-2019, 2019.](https://doi.org/10.5194/acp-19-407-2019)
- Nisbet, E. G., Dlugokencky, E. J., and Bousquet, P.: Methane on the Rise – Again, *Science*, 343, 493–495, doi:10.1126/science.1247828, 2014.
- Nisbet, E. G., Manning, M. R., Dlugokencky, E. J., Fisher, R. E., Lowry, D., Michel, S. E., Myhre, C. Lund, Platt, S. M., Allen, G., Bousquet, P., Brownlow, R., Cain, M., France, J. L., Hermansen, O., Hossaini, R., Jones, A. E., Levin, I., Manning, A. C., Myhre, G., Pyle, J. A., Vaughn, B., Warwick, N. J., White, J. W. C.: Very strong atmospheric methane growth in the four years 2014-2017: Implications for the Paris Agreement, *Global Biogeochem. Cy.*, <https://doi.org/10.1029/2018GB006009>, 2019.
- Nisbet, E. G., Dlugokencky, E. J., Manning, M. R., Lowry, D., Fisher, R. E., France, J. L., Michel, S. E., Miller, J. B., White, J. W. C., Vaughn, B., Bousquet, P., Pyle, J. A., Warwick, N. J., Cain, M., Brownlow, R., Zazzeri, G., Lanoisellé, M., Manning, A. C., Gloor, E., Worthy, D. E. J., Brunke, E.-G., Labuschagne, C., Wolff, E. W., and Ganesan, A. L.: Rising atmospheric methane: 2007–2014 growth and isotopic shift, *Global Biogeochem. Cy.*, 30, 1356–1370, <https://doi.org/10.1002/2016GB005406>, 2016.
- Patra, P. K., Houweling, S., Krol, M., Bousquet, P., Belikov, D., Bergmann, D., Bian, H., Cameron-Smith, P., Chipperfield, M. P., Corbin, K., Fortems-Cheiney, A., Fraser, A., Gloor, E., Hess, P., Ito, A., Kawa, S. R., Law, R. M., Loh, Z., Maksyutov, S., Meng, L., Palmer, P. I., Prinn, R. G., Rigby, M., Saito, R., and Wilson, C.: TransCom model simulations of CH_4 and CH_4 and

- related species: linking transport, surface flux and chemical loss with CH₄-variability in the troposphere and lower stratosphere, *Atmos. Chem. Phys.*, 11, 12813-12837, <https://doi.org/10.5194/acp-11-12813-2011>, 2011.
- 595 [Patra, P. K., Saeki, T., Dlugokencky, E. J., Ishijima, K., Umezawa, T., Ito, A., Aoki, S., Morimoto, S., Kort, E. A., Crotwell, A., Ravi Kumar, K., and Nakazawa, T.: Regional Methane Emission Estimation Based on Observed Atmospheric Concentrations \(2002–2012\), *J. Met. Soc. Jap.*, 94, 91–112, doi:10.2151/jmsj.2016-006, 2016.](#)
- Paulot, F., Ginoux, P., Cooke, W. F., Donner, L. J., Fan, S., Lin, M.-Y., Mao, J., Naik, V., and Horowitz, L. W.: Sensitivity of nitrate aerosols to ammonia emissions and to nitrate chemistry: implications for present and future nitrate optical depth, *Atmos. Chem. Phys.*, 16, 1459-1477, <https://doi.org/10.5194/acp-16-1459-2016>, 2016.
- 600 Prather, M. J., Holmes, C. D., and Hsu, J.: Reactive greenhouse gas scenarios: Systematic exploration of uncertainties and the role of atmospheric chemistry, *Geophys. Res. Lett.*, 39, L09803, doi:10.1029/2012gl051440, 2012.
- Rice, A. L., Butenhoff, C. L., Teama, D. G., Röger, F. H., Khalil, M. A. K., and Rasmussen, R. A.: Atmospheric methane isotopic record favors fossil sources flat in 1980s and 1990s with recent increase, *Proceedings of the National Academy of Sciences*, 113, 10791-10796, 10.1073/pnas.1522923113, 2016.
- 605 Rigby, M., Prinn, R. G., Fraser, P. J., Simmonds, P. G., Langenfelds, R. L., Huang, J., Cunnold, D. M., Steele, L. P., Krummel, P. B., Weiss, R. F., O'Doherty, S., Salameh, P. K., Wang, H. J., Harth, C. M., Mühle, J., and Porter, L. W.: Renewed growth of atmospheric methane, *Geophys. Res. Lett.*, 35, L22805, doi:10.1029/2008GL036037, 2008.
- Rigby, M., Manning, A. J., and Prinn, R. G.: The value of high frequency, high-precision methane isotopologue measurements for source and sink estimation, *J. Geophys. Res.-Atmos.*, 117, D12312, doi:10.1029/2011jd017384, 2012
- 610 Rigby, M., Montzka, S. A., Prinn, R. G., White, J. W. C., Young, D., O'Doherty, S., Lunt, M. F., Ganesan, A. L., Manning, A. J., Simmonds, P. G., Salameh, P. K., Harth, C. M., Mühle, J., Weiss, R. F., Fraser, P. J., Steele, L. P., Krummel, P. B., McCulloch, A., and Park, S.: Role of atmospheric oxidation in recent methane growth, *P. Natl. Acad. Sci.*, 114, 5373–5377, <https://doi.org/10.1073/pnas.1616426114>, 2017.
- 615 [Saeki, T., and Patra, P. K.: Implications of overestimated anthropogenic CO₂ emissions on East Asian and global land CO₂ flux inversion, *Geoscience Letters*, 4:9, <https://doi.org/10.1186/s40562-017-0074-7>, 2017.](#)
- Saunois, M., Bousquet, P., Poulter, B., Peregón, A., Ciais, P., Canadell, J. G., Dlugokencky, E. J., Etiope, G., Bastviken, D., Houweling, S., Janssens-Maenhout, G., Tubiello, F. N., Castaldi, S., Jackson, R. B., Alexe, M., Arora, V. K., Beerling, D. J., Bergamaschi, P., Blake, D. R., Brailsford, G., Brovkin, V., Bruhwiler, L., Crevoisier, C., Crill, P., Covey, K., Curry, C., Frankenberg, C., Gedney, N., Höglund-Isaksson, L., Ishizawa, M., Ito, A., Joos, F., Kim, H.-S., Kleinen, T., Krummel, P., Lamarque, J.-F., Langenfelds, R., Locatelli, R., Machida, T., Maksyutov, S., McDonald, K. C., Marshall, J., Melton, J. R., Morino, I., Naik, V., O'Doherty, S., Parmentier, F.-J. W., Patra, P. K., Peng, C., Peng, S., Peters, G. P., Pison, I., Prigent, C., Prinn, R., Ramonet, M., Riley, W. J., Saito, M., Santini, M., Schroeder, R., Simpson, I. J., Spahni, R., Steele, P., Takizawa, A., Thornton, B. F., Tian, H., Tohjima, Y., Viovy, N., Voulgarakis, A., van Weele, M., van der Werf, G. R., Weiss, R., Wiedinmyer, C., Wilton, D. J., Wiltshire, A., Worthy, D., Wunch, D., Xu, X., Yoshida, Y., Zhang, B., Zhang, Z., and Zhu, Q.: The global methane budget 2000–2012, *Earth Syst. Sci. Data*, 8, 697-751, <https://doi.org/10.5194/essd-8-697-2016>, 2016.

- 630 [Saunois, M., Bousquet, P., Poulter, B., Peregón, A., Ciais, P., Canadell, J. G., Dlugokencky, E. J., Etiope, G., Bastviken, D., Houweling, S., Janssens-Maenhout, G., Tubiello, F. N., Castaldi, S., Jackson, R. B., Alexe, M., Arora, V. K., Beerling, D. J., Bergamaschi, P., Blake, D. R., Brailsford, G., Bruhwiler, L., Crevoisier, C., Crill, P., Covey, K., Frankenberg, C., Gedney, N., Höglund-Isaksson, L., Ishizawa, M., Ito, A., Joos, F., Kim, H.-S., Kleinen, T., Krummel, P., Lamarque, J.-F., Langenfelds, R., Locatelli, R., Machida, T., Maksyutov, S., Melton, J. R., Morino, I., Naik, V., O'Doherty, S., Parmentier, F.-J. W., Patra, P. K., Peng, C., Peng, S., Peters, G. P., Pison, I., Prinn, R., Ramonet, M., Riley, W. J., Saito, M., Santini, M., Schroeder, R., Simpson, I. J., Spahni, R., Takizawa, A., Thornton, B. F., Tian, H., Tohjima, Y., Viovy, N., Voulgarakis, A., Weiss, R., Wilton, D. J., Wiltshire, A., Worthy, D., Wunch, D., Xu, X., Yoshida, Y., Zhang, B., Zhang, Z., and Zhu, Q.: Variability and quasi-](#)
- 635 [decadal changes in the methane budget over the period 2000–2012, *Atmos. Chem. Phys.*, 17, 11135–11161, <https://doi.org/10.5194/acp-17-11135-2017>, 2017.](#)
- 640 [Saunois, M., Stavert, A. R., Poulter, B., Bousquet, P., Canadell, J. G., Jackson, R. B., Raymond, P. A., Dlugokencky, E. J., Houweling, S., Patra, P. K., Ciais, P., Arora, V. K., Bastviken, D., Bergamaschi, P., Blake, D. R., Brailsford, G., Bruhwiler, L., Carlson, K. M., Carrol, M., Castaldi, S., Chandra, N., Crevoisier, C., Crill, P. M., Covey, K., Curry, C. L., Etiope, G., Frankenberg, C., Gedney, N., Hegglin, M. I., Höglund-Isakson, L., Hugelius, G., Ishizawa, M., Ito, A., Janssens-Maenhout, G., Jensen, K. M., Joos, F., Kleinen, T., Krummel, P. B., Langenfelds, R. L., Laruelle, G. G., Liu, L., Machida, T., Maksyutov, S., McDonald, K. C., McNorton, J., Miller, P. A., Melton, J. R., Morino, I., Müller, J., Murgia-Flores, F., Naik, V., Niwa, Y., Noce, S., O'Doherty, S., Parker, R. J., Peng, C., Peng, S., Peters, G. P., Prigent, C., Prinn, R., Ramonet, M., Regnier, P., Riley, W. J., Rosentreter, J. A., Segers, A., Simpson, I. J., Shi, H., Smith, S. J., Steele, P. L., Thornton, B. F., Tian, H., Tohjima, Y.,](#)
- 645 [Tubiello, F. N., Tsuruta, A., Viovy, N., Voulgarakis, A., Weber, T. S., van Weele, M., van der Werf, G. R., Weiss, R. F., Worthy, D., Wunch, D., Yin, Y., Yoshida, Y., Zhang, W., Zhang, Z., Zhao, Y., Zheng, B., Zhu, Q., Zhu, Q., and Zhuang, Q.: The Global Methane Budget 2000–2017, *Earth Syst. Sci. Data Discuss.*, <https://doi.org/10.5194/essd-2019-128>, in review, 2019.](#)
- 650 [Schaefer, H., Fletcher, S. E. M., Veidt, C., Lassey, K. R., Brailsford, G. W., Bromley, T. M., Dlugokencky, E. J., Michel, S. E., Miller, J. B., Levin, I., Lowe, D. C., Martin, R. J., Vaughn, B. H., and White, J. W. C.: A 21st century shift from fossil-fuel to biogenic methane emissions indicated by \$^{13}\text{CH}_4\$, *Science*, 352, 80–84, <https://doi.org/10.1126/science.aad2705>, 2016.](#)
- [Schnell, J. L., Naik, V., Horowitz, L. W., Paulot, F., Mao, J., Ginoux, P., Zhao, M., and Ram, K.: Exploring the relationship between surface \$\text{PM}_{2.5}\$ and meteorology in Northern India, *Atmos. Chem. Phys.*, 18, 10157–10175, <https://doi.org/10.5194/acp-18-10157-2018>, 2018.](#)
- 655 [Schumann, U. and Huntrieser, H.: The global lightning-induced nitrogen oxides source, *Atmos. Chem. Phys.*, 7, 3823–3907, <https://doi.org/10.5194/acp-7-3823-2007>, 2007.](#)
- [Schwietzke, S., Sherwood, O. A., Bruhwiler, L. M. P., Miller, J. B., Etiope, G., Dlugokencky, E. J., Michel, S. E., Arline, V. A., vaughn, B. H., White, J. W. C., and Tans, P. P.: Upward revision of global fossil fuel methane emissions based on isotope database, *Nature*, 538, 88–91, <https://doi.org/10.1038/nature19797>, 2016.](#)

- 660 Shindell, D., Kuylensstierna, J. C. I., Vignati, E., van Dingenen, R., Amann, M., Klimont, Z., Anenberg, S. C., Muller, N., JanssensMaenhout, G., Raes, F., Schwartz, J., Faluvegi, G., Pozzoli, L., Kupiainen, K., Höglund-Isaksson, L., Emberson, L., Streets, D., Ramanathan, V., Hicks, K., Oanh, N. T. K., Milly, G., Williams, M., Demkine, V., and Fowler, D.: Simultaneously mitigating near-term climate change and improving human health and food security, *Science*, 335, 183–189, 2012.
- Simpson, I. J., Sulbaek Andersen, M. P., Meinardi, S., Bruhwiler, L., Blake, N. J., Helmig, D., Rowland, F. S., and Blake, D.
665 R.: Long-term decline of global atmospheric ethane concentrations and implications for methane, *Nature*, 488, 490–494, 2012.
[Tans, P. P., Conway, T. J., and Nakazawa, T.: Latitudinal distribution of the sources and sinks of atmospheric carbon dioxide derived from surface observations and an atmospheric transport model, *J. Geophys. Res.*, 94, 5151–5172, doi:10.1029/JD094iD04p05151, 1989.](#)
- Taylor, K. E., Williamson, D., and Zwiers, F.: The sea surface temperature and sea-ice concentration boundary conditions of
670 AMIP II simulations, PCMDI Rep. 60, 20 pp, 2000.
- Thoning, K. W.: Curve Fitting Methods Applied to Time Series in NOAA/ESRL/GMD, path:
<https://www.esrl.noaa.gov/gmd/ccgg/mbl/crvfit/crvfit.html>, 2019.
- Thoning, K.W., Tans, P. P., and Komhyr, W. D.: Atmospheric carbon dioxide at Mauna Loa Observatory, 2. Analysis of the NOAA/GMCC data, 1974-1985, *J. Geophys. Res.*, 94, 8549-8565, 1989.
- 675 [Thompson, R. L., Stohl, A., Zhou, L. X., Dlugokencky, E., Fukuyama, Y., Tohjima, Y., Kim, S. Y., Lee, H., Nisbet, E. G., Fisher, R. E., Lowry, D., Weiss, R. F., Prinn, R. G., O'Doherty, S., Young, D., and White, J. W. C.: Methane emissions in East Asia for 2000–2011 estimated using an atmospheric Bayesian inversion, *J. Geophys. Res.-Atmos.*, 120, 4352–4369, doi:10.1002/2014JD022394, 2015.](#)
- Tsuruta, A., Aalto, T., Backman, L., Hakkarainen, J., van der Laan-Luijkx, I. T., Krol, M. C., Spahni, R., Houweling, S., Laine,
680 M., Dlugokencky, E., Gomez-Pelaez, A. J., van der Schoot, M., Langenfelds, R., Ellul, R., Arduini, J., Apadula, F., Gerbig, C., Feist, D. G., Kivi, R., Yoshida, Y., and Peters, W.: Global methane emission estimates for 2000–2012 from CarbonTracker Europe-CH4 v1.0, *Geosci. Model Dev.*, 10, 1261-1289, <https://doi.org/10.5194/gmd-10-1261-2017>, 2017.
- Turner, A. J., Frankenberg, C., Wennberg, P. O., and Jacob, D. J.: Ambiguity in the causes for decadal trends in atmospheric methane and hydroxyl, *P. Natl. Acad. Sci. USA*, 114, 5367–5372, <https://doi.org/10.1073/pnas.1616020114>, 2017.
- 685 van Marle, M. J. E., Kloster, S., Magi, B. I., Marlon, J. R., Daniau, A.-L., Field, R. D., Arneth, A., Forrest, M., Hantson, S., Kehrwald, N. M., Knorr, W., Lasslop, G., Li, F., Mangeon, S., Yue, C., Kaiser, J. W., and van der Werf, G. R.: Historic global biomass burning emissions for CMIP6 (BB4CMIP) based on merging satellite observations with proxies and fire models (1750–2015), *Geosci. Model Dev.*, 10, 3329-3357, <https://doi.org/10.5194/gmd-10-3329-2017>, 2017.
- Voulgarakis, A., Naik, V., Lamarque, J. F., Shindell, D. T., Young, P. J., Prather, M. J., Wild, O., Field, R. D., Bergmann, D.,
690 Cameron-Smith, P., Cionni, I., Collins, W. J., Dalsøren, S. B., Doherty, R. M., Eyring, V., Faluvegi, G., Folberth, G. A., Horowitz, L. W., Josse, B., MacKenzie, I. A., Nagashima, T., Plummer, D. A., Righi, M., Rumbold, S. T., Stevenson, D. S., Strode, S. A., Sudo, K., Szopa, S., and Zeng, G.: Analysis of present day and future OH and methane lifetime in the ACCMIP simulations, *Atmos. Chem. Phys.*, 13, 2563–2587, <https://doi.org/10.5194/acp13-2563-2013>, 2013.

- Wofsy, S. C., Daube, B., Jimenez, R., Kort, E., Pittman, J., Park, S., Commane, R., Xiang, B., Santoni, G. and Jacob, D., Fisher, J., Pickett-Heaps, C., Wang, H., Wecht, K., Wang, Q.-Q., Stephens, B., Shertz, S., Romashkin, P., Campos, T., Haggerty, J., Cooper, W., Rogers, D., Beaton, S., Hendershot, R., Elkins, J. W., Fahey, D. W., Gao, F. R. S., Moore, F., Montzka, S. A., Schwarz, D. J. P., Miller, Hurst, B., Sweeney, C., Oltmans, S. J., Nance, D., Hints, E., Dutton, G., Watts, L. A., Spackman, J. R., Rosenlof, K. H., Ray, E. A., Zondlo, M., Diao, M., Keeling, R., Bent, J., Atlas, E., Lueb, R., Mahoney, M., Chahine, M., Olson, E., Patra, P., Ishijima, K., Engelen, R., Flemming, J., Nassar, R., Jones, D. B. A., and Mikaloff Fletcher, S. E.: HIAPER Pole-to-Pole Observations (HIPPO): fine-grained, global-scale measurements of climatically important atmospheric gases and aerosols, *Philos. T. R. Soc. A*, 369, 2073–2086, doi:10.1098/rsta.2010.0313, 2011.
- Worden, J. R., Bloom, A. A., Pandey, S., Jiang, Z., Worden, H. M., Walker, T. W., Houweling, S., and Röckmann, T.: Reduced biomass burning emissions reconcile conflicting estimates of the post-2006 atmospheric methane budget, *Nature Commun.*, 8, 2227, <https://doi.org/10.1038/s41467-017-02246-0>, 2017.
- Wesely, M. L.: Parameterization of surface resistances to gaseous dry deposition in regional-scale numerical models, *Atmos. Environ.*, 23, 1293–1304, 1989.
- Zhao, M., Golaz, J.-C., Held, I. M., Guo, H., Balaji, V., Renson, R., Chen, J.-H., Chen, X., Donner, L. J., Dunne, J. P., Dunne, K., Durachta, J., Fan, S.-M., Freidenreich, S. M., Garner, S. T., Ginoux, P., Harris, L. M., Horowitz, L. W., Krasting, J. P., Langenhorst, A. R., Liang, Z., Lin, P., Lin, S.-J., Malyshev, S. L., Mason, E., Milly, P. C. D., Ming, Y., Naik, V., Paulot, F., Paynter, D., Phillipps, P., Radhakrishnan, A., Ramaswamy, V., Robinson, T., Schwarzkopf, D., Seman, C. J., Shevliakova, E., Shen, Z., Shin, H., Silvers, L. G., Wilson, J. R., Winton, M., Wittenberg, A. T., Wyman, B., and Xian, B.: The GFDL global atmosphere and land model AM4.0/LM4.0: 1. Simulation characteristics with prescribed SSTs. *J. Adv. Model. Earth Syst.*, 10, 691–734, <https://doi.org/10.1002/2017MS001208>, 2018a.
- Zhao, M., Golaz, J.-C., Held, I. M., Guo, H., Balaji, V., Renson, R., Chen, J.-H., Chen, X., Donner, L. J., Dunne, J. P., Dunne, K., Durachta, J., Fan, S.-M., Freidenreich, S. M., Garner, S. T., Ginoux, P., Harris, L. M., Horowitz, L. W., Krasting, J. P., Langenhorst, A. R., Liang, Z., Lin, P., Lin, S.-J., Malyshev, S. L., Mason, E., Milly, P. C. D., Ming, Y., Naik, V., Paulot, F., Paynter, D., Phillipps, P., Radhakrishnan, A., Ramaswamy, V., Robinson, T., Schwarzkopf, D., Seman, C. J., Shevliakova, E., Shen, Z., Shin, H., Silvers, L. G., Wilson, J. R., Winton, M., Wittenberg, A. T., Wyman, B., and Xian, B.: The GFDL global atmosphere and land model AM4.0/LM4.0: 2. Model description, sensitivity studies, and tuning strategies. *J. Adv. Model. Earth Syst.*, 10, 735–769, <https://doi.org/10.1002/2017MS001209>, 2018b.

Table 1. Emission inventories used in this study

Source Category	Database	Temporal Variability	References
Anthropogenic	CEDS v2017-05-18	1980-2014 monthly data	Hosely et al. (2018)
	SSP2-4.5	2015-2017 monthly data	Gidden et al. (2018)
Biomass Burning	BB4MIP	1980-2014 monthly data	van Marle et al. (2017)
	SSP2-4.5	2015-2017 monthly data	Gidden et al. (2018)
Wetlands	WetChart v1.0	Climatological monthly mean (with seasonal variability) for 1980-2017	Bloom et al. (2017)
Ocean	MOZART	Climatological monthly mean (with seasonal variability) for 1980-2017	Brasseur et al. (1998)
Near-shore	TransCom-CH4	Climatological annual mean (no seasonal variability) for 1980-2017	Lambert and Schmidt (1993), Patra et al. (2011)
Termites	NASA-GISS	Climatological annual mean (no seasonal variability) for 1980-2017	Fung et al. (1991)
Mud volcanoes	TransCom-CH4	Climatological annual mean (no seasonal variability) for 1980-2017	Etioppe and Milkov (2004), Patra et al. (2011)

Table 2. List of simulations conducted using GFDL-AM4.1 to explore trends and variability in methane

Simulations	Description
S0Aopt	Standard AM4.1 configuration, but with optimized anthropogenic emissions <u>for 1980-2017</u>
S0Wopt	Standard AM4.1 configuration, but with optimized wetland emissions <u>for 1980-2017</u>
<u>S0A06</u>	<u>S0Aopt emissions for 1980-2005, with repeating 2006 S0Aopt anthropogenic emissions for 2006-2014 and adjusting wetland emissions for 2006-2014 to ensure the total emissions are same as optimized totals</u>
<u>S0Comb</u>	<u>S0Aopt emissions for 1980-2005 and S0Wopt emissions for 2006-2014</u>
S1Wopt	AM4.1 configuration with low OH levels (LNO _x emissions scaled by a factor of 0.5), and optimized wetland emissions <u>for 1980-2017</u>
S2Wopt	AM4.1 configuration with high OH levels (LNO _x emissions scaled by a factor of 2), and optimized wetland emissions <u>for 1980-2017</u>

Table 3. Comparisons of simulated methane growth rates (annual mean \pm standard deviation) with observed methane growth rates (ppb yr⁻¹)

	<u>1984-1991</u>	<u>1992-1998</u>	<u>1999-2006</u>	<u>2007-2017</u>
<u>Observed</u>	<u>11.7\pm1.4</u>	<u>5.5\pm3.5</u>	<u>0.7\pm3.1</u>	<u>7.0\pm2.7</u>
<u>S0Aopt</u>	<u>13.7\pm3.2</u>	<u>5.4\pm3.4</u>	<u>1.3\pm4.1</u>	<u>6.1\pm2.7</u>
<u>S0Wopt</u>	<u>13.6\pm3.4</u>	<u>5.4\pm3.6</u>	<u>1.3\pm4.4</u>	<u>6.1\pm2.6</u>

1730

Table 4. Global methane budget (Tg CH₄ yr⁻¹) during 1980-2017

Period of time	1980-1989	1990-1999	2000-2009	2008-2017	1999-2006	2007-2017
Sources^a						
<u>Natural sources</u>	<u>203 [203-282]</u> <u>203 [150-267]^b</u> <u>355 [244-466]^c</u>	<u>203 [203-297]</u> <u>182 [167-197]^b</u> <u>336 [230-465]^c</u>	<u>203 [203-288]</u> <u>218 [179-273]^b</u> <u>347 [238-484]^c</u> <u>214 [176-243]^d</u> <u>369 [245-485]^e</u>	<u>203 [203-277]</u> <u>215 [176-248]^d</u> <u>371 [245-488]^e</u>	<u>203 [203-297]</u>	<u>203 [203-277]</u>
<u>Natural wetlands</u>	<u>166 [166-245]</u> <u>167 [115-231]^b</u> <u>225 [183-266]^c</u>	<u>166 [166-260]</u> <u>150 [144-160]^b</u> <u>206 [169-265]^c</u>	<u>166 [166-251]</u> <u>175 [142-208]^b</u> <u>217 [177-284]^c</u> <u>180 [153-196]^d</u> <u>147 [102-179]^e</u>	<u>166 [166-240]</u> <u>178 [155-200]^d</u> <u>149 [102-182]^e</u>	<u>166 [166-260]</u>	<u>166 [166-240]</u>
<u>Other natural sources</u>	<u>37</u>	<u>37</u>	<u>37</u> <u>35 [21-47]^d</u> <u>222 [143-306]^e</u>	<u>37</u> <u>37 [21-50]^d</u> <u>222 [143-306]^e</u>	<u>37</u>	<u>37</u>
<u>Oceans</u>	<u>9.5</u>	<u>9.5</u>	<u>9.5</u> <u>18 [2-40]^c</u> <u>13 [9-22]^e</u>	<u>9.5</u>	<u>9.5</u>	<u>9.5</u>
<u>Termites</u>	<u>20</u>	<u>20</u>	<u>20</u>	<u>20</u>	<u>20</u>	<u>20</u>
<u>Mud volcanoes</u>	<u>7.5</u>	<u>7.5</u>	<u>7.5</u>	<u>7.5</u>	<u>7.5</u>	<u>7.5</u>
<u>Anthropogenic sources</u>	<u>289 [289-368]</u> <u>348 [305-383]^b</u> <u>308 [292-323]^c</u>	<u>311 [311-405]</u> <u>372 [290-453]^b</u> <u>313 [281-347]^c</u>	<u>340 [340-425]</u> <u>335 [273-409]^b</u> <u>331 [304-368]^c</u> <u>331 [310-346]^d</u> <u>334 [325-357]^e</u>	<u>379 [379-452]</u> <u>357 [334-375]^d</u> <u>366 [348-392]^e</u>	<u>328 [328-422]</u>	<u>377 [377-450]</u>
<u>Agriculture and waste</u>	<u>159 [159-203]</u> <u>208 [187-220]^b</u> <u>185 [172-197]^c</u>	<u>172 [172-224]</u> <u>239 [180-301]^b</u> <u>188 [177-196]^c</u>	<u>185 [185-232]</u> <u>209 [180-241]^b</u> <u>200 [187-224]^c</u> <u>202 [173-219]^d</u> <u>192 [178-206]^e</u>	<u>201 [201-240]</u> <u>219 [175-239]^d</u> <u>206 [191-223]^e</u>	<u>181 [181-233]</u>	<u>200 [200-239]</u>
<u>Biomass burning</u>	<u>13 [13-16]</u>	<u>18 [18-24]</u>	<u>15 [15-18]</u> <u>19 [15-32]^e</u>	<u>14 [14-17]</u> <u>17 [14-26]^e</u>	<u>15 [15-20]</u>	<u>14 [14-17]</u>
<u>Fossil fuels</u>	<u>104 [104-132]</u> <u>94 [75-108]^b</u> <u>89 [89-89]^c</u>	<u>107 [107-139]</u> <u>95 [84-107]^b</u> <u>84 [66-96]^c</u>	<u>127 [127-159]</u> <u>96 [77-123]^b</u> <u>96 [85-105]^c</u> <u>100 [70-149]^d</u> <u>110 [93-129]^e</u>	<u>151 [151-180]</u> <u>109 [79-168]^d</u> <u>127 [111-154]^e</u>	<u>120 [120-153]</u>	<u>150 [150-179]</u>
<u>Other anthropogenic sources</u>	<u>14 [14-17]</u>	<u>14 [14-18]</u>	<u>13 [13-16]</u>	<u>13 [13-16]</u>	<u>12 [12-16]</u>	<u>13 [13-16]</u>
<u>ΔE^{f,g}</u>	<u>47 [23-79]</u>	<u>60 [36-94]</u>	<u>52 [29-85]</u>	<u>44 [21-79]</u>	<u>57 [34-93]</u>	<u>40 [17-73]</u>
Sinks^g						
<u>Total chemical loss</u>	<u>486 [462-519]</u> <u>490 [450-533]^b</u>	<u>540 [516-573]</u> <u>525 [491-554]^b</u>	<u>577 [553-610]</u> <u>518 [510-538]^b</u>	<u>584 [560-617]</u> <u>518 [474-532]^d</u>	<u>570 [546-603]</u>	<u>592 [568-625]</u>

	<u>539 [411-671]^c</u>	<u>571 [521-621]^c</u>	<u>604 [483-738]^c</u> <u>505 [459-516]^d</u> <u>595 [489-749]^e</u>			
<u>OH loss</u>	<u>442 [419-476]</u> <u>468 [382-567]^c</u>	<u>486 [462-519]</u> <u>479 [457-501]^c</u>	<u>526 [502-559]</u> <u>528 [454-617]^c</u> <u>553 [476-677]^e</u>	<u>534 [510-567]</u>	<u>519 [495-552]</u>	<u>542 [519-576]</u>
<u>OID loss</u>	<u>38</u> <u>46 [16-67]^c</u>	<u>47</u> <u>67 [51-83]^c</u>	<u>43</u> <u>51 [16-84]^c</u> <u>31 [12-37]^e</u>	<u>43</u>	<u>44</u>	<u>42</u>
<u>CI loss</u>	<u>5</u> <u>25 [13-37]^c</u>	<u>7</u> <u>25 [13-37]^c</u>	<u>7</u> <u>25 [13-37]^c</u> <u>11 [1-35]^e</u>	<u>7</u>	<u>8</u>	<u>7</u>
<u>Soils</u>	<u>13</u> <u>21 [10-27]^b</u> <u>28 [9-47]^c</u>	<u>14</u> <u>27 [27-27]^b</u> <u>28 [9-47]^c</u>	<u>14</u> <u>32 [26-42]^b</u> <u>28 [9-47]^c</u> <u>34 [27-41]^d</u> <u>30 [11-49]^e</u>	<u>14</u> <u>38 [27-45]^d</u>	<u>14</u>	<u>14</u>
<u>Totals^g</u>						
<u>Sum of sources</u>	<u>539 [515-571]</u> <u>551 [500-592]^b</u> <u>663 [536-789]^c</u>	<u>574 [549-608]</u> <u>554 [529-596]^b</u> <u>649 [511-812]^c</u>	<u>595 [572-628]</u> <u>548 [526-569]^b</u> <u>678 [542-852]^c</u> <u>545 [522-559]^d</u> <u>703 [570-842]^e</u>	<u>605 [582-640]</u> <u>572 [538-593]^d</u> <u>737 [593-880]^e</u>	<u>589 [565-625]</u>	<u>620 [597-653]</u>
<u>Sum of sinks</u>	<u>499 [475-532]</u> <u>511 [460-559]^b</u> <u>539 [420-718]^c</u>	<u>554 [530-586]</u> <u>542 [518-579]^b</u> <u>596 [530-668]^c</u>	<u>591 [567-624]</u> <u>540 [514-560]^b</u> <u>632 [592-785]^c</u> <u>540 [486-556]^d</u> <u>625 [600-798]^e</u>	<u>598 [574-632]</u> <u>556 [501-574]^d</u>	<u>584 [560-617]</u>	<u>606 [582-639]</u>
<u>Imbalance</u>	<u>40 [39-40]</u> <u>30 [16-40]^b</u>	<u>20 [19-22]</u> <u>12 [7-17]^b</u>	<u>4 [4-5]</u> <u>8 [-4-19]^b</u> <u>4 [-11-36]^d</u>	<u>7 [8-8]</u> <u>16 [0-47]^d</u>	<u>5 [5-8]</u>	<u>14 [15-14]</u>
<u>Atmospheric growth</u>	<u>36</u> <u>34^b</u> <u>32^h</u>	<u>19</u> <u>17^{b,h}</u>	<u>4.8</u> <u>6^{b,h}</u>	<u>7.4</u>	<u>3.5</u> <u>1.9±1.6^h</u>	<u>16.6-17.2</u> <u>18.9±1.7^h</u>

^a The decadal mean values are based on initial emission inventories. The lower and upper limits of the ranges are based on the minimum and maximum among all the optimized emission scenarios (i.e., S0Aopt, S0Wopt, S1Aopt, S1Wopt, S2Aopt, and S2Wopt) conducted in this work.

^b Values are based on Kirschke et al. (2013) top-down approach.

^c Values are based on Kirschke et al. (2013) bottom-up approach.

^d Values are based on Saunio et al. (2019) top-down approach.

^e Values are based on Saunio et al. (2019) bottom-up approach.

^f ΔE is calculated based on the methodology of Ghosh et al. (2015).

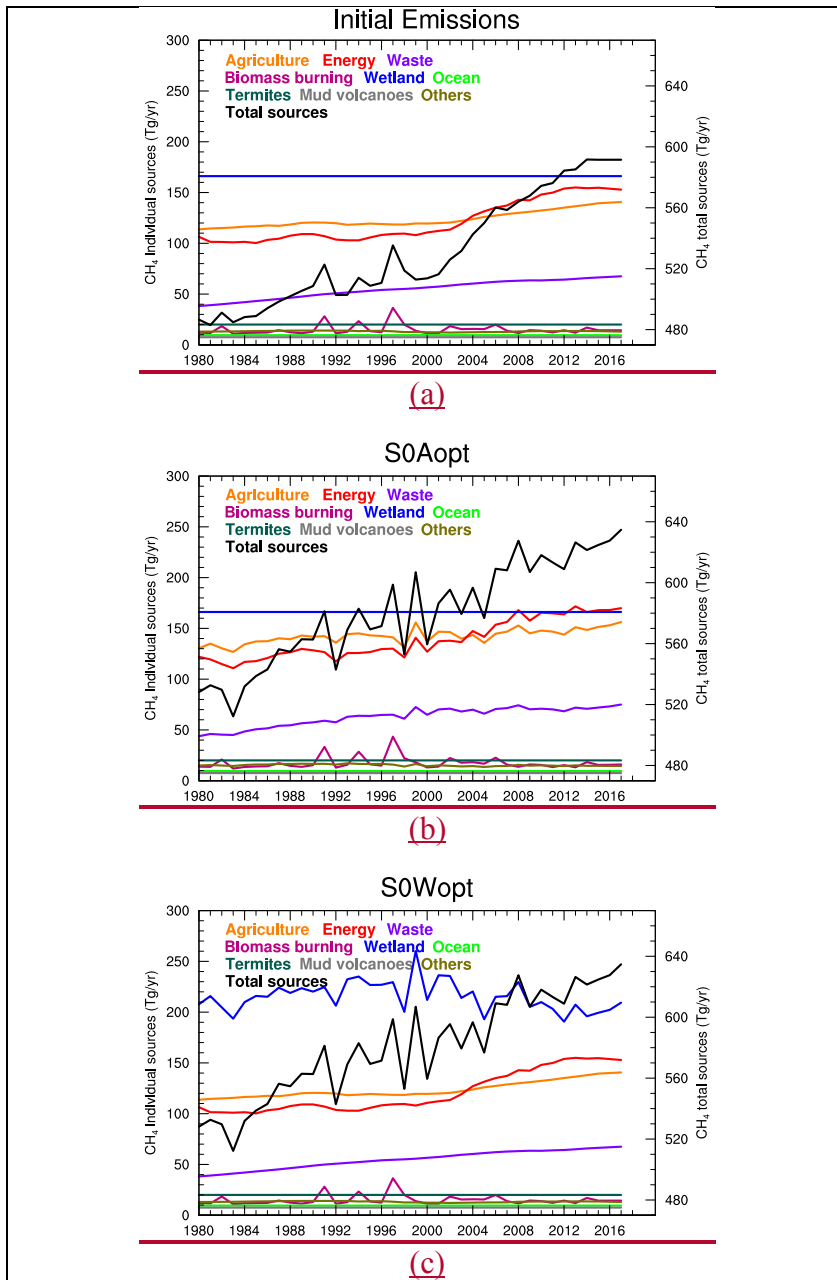
^g The ranges are based on the low OH (S1Wopt) and high OH cases (S2Wopt) and the decadal mean values shown in the table are based on the default OH (S0Wopt).

^h The observed atmospheric growth rates (Tg yr⁻¹) are estimated based on a few MBL sites (Dlugokencky et al., 2018), which are not the same as the Imbalance Row (based on the entire globe).

Table 5. Comparisons of estimated methane linear trend (ppb yr⁻¹)*

	<u>1984-1998</u>		<u>1999-2006</u>		<u>2007-2017</u>		<u>2007-2014</u>	
	<u>Total</u>	<u>Dominating tracers</u>	<u>Total</u>	<u>Dominating tracers</u>	<u>Total</u>	<u>Dominating tracers</u>	<u>Total</u>	<u>Dominating tracers</u>
<u>Observed</u>	<u>8.9</u>	<u>N./A.</u>	<u>0.6</u>	<u>N./A.</u>	<u>6.0</u>	<u>N./A.</u>	<u>5.4</u>	<u>N./A.</u>
<u>S0Aopt</u>	<u>10.5</u>	<u>CH4AGR</u> <u>(3.7)</u> <u>CH4ENE</u> <u>(2.2)</u> <u>CH4WST</u> <u>(3.6)</u>	<u>1.0</u>	<u>CH4ENE</u> <u>(2.6)</u> <u>CH4WST</u> <u>(2.3)</u>	<u>5.3</u>	<u>CH4AGR</u> <u>(0.6)</u> <u>CH4ENE</u> <u>(5.9)</u> <u>CH4WST</u> <u>(1.0)</u>		
<u>S0Wopt</u>	<u>10.4</u>	<u>CH4AGR</u> <u>(0.8)</u> <u>CH4WST</u> <u>(2.2)</u> <u>CH4WET</u> <u>(7.0)</u>	<u>1.1</u>	<u>CH4ENE</u> <u>(1.8)</u> <u>CH4WST</u> <u>(1.9)</u>	<u>5.4</u>	<u>CH4AGR</u> <u>(2.2)</u> <u>CH4ENE</u> <u>(7.0)</u> <u>CH4WST</u> <u>(1.6)</u>		
<u>S0A06</u>							<u>4.4</u>	<u>CH4ENE</u> <u>(3.4)</u> <u>CH4WST</u> <u>(1.1)</u>
<u>S0Comb</u>							<u>4.4</u>	<u>CH4ENE</u> <u>(2.8)</u> <u>CH4WET</u> <u>(5.9)</u>

*The linear trend is estimated by Mann-Kendall test. The estimated linear trend for source tagged tracers are shown in parentheses.



750 **Figure 1. Time series of methane emissions from the initial methane inventories (a), optimized methane emissions on**
anthropogenic sectors (S0Aopt, b) and wetland sector (S0Wopt, c) for the period of 1980-2017. The emissions for major
sectors are shown on the left y axis, including agriculture sector, energy production sector, waste sector, biomass
burning sector, wetland sector, ocean and near-shore fluxes, termites, mud volcanoes, and other sources (i.e., industrial
processes, surface transportation, international shipping, residential, commercial, and others). The total methane
emissions from the initial emission inventories (black line) are shown on the right y axis.
 755

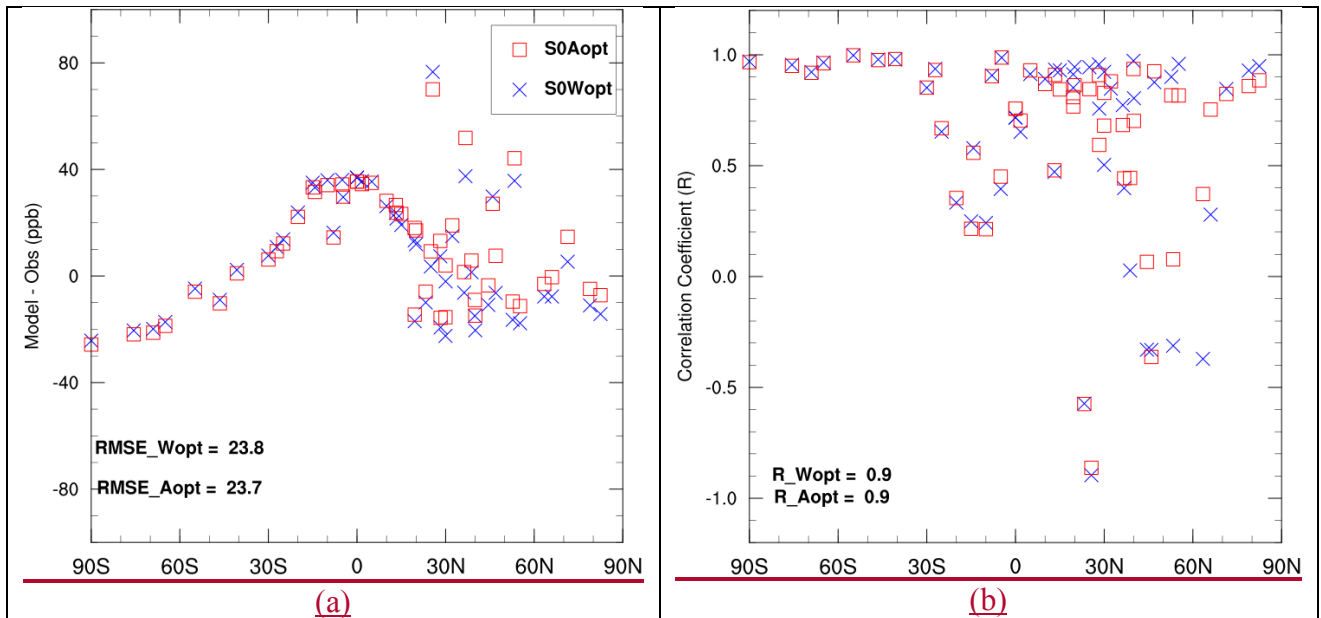


Figure 2. Model bias (a) and correlation coefficient (b) of simulated climatological mean surface methane concentrations against NOAA GMD observations for the 1983-2017 time period. GMD sites with at least 20-year observations are selected for model climatological evaluation. In Fig.2a, each red square or blue cross represents model mean bias by S0Aopt or S0Wopt at the corresponding GMD site. Root-mean-square-error (RMSE) is shown for all the GMD sites in Fig.2a. In Fig.2b, each red square or blue cross represents correlation of climatological seasonal variability by S0Aopt or S0Wopt at the corresponding GMD site. Spatial correlation (R) is shown for all the GMD sites in Fig.2b.

760

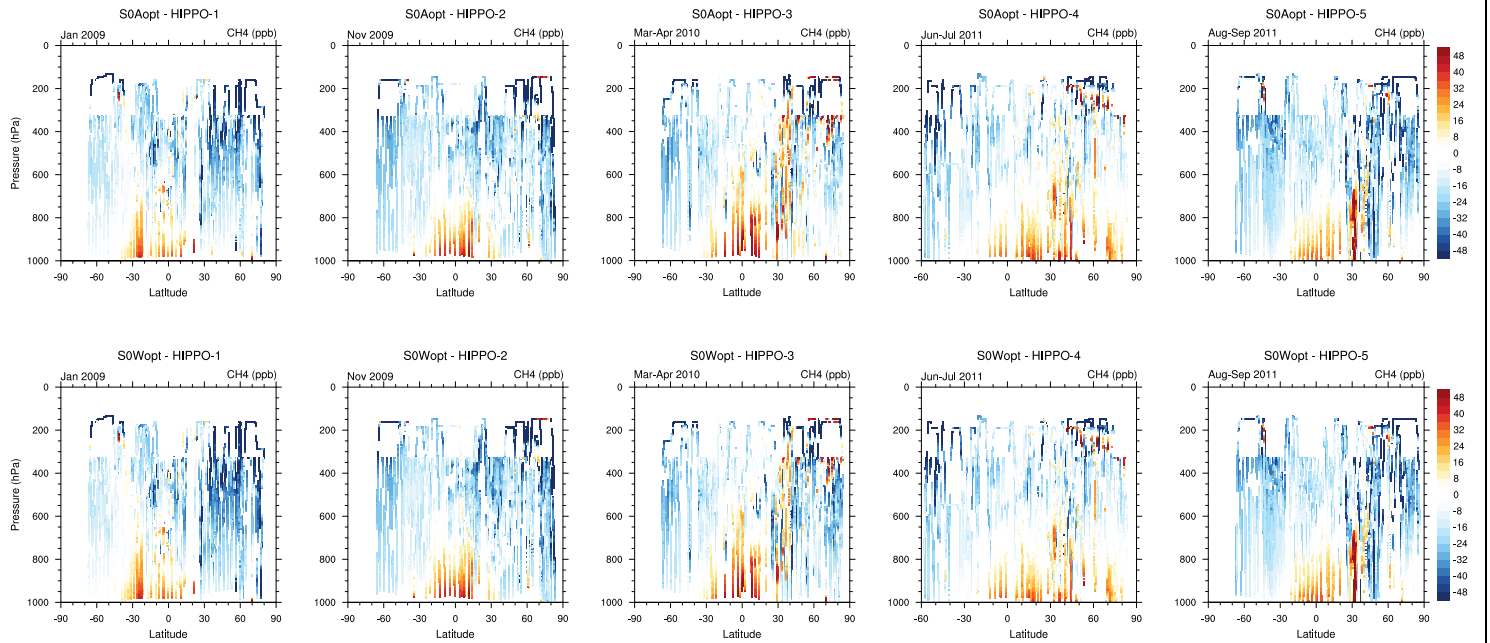


Figure 3. Comparison of vertical distribution of methane from S0Aopt and S0Wopt simulations with measurements from individual HIPPO campaigns. Months of campaign are given at the top left of the individual plots.

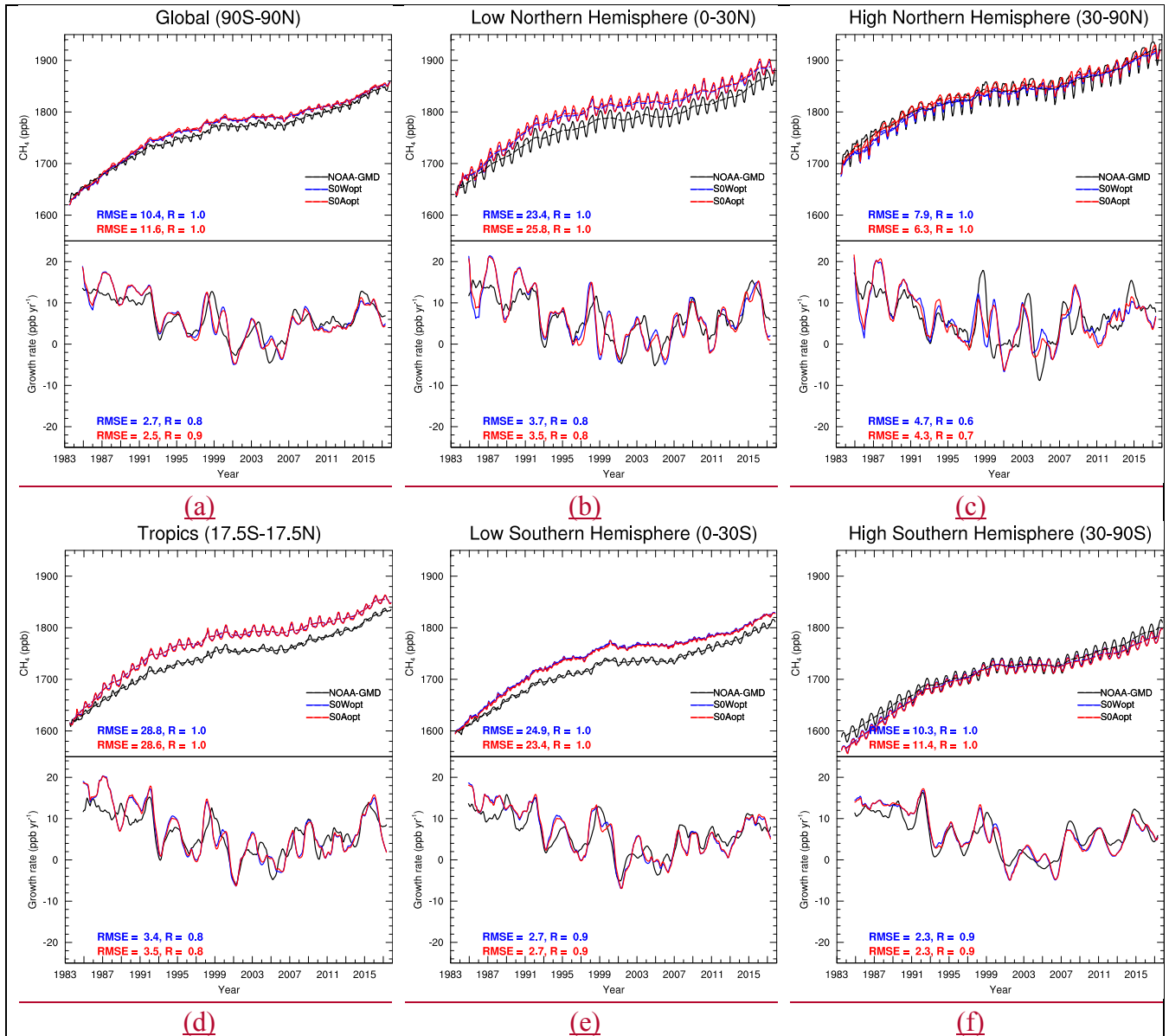


Figure 4. Comparison of GFDL-AM4.1 simulated methane concentrations and growth rates with NOAA-GMD surface observations. For the upper plot in each panel, dash line represents smoothed trends (i.e., 12-month running mean) from deseasonalized monthly data. A meridional curve (Tans et al., 1989) was fitted through NOAA-GMD site observations to get the latitudinal distribution of methane. A function fit consisting of yearly harmonics and a polynomial trend, with fast fourier transform and low pass filtering of the residuals are applied to the monthly mean methane DMF (Thoning et al., 1989; Thoning, 2019) to approximate the long-term trend. For the lower plot in each panel, the growth rates are calculated from the time derivative of the dash line in the corresponding upper plot.

770

775

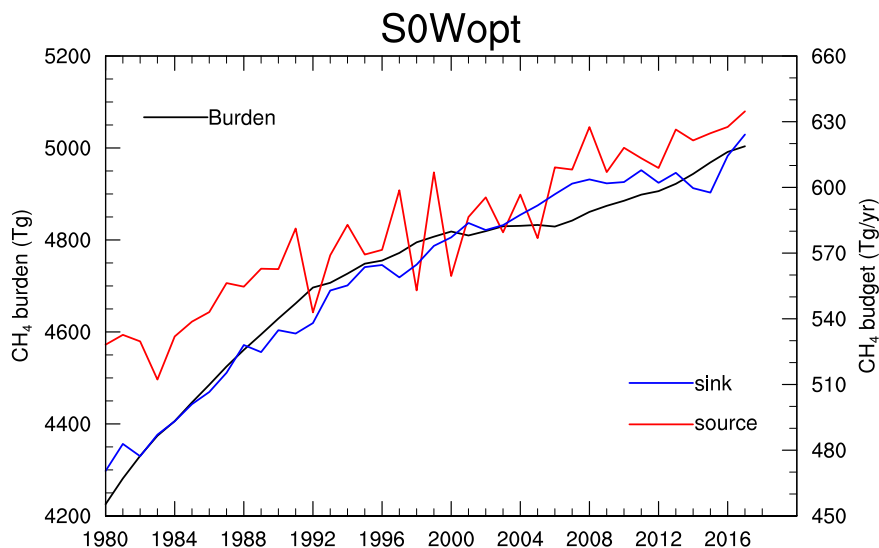


Figure 75. Time series of global methane burden (black line, left Y axis), methane sources (red line, right Y axis), and methane sinks (blue line, right Y axis) by S0Wopt.

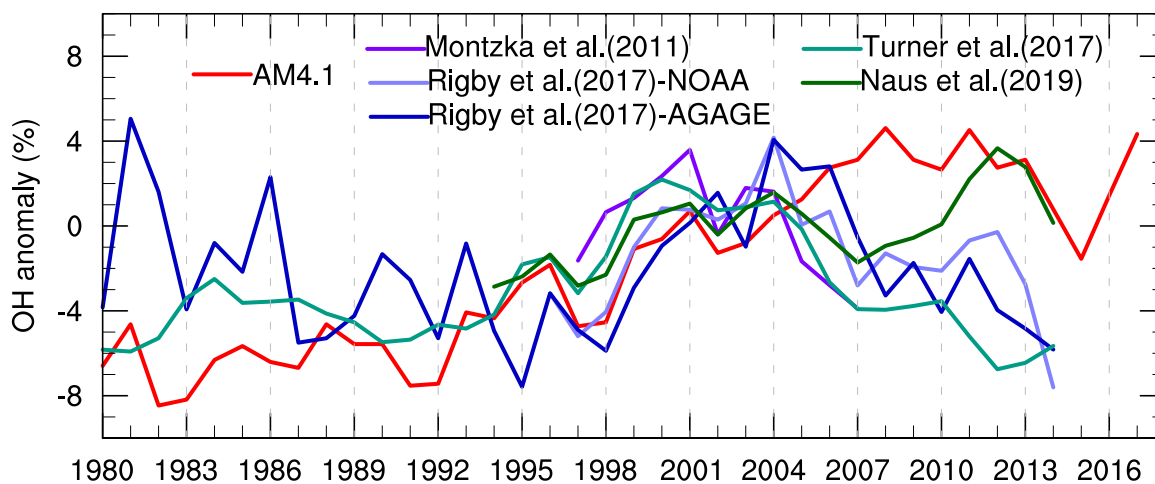


Figure 6. Time series of global tropospheric OH anomalies with respect to 1998-2007. Results of Montzka et al. (2011) are shown in dark purple (with the mean interannual variability of OH as $\pm 2.3\%$ for the period of 1998-2007). Results of Rigby et al. (2017) derived from NOAA observations are shown in light blue (with the mean interannual variability of OH as $\pm 2.3\%$ for the period of 1998-2007 and $\pm 2.6\%$ for the period of 1980-2014), and derived from AGAGE observations are shown in dark blue (with the mean interannual variability of OH as $\pm 3.0\%$ for the period of 1998-2007 and $\pm 3.1\%$ for the period of 1980-2014). Results from Turner et al. (2017) are shown in green (with the mean interannual variability of OH as $\pm 2.0\%$ for the period of 1998-2007 and $\pm 2.5\%$ for the period of 1980-2014). Results from Naus et al. (2019) are shown in dark green (with the mean interannual variability of OH as $\pm 1.2\%$ for the period of 1998-2007 and $\pm 1.8\%$ for the period of 1994-2014). OH anomalies in this work are shown in red (with the mean interannual variability of OH as $\pm 2.2\%$ for the period of 1998-2007 and $\pm 4.1\%$ for the period of 1980-2014).

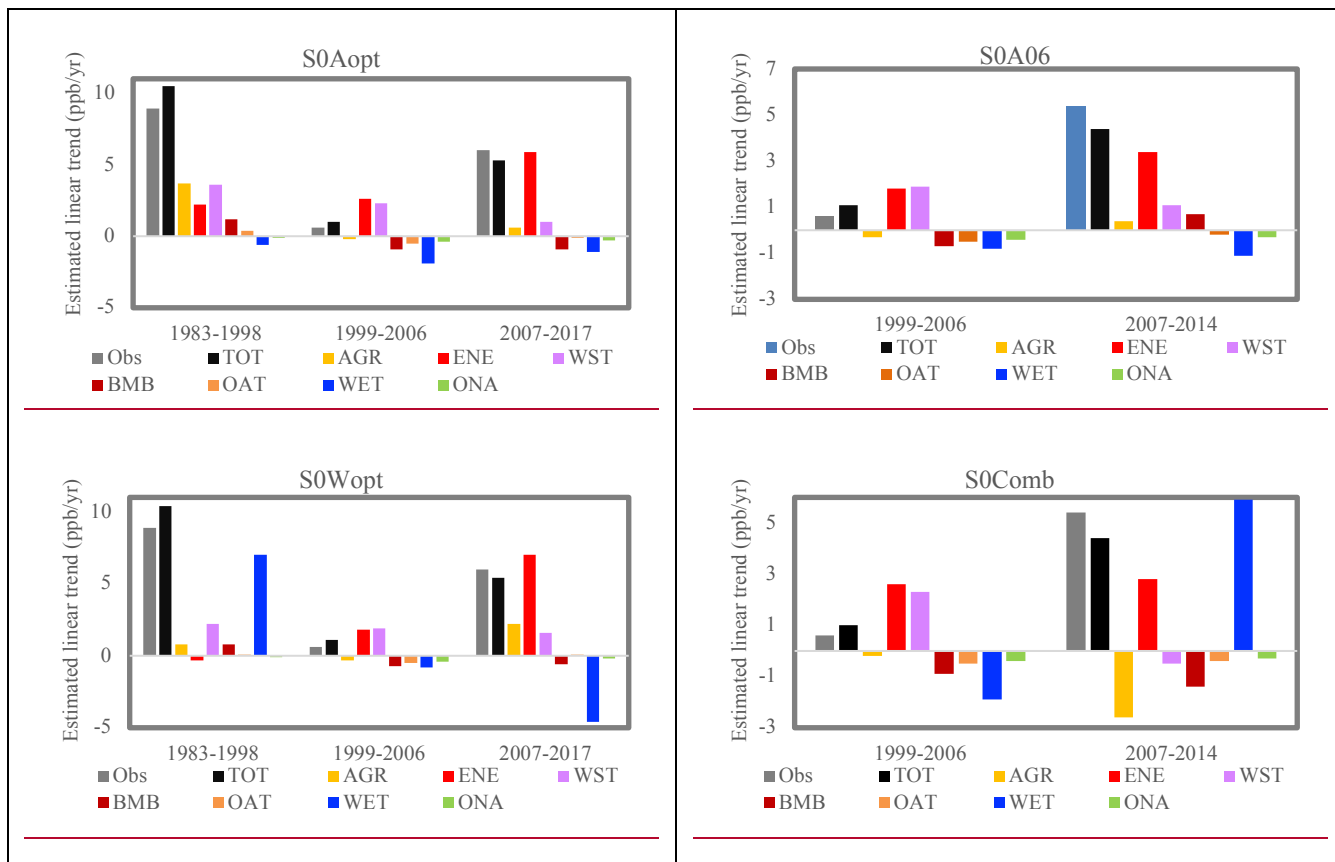
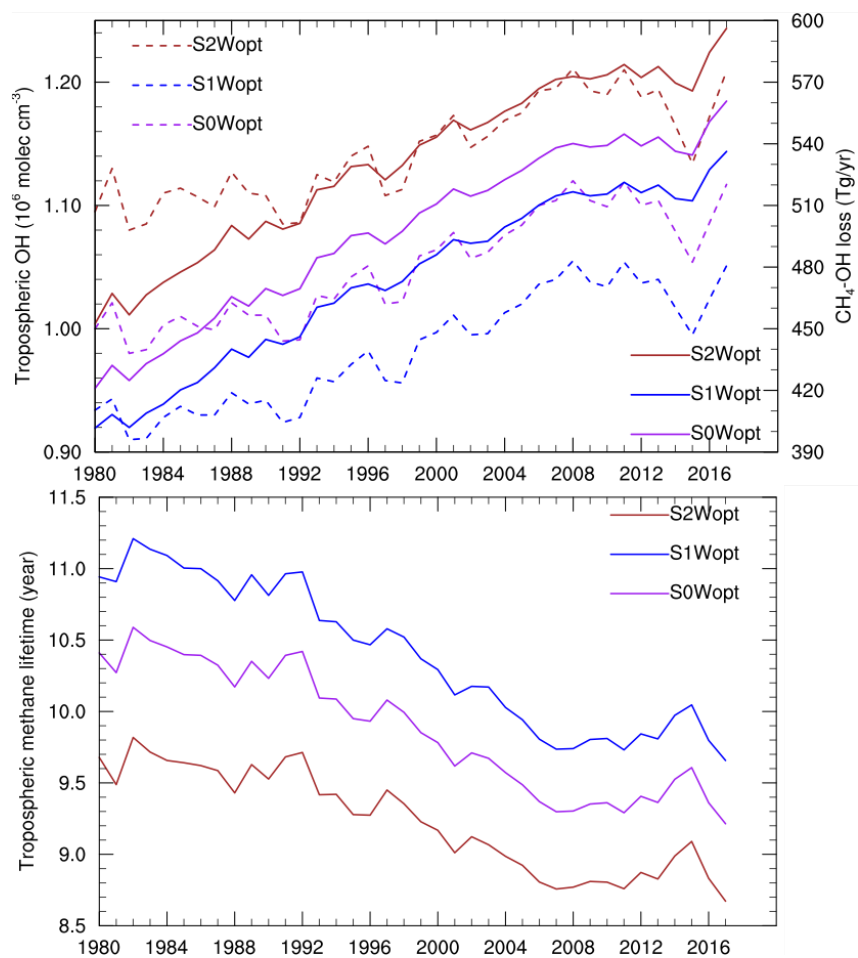


Figure 7. Estimated global linear trends for source tagged tracers and total methane (TOT). The source tagged tracers include tracers from the agriculture sector (AGR), energy sector (ENE), waste sector (WST), biomass burning sector (BMB), other anthropogenic sectors (OAT), wetland sector (WET), and other natural sectors (ONA). The grey bar represents total methane trend from NOAA-GMD observation. In the left panel (i.e., S0Aopt and S0Wopt), the trends are estimated for the periods of 1983-1998, 1999-2006, and 2007-2017. In the right panel (i.e., S0A06 and S0Comb), the trends are estimated for the period of 2007-2014, with 1999-2006 trends from S0Wopt and S0Aopt respectively.



805

Figure 813. Time series of global tropospheric OH levels (left Y axis, dash line) and methane OH loss (right Y axis, solid line) from S0Wopt (purple), S1Wopt (blue), and S2Wopt (brown) in the upper panel and time series of methane tropospheric lifetime from S0Wopt (purple), S1Wopt (blue), and S2Wopt (brown) in the lower panel.

Investigation of the global methane budget over 1980-2017 using GFDL-AM4.1

Jian He^{1,2}, Vaishali Naik², Larry W. Horowitz², Ed Dlugokencky³, and Kirk Thoning³

810 ¹Program in Atmospheric and Oceanic Sciences, Princeton University, Princeton, New Jersey, USA

²NOAA Geophysical Fluid Dynamics Laboratory, Princeton, New Jersey, USA

³NOAA Earth System Research Laboratory, Boulder, Colorado, USA

Correspondence to: Jian He (jian.he@noaa.gov)

Abstract. Changes in atmospheric methane abundance have implications for both chemistry and climate as methane is both a
815 strong greenhouse gas and an important precursor for tropospheric ozone. A better understanding of the drivers of trends and
variability in methane abundance over the recent past is therefore critical for building confidence in projections of future
methane levels. In this work, the representation of methane in the atmospheric chemistry model AM4.1 is improved by
optimizing total methane emissions (to an annual mean of 580 ± 34 Tg yr⁻¹) to match surface observations over 1980-2017. The
simulations with optimized global emissions are in general able to capture the observed trend, variability, seasonal cycle, and
820 latitudinal gradient of methane. Simulations with different emission adjustments suggest that increases in methane emissions
(mainly from agriculture, energy, and waste sectors) balanced by increases in methane sinks (mainly due to increases in OH
levels) lead to methane stabilization (with an imbalance of 5 Tg yr⁻¹) during 1999-2006, and that increases in methane emissions
(mainly from agriculture, energy, and waste sectors) combined with little change in sinks (despite small decreases in OH
levels) during 2007-2012 lead to renewed growth in methane (with an imbalance of 14 Tg yr⁻¹ for 2007-2017). Compared to
825 1999-2006, both methane emissions and sinks are greater (by 31 Tg yr⁻¹ and 22 Tg yr⁻¹, respectively) during 2007-2017. Our
tagged tracer analysis indicates that anthropogenic sources (such as agriculture, energy, and waste sectors) are more likely
major contributors to the renewed growth in methane after 2006. A sharp increase in wetland emissions (a likely scenario)
with concomitant sharp decrease in anthropogenic emissions (a less likely scenario), would be required starting in 2006 to
drive the methane growth by wetland tracer. Simulations with varying OH levels indicate that a 1% change in OH levels could
830 lead to an annual mean difference of ~ 4 Tg yr⁻¹ in the optimized emissions and 0.08 year difference in the estimated
tropospheric methane lifetime. Continued increases in methane emissions along with decreases in tropospheric OH
concentrations during 2008-2015 prolong methane's lifetime and therefore amplify the response of methane concentrations to
emission changes. Uncertainties still exist in the partitioning of emissions among individual sources and regions.

1 Introduction

835 Atmospheric methane (CH₄) is the second most important anthropogenic greenhouse gas with a global warming potential 28-
34 times that of carbon dioxide (CO₂) over a 100-year time horizon (Myhre et al., 2013). Methane is also a precursor for

1840 tropospheric ozone (O₃)—both an air pollutant and greenhouse gas—influencing ozone background levels (Fiore et al., 2002). Controlling methane has been shown to be a win-win, benefiting both climate and air quality (Shindell et al., 2012). From a preindustrial level of 722±25 ppb (Etheridge et al., 1998; Dlugokencky et al., 2005), methane has increased by a factor of ~2.5 to a value of 1857±1 ppb in 2018 (Dlugokencky et al., 2018), mostly due to anthropogenic activities (Dlugokencky et al., 2011). The global network of surface observations over the past 3-4 decades indicates that methane went through a period of rapid growth from the 1980s to 1990s, nearly stabilized from 1999 to 2006, and then renewed its rapid growth. Here, we estimate the methane budget and explore the contributions of methane sources and sinks to its observed trends and variability during 1980-2017.

1845 Methane is emitted into the atmosphere from both anthropogenic activities (e.g., agriculture, energy, industry, transportation, waste management, and biomass burning) and natural processes (e.g., wetland, termites, oceanic and geological processes, and volcanoes), and is removed from the atmosphere mainly by reaction with hydroxyl radical (OH) in the troposphere, with lesser contributions to destruction by reactions with excited atomic oxygen (O(¹D)) and atomic chlorine (Cl) in the stratosphere and uptake by soils (Saunio et al., 2016). Measurements of the global distribution of surface methane beginning in 1983 have revealed that atmospheric methane approached steady state during 1983-2006 and renewed its growth since then. During 1983-2006, methane growth rates decreased from 12 ppb yr⁻¹ during 1984-1991 to 5 ppb yr⁻¹ during 1992-1998 (Nisbet et al., 2014; Dlugokencky et al., 2018) and to 0.7±0.6 ppb yr⁻¹ during 1999-2006 (Dlugokencky et al., 2018). After 2006, methane started increasing again with a growth rate of 5.7±1.2 ppb yr⁻¹ in 2007-2013 and reached 12.6±0.5 ppb yr⁻¹ in 2014 and 10.0±0.7 ppb yr⁻¹ in 2015 (Nisbet et al., 2016; Dlugokencky et al., 2018). While anthropogenic activities are widely considered responsible for the long-term methane increase since pre-industrial times (Dlugokencky et al., 2011), there is no consensus on the drivers for the methane stabilization during 1999-2006 and renewed growth since 2007. Previous studies have attributed the stabilization during 1999-2006 to the combined effects of increased anthropogenic emissions with decreased wetland emissions (Bousquet et al., 2006), decreased fossil fuel emissions (Dlugokencky et al., 2003; Simpson et al., 2012; Schaefer et al., 2016) or rice paddies emissions (Kai et al., 2011), stable emissions from microbial and fossil fuel sources (Levin et al., 2012), or variations of methane sinks (Rigby et al., 2008; Montzka et al., 2011; Schaefer et al., 2016). The observed renewed growth since 2007 has been explained alternatively through increases in tropical emissions (Houweling et al., 2014; Nisbet et al., 2016) such as agricultural emissions (Schaefer et al., 2016; Patra et al., 2016) and tropical wetland emissions (Bousquet et al., 2011; Maasakkers et al., 2019), increases in fossil fuel emissions (Rice et al., 2016; Worden et al., 2017), decreases in sources compensated by decreases in sinks due to OH levels (Turner et al., 2017; Rigby et al., 2017), or a combination of changes in different sources such as increases in fossil, agriculture, and waste emissions with decreases in biomass burning emissions (Saunio et al., 2017). These different explanations reflect limitations in our understanding of recent changes in methane and its budget.

1870 Previous work has generally combined observations of methane and its isotopic composition (δ¹³CH₄) with inverse models (top-down), process-based models (bottom-up), or box models to estimate methane emissions and sinks and their variability (Bousquet et al., 2006; Monteil et al., 2011; Rigby et al., 2012; Bloom et al., 2012; Kirschke et al., 2013; Ghosh et al., 2015;

Schwietzke et al., 2016; Schaefer et al., 2016; Nisbet et al., 2014, 2016; Dalsøren et al., 2016; Turner et al., 2017; Rigby et al., 2017). Inverse models use observations to derive emissions, but usually prescribe climatological OH, O(¹D), and Cl levels or loss rates (e.g., Rice et al., 2016; Tsuruta et al., 2017). Box models, on the other hand, use methane observations together with those of other proxy chemicals (e.g., ¹³C/¹²C ratio, ethane, carbon monoxide, methyl chloroform) to provide information on the global methane budget (e.g., Schaefer et al., 2016; Turner et al., 2017), but lack information on spatial variability or regional characteristics. With process-based models (e.g., wetlands) and inventories representing different source types (e.g., fossil fuel emissions) to drive chemical transport models, the bottom-up approach is able to estimate the methane budget for all individual sources and sinks. However, without observational constraints, there is considerable uncertainty in the total methane emissions derived from a combination of independent bottom-up estimates (Saunois et al., 2016).

Bottom-up global Earth System Models (ESMs) that realistically simulate the physical, chemical, and biogeochemical processes, as well as interactions and feedbacks among these processes, are useful tools to characterize the global methane cycle and quantify the global methane budget and impacts on composition and climate. Dalsøren et al. (2016) investigated the evolution of atmospheric methane by driving a chemical transport model with bottom-up emissions. While their model results are able to match the observed time evolution of methane without emission adjustments, surface methane is largely underpredicted in their study. Ghosh et al. (2015) optimized bottom-up emissions to investigate methane trends; however, OH trends and interannual variability were not considered in their chemical transport model. Here, we apply a prototype of the full-chemistry version of the Geophysical Fluid Dynamics Laboratory (GFDL) new-generation Atmospheric Model, version 4.1 (AM4.1, Zhao et al., 2018a, b; Horowitz et al., manuscript in preparation) to investigate the evolution of methane over 1980-2017. Our main objectives are to improve the representation of methane in GFDL-AM4.1, to comprehensively evaluate the model performance of methane predictions with an improved representation of the methane budget, and to investigate possible drivers of the methane trends and variability. This paper is structured as follows: Section 2 describes the modeling approach, emission inventories, and observations used for model evaluation. Results of the model evaluation, global methane budget analysis, and model sensitivities are presented in Section 3. Finally, Section 4 summarizes the results and discusses the implication of these results.

2 Methodology and data

2.1 Model description and initialization

We use a prototype version of the new generation GFDL chemistry-climate model, GFDL-AM4.1 (Zhao et al., 2018a, b; Horowitz et al., manuscript in preparation). A detailed description of the physics and dynamics in AM4.1 is provided by Zhao et al. (2018a, b). The version of AM4.1 with full interactive chemistry used in this work is described by Schnell et al. (2018).

In its standard form, this model setup consists of a cubed sphere finite-volume dynamical core with a horizontal resolution of ~100 km and 49 vertical levels extending from the surface up to ~80 km. The model's lowermost level is approximately 30 m thick. The chemistry and aerosol physics in this model have been updated from the previous version (GFDL-AM3; Naik et al.,

2013a), as described by Mao et al. (2013a, b) and Paulot et al. (2016). There are a total of 102 advected gas tracers and 18 aerosol tracers, 44 photolysis reactions, and 205 gas-phase reactions included in the chemical mechanism in this version of AM4.1 to represent tropospheric and stratospheric chemistry.

The standard AM4.1 configuration uses global annual-mean methane concentrations as a lower boundary condition to simulate the atmospheric distribution of methane. This modeling framework does not allow for the full characterization of the drivers of methane trends and variability, nor does it capture latitudinal or seasonal variations in methane. To overcome this issue, we updated AM4.1 to be driven by methane emissions. Table 1 provides information on the methane emission datasets used in this work. Our initial estimates of surface emissions from anthropogenic sources—including agriculture (AGR), energy production (ENE), industry (IND), road transportation (TRA), residential, commercial, and other sectors (RCO), waste (WST), and international shipping (SHP)—are from the Community Emissions Data System (CEDS, version 2017-05-18, Hoesly et al., 2018) developed in support of the Coupled Model Intercomparison Project Phase 6 (CMIP6) for 1980-2014. Emissions for 2015-2017 are from a middle-of-the-road scenario of Shared Socioeconomic Pathways targeting a forcing level of 4.5 W m^{-2} (SSP2-4.5), developed in support of the ScenarioMIP experiment within CMIP6 (Gidden et al., 2019). Biomass burning (BMB) emissions are from van Marle et al. (2017) for 1980-2014 and from SSP2-4.5 for 2015-2017, and are vertically distributed over seven ecosystem-dependent altitude levels between the surface and 6 km above the surface, following the methodology of Dentener et al. (2006). Anthropogenic and biomass burning emissions are represented by monthly gridded emissions including seasonal and interannual variability. Natural emissions include wetland (WET) emissions from the WetCHARTs version 1.0 inventory (Bloom et al., 2017), ocean (OCN) emissions from Brasseur et al. (1998) with near-shore methane fluxes from Lambert and Schmidt (1993) and Patra et al. (2011), termites (TMI) from Fung et al. (1991), and mud volcanoes (VOL) from Etiope and Milkov (2004) and Patra et al. (2011). Wetland emissions and ocean emissions are climatological monthly means without interannual variability. The remaining natural emissions are based on a climatological annual mean (repeated every month without seasonal variability). Timeseries of the total emissions and emissions from major sectors over 1980-2017 are shown in Figure 1. Trends in total emissions are primarily driven by trends in ENE, AGR, and WST emissions. Although wetlands are in reality a major contributor to interannual variability in methane emissions (Bousquet et al., 2006; Kirschke et al., 2013), our use of climatological wetland emissions causes the interannual variability in our methane emissions to be dominated by BMB emissions. Anthropogenic and biomass burning emissions of other short-lived species also follow CEDS and SSP2-4.5 inventories. Natural emissions of other short-lived species are from Naik et al. (2013a). Biogenic isoprene emissions are calculated interactively following Guenther et al. (2006).

The methane sinks considered in AM4.1 include oxidation by OH, Cl, and $\text{O}(^1\text{D})$, and dry deposition. Since the model does not represent tropospheric halogen chemistry, it does not consider removal of methane by Cl in the troposphere, a sink that remains poorly constrained (Hossaini et al., 2016; Gromov et al., 2018; Wang et al., 2019). The dry deposition flux of methane is estimated based on a monthly climatology of deposition velocities (Horowitz et al., 2003) calculated by a resistance-in-series scheme (Wesely, 1989; Hess et al., 2000) and used to mimic methane loss by soil uptake, which accounts for about 5% of the total methane sink (Kirschke et al., 2013; Saunio et al., 2016).

In this work, we included 12 additional methane tracers tagged by source sector to attribute methane from agriculture (CH4AGR), energy (CH4ENE), industry (CH4IND), transportation (CH4TRA), residents (CH4RCO), waste (CH4WST), shipping (CH4SHP), biomass burning (CH4BMB), ocean (CH4OCN), wetland (CH4WET), termites (CH4TMI), and mud volcanoes (CH4VOL). The tracers are emitted from corresponding sources, and undergo the same chemical and transport pathways as the full CH₄ tracer. For analysis, we combine CH4IND, CH4TRA, CH4RCO, and CH4SHP as other anthropogenic tracers (i.e., CH4OAT), and combine CH4OCN, CH4TMI, and CH4VOL as other natural tracers (i.e., CH4ONA).

Initially the model was spun up in a 50-year run with repeating 1979 emissions driven by 1979 sea surface temperatures and sea ice until stable atmospheric burdens of methane and tagged tracers were obtained. After spin-up, several sets of simulations were conducted for 1980-2017 to quantify the methane budget and investigate the impacts of changes in methane sources and sinks on methane abundance (see Section 2.3). All model simulations are forced with interannually-varying sea surface temperatures and sea ice from Taylor et al. (2000), prepared in support of the CMIP6 Atmospheric Model Intercomparison Project (AMIP) simulations. Horizontal winds are nudged to the National Centers for Environmental Prediction (NCEP) reanalysis (Kalnay et al., 1996) using a pressure-dependent nudging technique (Lin et al., 2012).

1950 **2.2 Observations**

We evaluate the simulated methane dry-air mole fraction (DMF) against a suite of ground-based and aircraft observations to thoroughly evaluate the model simulated spatial and temporal distribution of methane. To evaluate surface CH₄, we use measurements from a globally distributed network of air sampling sites maintained by the Global Monitoring Division (GMD) of the Earth System Research Laboratory at the National Oceanic and Atmospheric Administration (NOAA) (Dlugokencky et al., 2018). The global estimates are based on spatial and temporal smoothing of CH₄ measurements from 45 surface marine boundary layer (MBL) sites. Locations of the MBL sites are shown in Figure S1, and information for each MBL site is listed in Table S1 in the Supplement. First, the average trend and seasonal cycle are approximated for each sampling site by fitting a second-order polynomial and four harmonics to the data. We characterize deviations from this average behaviour by transforming the residuals to frequency domain, then multiplying by a low pass filter (Thoning et al., 1989; Thoning, 2019). Zonal and global averages are determined by extracting values at synchronized time steps from the smoothed fits to the data, then fitting another curve as a function of latitude (Tans et al., 1989). We divide these fits into sine (latitude) = 0.05 intervals, which define a matrix of zonally averaged CH₄ as a function of time and latitude. The same sampling and processing approach (Thoning et al., 1989; Tans et al., 1989) is applied to the simulated monthly mean methane DMF to calculate global and zonal averages to facilitate consistent model-observation comparison. Besides the comparison with global estimates from MBL sites, we also evaluate model performance at individual GMD sites to investigate regional emission representation. For site-specific evaluation, we sample the model grid cell at the location of the corresponding site and at the model layer with height closest to the altitude of the corresponding site.

To investigate background tropospheric methane variability, we compare the simulated vertical profiles with aircraft measurements from the High-performance Instrumented Airborne Platform for Environmental Research (HIAPER) Pole-to-

1970 Pole observation (HIPPO) campaigns from January 2009 to September 2011 (Wofsy et al., 2012). A total of 787 profiles were
flown during 5 campaigns with continuous profiling between approximately 150 m and 8500 m altitudes, but also including
many profiles up to 14 km altitude. For each HIPPO mission, we spatially sample the model consistent with the observations
and average the model for the months of the campaign to create climatological monthly means.

2.3 Simulation design

1975 We conduct several sets of hindcast simulations for 1980-2017, as listed in Table 2, to quantify the methane budget and
investigate the contributions of sources and sinks to the trend and variability of methane. The model simulation using the initial
methane emissions inventory (E_{init}) described in Section 2.1 was found to largely underestimate the methane DMF by 126 ppb
(see Figures S2 and S3 in the Supplement). Assuming that this mismatch is due to a bias in the simulated methane budget, we
can either increase methane sources or decrease methane sinks to match the observations. We perform several optimization
1980 simulations that explore the sensitivity of methane to uncertainties in emissions of methane and levels of OH, the dominant
sink for methane. Because OH trends and variability depend on a number of factors, including temperature, water vapor, O_3 ,
and emissions of nitrogen oxide (NO_x), carbon monoxide (CO), and volatile organic compounds (VOCs), it is not
straightforward to perturb OH. Previous work has shown that interannual variability of global OH is highly correlated with
 NO_x from lightning (Fiore et al., 2006; Murray et al., 2013). Therefore, we apply scaling factors to lightning NO_x (LNO_x)
1985 emissions to indirectly adjust OH levels without influencing its variability. The LNO_x emissions are calculated interactively
as described by Horowitz et al. (2003) as a function of subgrid convection parameterized in the model. The climatological
global mean LNO_x emission simulated by standard AM4.1 is about 3.6 TgN yr^{-1} , within the range of 2-8 TgN yr^{-1} estimated
by previous studies (e.g., Schumann and Huntrieser, 2007). We additionally apply scaling factors (e.g., 0.5 and 2.0) to LNO_x
emissions, producing LNO_x at the lower and upper limits of the estimated range for sensitivity simulations described below.
1990 We test the sensitivity of simulated methane to changes in OH using: 1) standard OH levels simulated by AM4.1 (referred as
“S0”); 2) low OH levels via applying a scaling factor of 0.5 to the default LNO_x emission calculations (referred as “S1”); 3)
high OH levels via applying a factor of 2 to the default LNO_x emission calculation (referred as “S2”). For each OH option, we
begin with initial methane emissions and then optimize global total emissions as described below to match simulated methane
with surface observations. Different OH levels lead to different estimations of the optimized total emissions, which provides
1995 a measure of uncertainties in our optimized total methane emissions.

The estimates of optimized emissions are based on comparison of simulated surface methane with NOAA-GMD MBL
observations. We apply a simple mass balance approach to optimize global total methane emissions, following the
methodology of Ghosh et al. (2015). In this approach, we calculate an increment ΔE , by which global emissions need to be
modified for each year. We do so by converting the differences in surface methane DMFs between observations and model
2000 estimates to the differences in methane burden growth rate and in total methane loss. We iterate the optimization process a
couple of times to account for the methane-OH feedback until the simulated surface methane DMF matches the observations.
Unlike inverse modeling studies (Houweling et al., 2017), we do not optimize emissions for each grid cell. Instead, we

uniformly scale emissions for particular sectors (as described below) globally for each year by the rate of the optimized emission total ($E_{opt} = E_{init} + \Delta E$) to the initial emissions (E_{init}). We assume that the spatial distribution of methane emissions from the initial emission inventories are the best available information we have. Considering the large uncertainties in the anthropogenic and wetland emissions, we perform two simulations for the standard (S0) LNO_x scenario, in which we achieve the optimized emission totals by scaling either anthropogenic and biomass burning sources only (referred to as “Aopt”) or the wetland sector only (referred to as “Wopt”). The purpose of conducting these simulations is to investigate the impact of optimizing emissions from different sectors on methane predictions. For the Aopt case, eight anthropogenic sectors (i.e., AGR, ENE, IND, TRA, RCO, WST, SHP, and BMB) are uniformly scaled by the ratio of ΔE to total anthropogenic emissions ($\Delta E/E_{anthro.}$), keeping the fractions of individual sources unchanged. For the Wopt case, wetland emissions are rescaled to increase this source by ΔE . For S1 and S2 scenarios, we scale the wetland sector only. The total E_{opt} emissions are the same for both Aopt and Wopt cases. Time series of optimized total emissions and emissions from major sectors from S0Aopt and S0Wopt over 1980-2017 are shown in Figure 1. As shown in Figure 1, the emission optimization to match observations resulted in higher interannual variability in total emissions than in the initial emissions. Although the interannual variability of methane emissions is mainly dominated by that from wetland and biomass burning, it could also exist in anthropogenic emissions due to the dependence of microbial methane sources, such as rice paddies, on soil temperature and precipitation (e.g., Knox et al., 2016). Because the purpose of S0Aopt is to investigate the role of changes in total anthropogenic emissions (including BMB) rather than individual sectors, we applied this interannual variability to all anthropogenic sectors which we acknowledge introduces some unrealistic interannual variability in the anthropogenic emissions. We chose this experimental construct to limit the number of sensitivity simulations.

Based on evidence from $\delta^{13}CH_4$, recent studies suggest increasing wetland emissions may be responsible for the renewed growth of methane (Dlugokencky et al., 2009; Nisbet et al., 2016). We perform two additional sensitivity simulations to test the possibility of wetland emissions driving the renewed methane growth during 2006-2014. One simulation is driven by repeating 2006 S0Aopt anthropogenic and biomass burning emissions for 2006-2014 but adjusting wetland emissions to ensure that the total methane emissions are the same as in S0Wopt (or S0Aopt), which would imply that the increases in methane emissions are only due to the increases in wetland emissions. This sensitivity simulation is referred to as “S0A06”. Another sensitivity simulation is driven by a combination of emissions for S0Aopt and S0Wopt as follows: S0Aopt emissions for 1980-2005 and S0Wopt emissions for 2006-2014. This simulation is referred to as “S0Comb”.

2030 **3 Results and discussions**

3.1 Model evaluation

The detailed model evaluation for S0Aopt and S0Wopt are discussed below. We first evaluate the mean climatological spatial distribution and seasonal variability simulated by the model and then evaluate the trends and variability.

3.1.1 Climatological evaluation

2035 Figure 2 shows the model bias and correlation coefficient of simulated climatological mean surface methane DMF against
NOAA GMD surface observations (Dlugokencky et al., 2018) for 1983-2017. The mean seasonal cycle at individual GMD
sites is shown in Figure S4 in the Supplement. GMD sites with at least 20 years of observations are selected for model
climatological evaluation. Information about these sites is shown in Table S2 in the Supplement. As shown in Figure 2a,
simulations with optimization of either anthropogenic (S0Aopt) or wetland (S0Wopt) emissions are generally able to reproduce
2040 surface methane DMF with model biases within ± 30 ppb at most sites. Both S0Wopt and S0Aopt simulate methane DMF
relatively well over the Southern Hemisphere. Going from south to north, the low bias in methane DMF decreases and becomes
a high bias over the tropics. Simulated methane in both S0Aopt and S0Wopt are biased moderately high over the tropical
Pacific Ocean (by up to ~ 40 ppb), indicating possible overestimation of methane emissions over the tropics and possible
underestimation in tropical OH levels. Large positive biases occur at Key Biscayne (KEY, 25.7 N, 80.2 W) and Mace Head
2045 (MHD, 53.3 N, 9.9 W) for both S0Wopt and S0Aopt, likely due to a model sampling bias, with model grid box overlapping
land while samples are collected with onshore winds. Over middle and high latitudes of the Northern Hemisphere, the
simulated surface methane DMF shows low and high biases at individual sites, possibly due in part to uncertainties in the local
emissions. As shown in Figure 2b, both S0Aopt and S0Wopt are able to capture the methane seasonal cycle at most sites (with
a correlation coefficient (R) larger than 0.5 for about 80% of sites). Both S0Aopt and S0Wopt are able to reproduce the methane
2050 seasonal cycle over the Southern Hemisphere. However, both S0Aopt and S0Wopt show poor performance in the seasonal
cycle over the southern tropical Pacific Ocean, with $R < 0.5$ (e.g., POCS10 and POCS15 in Figure S4 in the Supplement), but
show good performance in the seasonal cycle over the northern tropical Pacific Ocean, with $R = 0.9$ (e.g., POCN05, POCN10,
and POCN15 in Figure S4 in the Supplement). Poor performance also exists at a few sites in middle and high northern latitudes
(e.g., AZR, UUM, LEF, MHD, and ICE shown in Figure S4 in the Supplement), mainly due to overestimates of methane
2055 during summer. The major differences in simulated methane seasonal cycles between S0Aopt and S0Wopt occur over the
Northern Hemisphere, with slightly better performance by S0Wopt over the Pacific Ocean and by S0Aopt over continental
sites (e.g., UUM, WLG, UTA, and NWR). Uncertainties in the seasonality of methane emissions, OH abundances, and long-
range transport could lead to biases in the seasonal cycle. In general, both S0Aopt and S0Wopt are able to capture the methane
latitudinal gradient (e.g., $R = 0.9$). This suggests that the spatial distribution of methane in emissions is reasonable on the large
2060 scale despite uncertainties in representing local sources.

To investigate background tropospheric methane variability, Figure 3 shows the bias in the simulated vertical distribution of
methane with respect to HIPPO observations for the S0Aopt and S0Wopt simulations. S0Aopt and S0Wopt simulations
produce very similar methane profiles. Both S0Aopt and S0Wopt match observed methane profiles very well over the Southern
Hemisphere. Compared to HIPPO measurements, methane in both simulations is consistently high over the tropical Pacific
2065 Ocean (by up to ~ 50 ppb) from the surface to 700 mb during all HIPPO campaigns. These biases decrease with altitude and
decrease with latitude except for summer. In the Northern Hemisphere, both S0Wopt and S0Aopt simulations capture observed

methane from near the surface to 700 mb, but are generally biased low, except in summer when they are biased high, especially at mid-latitudes. Mid-latitude background methane is affected by both high-latitude and low-latitude air masses on synoptic scales. Biases over these regions could result from many processes (e.g., overestimation of the summer emissions, insufficient OH levels, and model transport). In general, the relative differences between the simulated methane profiles and HIPPO measurements are within 2% over most regions, demonstrating the capability of the improved GFDL-AM4.1 for simulating tropospheric methane.

3.1.2 Timeseries evaluation

As described in Section 2.2, we fit a function consisting of yearly harmonics and a polynomial trend, with fast fourier transform and low pass filtering of the residuals, to the monthly mean methane DMF (Thoning et al., 1989; Thoning, 2019) to estimate the timeseries and growth rates discussed below. The comparisons of simulated global mean background surface methane timeseries and growth rates to NOAA-GMD observations are shown in Figure 4. Both S0Wopt and S0Aopt predict similar global mean surface methane DMF, timeseries, and growth rates, since the global methane budget (emissions and sinks) is the same in the two simulations. S0Wopt and S0Aopt are also able to reproduce global annual mean surface methane DMF (with root-mean-square-error (RMSE) = 10.4 ppb in S0Wopt and 11.6 ppb in S0Aopt) over 1983-2017, which is expected from emission optimization. Meanwhile, both simulations are able to reproduce the methane timeseries very well (with $R = 1.0$ in both S0Wopt and S0Aopt) over different latitude bands as shown in Figure 4. The major discrepancies in surface methane DMF between model simulations and observations are mainly over low latitudes, especially the tropics, where the RMSE is greater than 20 ppb. Over the high northern latitudes, both S0Aopt and S0Wopt reproduce background methane DMF very well with RMSE less than 10 ppb. Over the high southern latitudes, both S0Aopt and S0Wopt underestimate background methane DMF by up to 35 ppb in the 1980s, which could be due in part to the fewer observational sites in the Southern Hemisphere used for emission optimization during this time period. In general, the agreement between the evolution of the simulated and observed global methane DMFs increases our confidence in the optimized methane emission trends used in this work.

Table 3 summarizes methane growth rates during 1984-1991, 1992-1998, 1999-2006, and 2007-2017. S0Aopt and S0Wopt simulate very similar methane growth rates as their emission totals are the same. During 1984-1991, both S0Aopt and S0Wopt slightly overestimate methane growth rates by ~ 2 ppb yr^{-1} , possibly due to fewer available observations used for emission optimization during this time period than afterwards. After 1991, the simulated methane growth rates are in general comparable to the observations (with annual mean difference within ± 1 ppb yr^{-1}). The major discrepancies in the simulated methane growth rates and observations occur over the tropics and high northern latitudes as shown in Figure 4. Over the tropics, both S0Aopt and S0Wopt overestimate methane growth rates (by about 5-10 ppb yr^{-1}) during 1984-1990 when there were limited observations available, but are able to reproduce methane growth rates relatively well afterwards. Agreement of the methane growth rate is worse in the Northern Hemisphere than in the Southern Hemisphere, especially at high northern latitudes, mainly due to the large bias during 1984-1988 and a slight shift in peak growth (or peak decrease) during 1997-2005. The number of

2100 observational MBL sites does not provide adequate coverage of the globe, especially in the 1980s, which could have different impacts on the Northern and Southern Hemisphere when optimizing global total emissions. In general, S0Aopt estimates slightly better methane growth rates than S0Wopt, especially over 30-90° N. The biases in methane growth rates also suggest a need to refine regional emissions.

S0Aopt and S0Wopt simulate very similar surface methane DMF and their comparison with NOAA-GMD observations at individual sites show both simulations to be biased low over Southern Hemisphere sites, but the low bias decreases northward (Figure S5 in the Supplement). The simulations are biased moderately high (by up to ~40 ppb) over tropical regions (e.g., POCS15, POCS10, SMO, POCS05, POCN00, CHR, and POCN05). These sites are mainly remote sites and surface methane DMF represents background methane levels. The overestimates are likely due to overestimation of emissions over Southeast Asia (e.g., Saeki and Patra, 2017, Patra et al., 2016, and Thompson et al., 2015), which could affect these remote sites through transport. However, the model predicts surface methane DMF relatively well at Ascension Island (ASC, 8°S, 14.4°W, 85 m), which is also a remote site without impacts from East Asia. The high biases over the tropics suggest a need to improve regional emissions (e.g., Southeast Asia). Moderate overestimates also occur at Mahe Island (SEY, 4.7°S, 55.5°E), a location that could be affected by air masses from polluted areas over the tropics and Northern Hemisphere. Over middle and high latitudes of the Northern Hemisphere, both S0Aopt and S0Wopt simulate surface methane DMF relatively well at most sites, except at Key Biscayne (KEY, 25.7°N, 80.2°W), Tae-ahn Peninsula (TAP, 36.7°N, 126.1°W), Park Falls (LEF, 45.9°N, 113.7°W), and Mace Head (MHD, 53.3°N, 9.9°W). KEY, MHD, and TAP are sampled under onshore winds, whereas LEF are affected by local sources and transport. The high biases at these sites could be due in part to model sampling bias (e.g., model grid box overlapping land while samples are collected at coast with onshore winds) and uncertainties in local emissions (e.g., possible overestimation in the emissions over East Asia). In general, both S0Wopt and S0Aopt are able to reproduce the surface methane DMF and capture the monthly variations at most sites (e.g., with R greater than 0.5 at 98% of total sites and with RMSE less than 30 ppb at 74% of total sites). As shown in Figure S5, S0Aopt in general better estimates methane timeseries and growth over low latitudes of the Southern Hemisphere (e.g., SMO) and middle/high latitudes of the Northern Hemisphere (e.g., ASK, KEY, WIS, UTA, NWR, UUA, LEF, CBA, STM, and ALT) than S0Wopt. Based on the site-level comparisons between S0Wopt and S0Aopt, anthropogenic emissions over Southeast Asia are likely overestimated in both S0Aopt and S0Wopt, while they could be underestimated at WLG and NWR in S0Wopt but be reasonably well represented in S0Aopt.

3.2 Global methane budget

Figure 5 shows time series of optimized total emissions, global sink, and global burden of methane based on S0Wopt. Since global totals in the S0Aopt and S0Wopt simulations are very similar, we only show the budget for S0Wopt. As depicted in Figure 5, the simulated global methane burden steadily increases from 1980 to 1992, with a growth rate of 39 Tg yr⁻¹. During 1993-1998, the global methane burden growth slows with a growth rate of 16 Tg yr⁻¹. The simulated growth rate in global methane burden decreases to 4 Tg yr⁻¹ during 1999-2006 while it increases to 16 Tg yr⁻¹ during 2007-2017 and reaches over 20 Tg yr⁻¹ during 2014-2016. The changes in the global burdens are due to the imbalance between methane emissions and

sinks. As shown in Figure 5, the optimized emissions in general increase during 1980-2017, with an annual mean of 580 ± 34 Tg yr⁻¹ (mean \pm standard deviation) and show much larger interannual variability during 1991-1993 and 1997-2000, which is likely due to the strong El Niño events during 1991-1992 and 1997-1998 as well as the Mt Pinatubo eruption in 1991 (Dlugokencky et al., 1996; Bousquet et al., 2006; Bândă et al., 2016). Although there is an overall increasing trend in total global emissions, growth in annual mean emissions has increased from the 1980s (with an annual emission growth rate of 3.9 Tg yr⁻¹) to the 1990s (4.4 Tg yr⁻¹), but decreased to 0.3 Tg yr⁻¹ during 2000-2006, and increased again to 2.3 Tg yr⁻¹ during 2007-2017. Interannual variability of the optimized emissions mainly results from interannual variability in simulated OH levels during emission optimization. Uncertainties in the interannual variability of simulated OH levels and therefore methane sinks could lead to uncertainties in the interannual variability of the optimized emissions.

Unlike methane emissions, the methane sink increases during 1980-2007, with relative stabilization during 2008-2014 but a resumed increase during 2015-2017. The annual mean methane sink during 1980-2017 is 560 ± 44 Tg yr⁻¹ (mean \pm standard deviation). The trends in methane sink are affected by the changes in both methane and OH levels (assuming that other sinks are minor) and temperature. Figure 6 shows the tropospheric OH anomalies with respect to 1998-2007. An interesting finding is that AM4.1 predicts higher OH levels during 2008-2014 than 1998-2007 by 3.1%, whereas previous studies applying multispecies inversion with a box-model framework (e.g., Rigby et al., 2017; Turner et al., 2017) suggest a decline in OH levels after 2007. However, a recent study by Naus et al. (2019) found a shift to positive OH trend over 1994-2015 after applying bias corrections based on a 3-D chemical transport model to a similar box model setup. In addition, OH levels simulated by AM4.1 decrease from 2013 to 2015 but increase again afterwards, leading to an increase in methane sinks during 2015-2017. As shown in Figure 5, larger methane emissions than sinks during 1980-1998 lead to an increase in methane burden. A relative balance between methane sources and sinks during 1999-2006 leads to the methane stabilization. Compared to 1999-2006, both methane sources and sinks are greater during 2007-2017, but methane emissions outweigh sinks after 2007 leading to renewed methane growth.

Table 4 provides a summary of the decadal mean methane budget for 1980-2017. Compared to Kirschke et al. (2013) and Saunio et al. (2019), total natural emissions from the initial emission inventories (203 Tg yr⁻¹) are at the lower range of top-down estimates during this period, except for the 1990s, when they are slightly greater than top-down estimates but still much lower than the bottom-up estimates. Since there is no observational constraint on bottom-up estimates, total natural emissions are simply summed over independent individual sources, which could be overestimated in the bottom-up approach considering the relatively large uncertainties in each individual source. In addition, in the bottom-up estimate from Kirschke et al. (2013) and Saunio et al. (2016), some other natural sources, such as freshwater, are not included in the initial emission inventories in this work; however, they are likely double counted in the bottom-up estimates (e.g., high-latitude inland waters are likely also considered as wetland areas) as pointed out in Saunio et al. (2019). The natural emissions estimated in this work (e.g., 203 - 297 Tg yr⁻¹) are much more comparable to previous top-down estimates (e.g., 150 - 273 Tg yr⁻¹ as shown in Kirschke et al., 2013), which demonstrates confidence in the natural source estimates. Total anthropogenic emissions from the initial emission inventories are overall within the range of top-down or bottom-up estimates, except for 1980-1989, when they are

less than the estimates in Kirschke et al. (2013). The low values in the 1980s result mainly from low estimated emissions from agriculture and waste sectors in the CEDS inventory. With the optimized global total emissions, the total sources used in this work and the total sinks estimated by AM4.1 are in the range of either top-down or bottom-up estimates by previous studies. As a result, the imbalance between total emissions and total sinks estimated in this work is, overall, within the range of estimates by previous studies although we find a smaller imbalance than previous estimates for the 2000s and afterwards. The atmospheric growth rates simulated by the model (sampled identically as for observations) are also comparable to the observed atmospheric growth rates.

3.3 Source tagged tracers

In this section, we apply the Mann-Kendall (M-K) test to estimate the linear trend of global mean source tagged tracers and total methane for 1983-1998, 1999-2006, and 2007-2017 to investigate possible drivers of total methane trends. Figure 7 compares the trends of source tagged tracers and total methane from S0Aopt and S0Wopt during each time period. For S0Aopt, total methane increases strongly at 10.5 ppb yr^{-1} during 1983-1998. The tagged anthropogenic tracers all show increasing trends during 1983-1998 despite the increases in OH levels, with dominant increasing trends by CH4AGR and CH4WST consistent with emission trends. Since wetland emissions and other natural emissions are kept constant every year in S0Aopt, with increases in OH levels during 1983-1998, all tagged natural tracers show a weak decreasing trend. During 1999-2006, total methane shows a small increasing trend of 1.0 ppb yr^{-1} , due to the increasing trends of CH4ENE and CH4WST compensated by the decreasing trends of other source tagged tracers. The increasing trends of CH4ENE and CH4WST are mainly driven by the increases in the emissions from energy and waste sectors in S0Aopt whereas the decreasing trends of other source tagged tracers are mainly driven by the increases in OH levels. Compared to the rapid growth during 1983-1998, only CH4ENE growth rate shows a small increase during 1999-2006 (2.6 ppb yr^{-1} vs. 2.2 ppb yr^{-1} in 1983-1998), with all other tracers show a decrease in their growth rates. Despite higher anthropogenic emissions during 1999-2006 than previous periods, the sinks are also higher, leading to a relative stabilization. During 2007-2017, total methane shows a renewed increasing trend of 5.3 ppb yr^{-1} , dominated by a strong increasing trend of CH4ENE (5.9 ppb yr^{-1}) and smaller increasing trends of CH4AGR and CH4WST. Compared to 1999-2006, there is a significant increase in CH4ENE growth rate with smaller increases in CH4AGR growth rate during 2007-2017. Although the CH4WST growth rate decreased in 2007-2017, the continued increasing trend of CH4WST together with those of CH4AGR and CH4ENE contributes to the renewed growth in methane. The results from S0Aopt suggest that globally, anthropogenic tracers dominate total methane trends during the entire simulation period. During the 1980s and 1990s, emissions from agriculture, energy, and waste sectors are the major contributors to the methane increase. During 1999-2006, when atmospheric methane stabilizes, increases in methane sinks and methane sources alternatively dominate the trend for different tracers. Compared to 1999-2006, higher emissions from agriculture, energy, and waste sectors during 2007-2017 are the major drivers for the renewed growth in methane, with energy sector as the largest contributor

The source tagged tracers behave slightly differently in S0Wopt. For S0Wopt, total methane shows a similar increasing trend as S0Aopt. During 1983-1998, the tagged anthropogenic tracers all show increasing trends except CH4ENE, with overall smaller increasing trends than those in S0Aopt. CH4WET shows a strong increasing trend (7.0 ppb yr⁻¹), dominating the total methane trend. This is mainly because wetland emission growth is larger than anthropogenic emission growth due to the emission optimization in S0Wopt during this period. During 1999-2006, similar to S0Aopt, the total methane trend results from the increasing trends of CH4ENE and CH4WST compensated by the decreasing trends of other source tagged tracers. During this time, CH4WET shows a slightly decreasing trend (-0.8 ppb yr⁻¹), reflecting the slightly greater CH4WET sinks (226 Tg yr⁻¹) than emissions (223 Tg yr⁻¹). Similar to S0Aopt, only CH4ENE shows an increase in its growth rate during this time period compared to previous time periods. During 2007-2017, the total methane trend is dominated by the increasing trends of CH4AGR, CH4ENE, and CH4WST, with CH4ENE as the largest contributor, similar to S0Aopt. On the other hand, CH4WET shows a significant decreasing trend during this period, with CH4WET sinks (217 Tg yr⁻¹) larger than emissions (206 Tg yr⁻¹). Compared to 1999-2006, there is a significant increase in CH4ENE growth rate with a noticeable increase in CH4AGR growth rate during 2007-2017. Although the CH4WST growth rate also decreased in 2007-2017, similar to S0Aopt, the continued increasing trend of CH4WST together with those of CH4AGR and CH4ENE contributes to the renewed growth in methane. On the other hand, CH4WET shows a significant decrease in its growth rate during this time period compared to 1999-2006, mainly due to lower emissions (206 Tg yr⁻¹ in 2007-2017 vs. 223 Tg yr⁻¹ in 1999-2006) imposed in this scenario. Compared to the S0Aopt results, S0Wopt suggests CH4WET as the largest contributor for the methane trends during 1980s and 1990s, mainly due to emission optimization of different sectors. However, both scenarios suggest CH4AGR, CH4WST, and CH4ENE are the major contributors to the renewed growth in methane, with CH4ENE as the largest contributor. As shown in Figures 5 and 6, OH levels slightly decrease and methane sinks are relatively stable during 2007-2013, but large interannual variability exists during 2013-2017. Decreasing OH levels could lead to increases in methane lifetime and therefore methane buildup. Combined with increases in the emissions, methane starts to increase again during this period. However, it is difficult to separate the contributions from methane emissions and sinks as optimized methane emissions are based on methane mass balance (e.g., changes in methane loss would act as a feedback on estimates of optimized total emissions). Nevertheless, it is clear that the decrease in OH levels alone (e.g., if emissions are kept constant) would not be enough to reproduce the renewed growth. The remaining question then is which emission sector(s) is (are) the major contributor(s) to the renewed growth over 2007 to 2017. Both S0Wopt and S0Aopt suggest that agriculture, waste, and energy sectors are the major contributors to renewed methane growth. However, both cases depend largely on the initial emission inventory and the scaling methods chosen. For example, S0Wopt relies on the emission growth of other sectors from the initial emission inventory, which means if the emission growth of a certain sector is overestimated or underestimated in the initial emission inventory, it would lead to different results. Therefore, we conducted two additional sensitivity simulations (i.e., S0A06 and S0Comb as described in Section 2.3) with different emission growths for anthropogenic and wetland sectors as in S0Aopt and S0Wopt for 2006-2014.

The trends for source tagged tracers and total methane by S0A06 and S0Comb are shown in Figure 7. Interestingly, in S0A06, where anthropogenic and biomass burning emissions are kept constant every year for 2006-2014, anthropogenic tracers, particularly CH4ENE and CH4WST, still show increasing trends during 2007-2014, whereas CH4WET shows a small decreasing trend despite rising emissions. As OH levels slightly decrease during this time (but are still higher than 1999-2006), with constant emissions except wetland, one might expect possible increasing trends in all tagged tracers except CH4WET. In fact, major anthropogenic tracers such as CH4AGR, CH4ENE, CH4WST, and CH4BMB increase over 2007-2014 in S0A06, but at a slower rate than in S0Wopt (and S0Aopt) due to no emission growth for these tracers. On the other hand, the decreasing OH levels (Figure 8) would lead to a smaller methane sink and therefore higher methane concentrations. Since methane loss is proportional to the product of OH levels and methane concentrations, and concentrations of CH4WET are much greater than other source tagged tracers, the loss of CH4WET is also much greater than other tracers. Higher CH4WET loss (223 Tg yr^{-1}) than CH4WET emissions (222 Tg yr^{-1}) leads to a slightly decreasing trend in CH4WET. In other words, despite the increasing source contributions from wetlands to total methane emissions, the relative contributions of wetland tracer to total methane abundance is declining. Compared to 1999-2006, there are major increases in the growth rates of CH4ENE and CH4BMB, with smaller increase in CH4AGR and CH4OAT growth rates, which drives the renewed methane growth. Meanwhile, CH4WET is still declining during 2007-2014 (-1.1 ppb yr^{-1}), but at a larger decrease rate than 1999-2006 (-0.8 ppb yr^{-1}). Nevertheless, S0A06 results suggest that the renewed growth during 2007-2014 is contributed by the increased growth rates of CH4ENE, CH4BMB, and CH4AGR as well as increasing trend of CH4WST, mainly due to higher anthropogenic emissions than 1999-2006 and decreases in OH levels during 2008-2014. The results also suggest OH trends play an important role in determining the increasing trend of total methane since emissions of the energy and waste sectors are kept constant in this sensitivity simulation. In addition, increases in wetland emissions alone are not able to drive increases in CH4WET over this period, as CH4WET sinks are equally important for determining the trend in CH4WET. Our analysis also suggests that increased emissions from other microbial sources (e.g., agriculture and waste) are needed to match the observed negative trend in $\delta^{13}\text{CH}_4$ since 2007 (Nisbet et al., 2019).

The trends for source tagged tracers and total methane behave differently in S0Comb, where we combine S0Aopt emissions for 1980-2005 and S0Wopt emissions for 2006-2014. During 2007-2014, all anthropogenic tracers show decreasing trends except CH4ENE (2.8 ppb yr^{-1}), whereas CH4WET shows a significant increasing trend (5.9 ppb yr^{-1}) and dominates the total methane trend. This is mainly due to lower anthropogenic emissions during this period than previous periods, allowing sinks of anthropogenic methane tracers to start to take over their trends except for CH4ENE. At the same time, significantly higher wetland emissions during this period than previous periods dominate the increasing trend of CH4WET. Interestingly, even with the same wetland emissions in S0Wopt and S0Comb for 2006-2014, CH4WET shows different trends. This is mainly because the CH4WET concentrations at the beginning of 2006 are much lower in S0Comb than in S0Wopt. Therefore, CH4WET loss is much lower in S0Comb (190 Tg yr^{-1}) compared to S0Wopt (220 Tg yr^{-1}) over this time, leading to an increasing CH4WET trend in S0Comb, but a decreasing trend in S0Wopt. Compared to 1999-2006, there is a significant increase in CH4WET growth rate with a minor increase in CH4ENE growth rates during 2007-2014, which drives the renewed

growth in methane. S0Comb results suggest the need for a sharp increase in wetland emissions with concomitant sharp decrease in anthropogenic emissions in 2006 to drive the methane growth by wetland tracer. It is a likely scenario for a sharp increase in wetland emissions considering the interannual variability. However, it is a less likely scenario for a concomitant sharp decrease in anthropogenic emissions as both top-down and bottom-up inventories indicate anthropogenic emissions increasing over 2000s. A more likely scenario is that both anthropogenic and wetland emissions increase (i.e., higher during 2007-2014 than 1999-2006). However, in that case, the dominance of wetland emissions in driving the total methane trend would decrease based on our analysis.

3.4 Sensitivity to OH levels

As described in Section 2.3, we perform two additional simulations for low and high OH levels (i.e., S1 and S2) for 1980-2017 to investigate the sensitivity of methane predictions to different OH levels. For both OH cases, the interannual variations in OH levels are the same as in S0 because the simulations are driven by the same meteorology. Figures 8(a) and (b) show global tropospheric OH concentrations, OH-driven methane loss, and tropospheric methane lifetime for the three cases (i.e., S0, S1, and S2) in which wetland emissions are optimized (Wopt; Aopt has a very similar global OH trend as Wopt). Compared to S0, scaling LNO_x production in the model by a factor of 0.5 leads to a reduction in simulated annual global mean OH levels by -6.4 % and an increase in methane lifetime by 0.5 years in S1 over 1980-2017; scaling by a factor of 2 leads to an increase in simulated annual global mean OH by +9.1% and a decrease in methane lifetime by 0.7 years in S2. The global mean OH levels increase from 1980 to 2008 (by 3.6%, with respect to 1980 level), decrease from 2008 to 2015 (by 2.3%, with respect to 2008 level), and increase from 2015 to 2017 (by 4.6%, with respect to 2015 level). However, compared to 1998-2007 average, OH levels during 2008-2015 and 2015-2017 are still greater by 2.5% and 1.3%, respectively. Changes in OH levels depend on a number of factors (e.g., temperature, water vapor, O₃, NO_x, CO, and VOCs). Therefore, OH is influenced by the specific chemistry and forcing data used in the model. Nevertheless, our estimates in OH trends and variabilities from all three cases are quite comparable to the those estimated by the Chemistry-Climate Model Initiative (CCMI) models (e.g., Zhao et al., 2019). Since emission optimization is also based on methane sinks, the total optimized emissions in S1 are lower than those in S0 by about 4.1% (with an annual mean of -24 Tg yr⁻¹), and the total optimized emissions in S2 are higher than those in S0 by about 5.8% (or 33 Tg yr⁻¹). This indicates that a 1% change in OH levels could lead to about 4 Tg yr⁻¹ difference in the optimized emissions. Increasing methane loss due to OH is simulated for 1980-2007 in the three cases due to increases in OH and methane concentrations (except over the stabilization period when methane was not increasing but OH was increasing). During 2007-2013, the simulated decrease in OH levels combined with increasing methane concentrations leads to relative stabilization in OH-driven methane loss in the three cases. The large interannual variability in OH levels during 2013-2017 dominates the interannual variability in methane OH loss despite the continued increases in methane.

All three simulations show a similar trend for tropospheric methane lifetime, with a decreasing trend from 1980 to 2007 (-0.04 year yr⁻¹ in S0, -0.05 year yr⁻¹ in S1, and -0.03 year yr⁻¹ in S2), a clear increasing trend during 2011-2015 (0.08 year yr⁻¹ in all three simulations), and a decreasing trend during 2015-2017 (-0.2 year yr⁻¹ in all three simulations). The mean tropospheric

methane lifetime due to OH loss for 1980-2017 is 9.9 ± 0.4 years in S0Wopt, which is about 0.5 year lower than S1Wopt (10.4 \pm 0.5 years), and about 0.7 year higher than S2Wopt (9.2 \pm 0.3 years), due to different OH levels and therefore methane sinks, but with similar methane burdens. This indicates that a 1% change in OH levels could lead to about 0.08 year difference in the tropospheric methane lifetime. The mean tropospheric methane lifetime simulated by the three simulations is within the uncertainty range of model estimates of $9.3 \pm 0.9 \sim 9.8 \pm 1.6$ years (Voulgarakis et al., 2013; Naik et al., 2013b) and in general comparable to the observation-derived estimates of 9.1 ± 0.9 years for the present-day (Prather et al., 2012), with a slightly higher estimate by S1Wopt. All simulations show an increase in methane lifetime during 2011-2015, which could be a signal of the methane feedback on its lifetime (Holmes, 2018) in the model. Continued increases in methane emissions (Figure 5) during this time, along with decreases in tropospheric OH concentrations (Figure 8), lengthen the lifetime of methane and therefore amplify methane's response to emission changes. If methane emissions continue to increase, we can expect stronger increases in atmospheric methane due to the amplifying effect of the methane-OH feedback as occurred in the significant increases in methane growth rates during 2014 and 2015.

4 Conclusions

In this work, we thoroughly evaluate the atmospheric methane budget simulated by the GFDL atmospheric chemistry model AM4.1 and apply the model to attribute the drivers of changes in global methane over the past four decades. We simulate methane and related tracers for 1980-2017 by driving the model with gridded emissions compiled from various sources. To match the long-term record of surface methane measurements, we optimize global total methane emissions using a simple mass-balance approach. Our optimized global total methane emissions are within the range of estimates by previous studies (both bottom-up and top-down). The GFDL-AM4.1 simulations with emissions following two different optimizations (anthropogenic sources and wetlands) both reproduce observed global methane trends and variabilities, despite the different contributions from anthropogenic and wetland emissions. This, therefore, suggests that accurate estimates of global total emissions and of their interannual variability are critical in predicting the global methane trend and its variability, despite uncertainties in the estimates of individual sources. In addition, both simulations are in general able to capture the spatial distribution and seasonal cycle of methane as observed by NOAA GMD sites and vertical distribution of methane as measured from aircraft, demonstrating the reasonable spatial and temporal representations of the optimized emissions derived in this work.

We then explore the contributions of changes in methane sources and sinks to methane trends and variability over 1980-2017. The simulation with optimization of anthropogenic emissions shows increasing anthropogenic emissions to drive the rapid methane growth during 1980s and 1990s, whereas the simulation with optimization of wetland emissions also shows wetland to be one of the major contributors during these periods. However, both simulations suggest increases in methane sources (mainly from agriculture, energy, and waste sectors), balanced by the increases in methane sinks (mainly due to increases in

OH levels), lead to methane stabilization during 1999-2006, and that the agriculture, energy, and waste sectors are the major contributors to the renewed growth in methane after 2006.

Two additional sensitivity simulations further investigate the contributions of wetlands to the methane renewed growth during 2007-2014. The simulation with repeating 2006 emissions for all the sectors except wetland shows a declining contribution of wetland tracer to total methane abundance despite of the increasing contribution of wetland emissions to total emissions, because sinks are equally important for determining the tracer trend. Results from a simulation with combined optimizations (i.e., 1980-2005 optimized anthropogenic emissions and 2006-2014 optimized wetland emissions) suggest that a sharp increase in wetland emissions (a likely scenario) with concomitant sharp decrease in anthropogenic emissions (a less likely scenario), would be required starting in 2006 to drive the methane growth by wetland tracer.

Two additional sensitivity simulations, with low and high OH levels (by scaling LNO_x production in the model by a factor of 0.5 and 2), further investigate methane OH loss and tropospheric methane lifetime. In general, OH trends dominate methane OH loss trends during different methane growth periods except 2007-2013, when methane OH loss shows little change due to the decrease in OH levels combined with the increase in methane concentrations. The results also indicate that a 1% change in OH levels could lead to about 4 Tg yr⁻¹ difference in the optimized emissions and 0.08 year difference in the estimated tropospheric methane lifetime. The increasing methane lifetime during 2011-2015 in all the OH sensitivity simulations indicate a possible methane feedback on its lifetime in the model. Continued increases in methane emissions along with decreases in tropospheric OH concentrations extend the lifetime of methane and therefore amplify methane's response to emission changes. Essentially, the global atmospheric methane trend is driven by the competition between its emissions and sinks. Our model results suggest that the methane stabilization during 1999-2006 is mainly due to increasing emissions balanced by increasing sinks, whereas the methane renewed growth during 2007-2013 is mainly due to increasing sources combined with little change in sinks despite small decreases in OH levels. The significant increases in methane growth during 2014-2015 are mainly due to increasing sources combined with decreasing sinks. Most of the model simulations conducted here suggest that increases in energy sources drive the renewed methane growth, in agreement with previous studies (e.g., Rice et al., 2016; Hausmann et al., 2016; Worden et al., 2017), with second largest contributor from waste sector and third largest contributor from agriculture sector, consistent with the shift in the isotopic ratio $\delta^{13}\text{CH}_4$. However, optimization of emissions from anthropogenic sources depends on the "shares" of individual anthropogenic sectors in the initial emission inventories. Uncertainties in these shares could lead to uncertainties in the emission adjustment for each anthropogenic sector. Recent studies using methane isotopic composition suggest that renewed growth in methane since 2007 is more likely due to the increases in biogenic sources (e.g., Schaefer et al., 2016) as $\delta^{13}\text{CH}_4$ is shifting to more negative values after increasing during the 1980s and 1990s and relatively stable during 1999-2006. However, this shift could also imply increases in isotopically lighter fossil fuel emissions, or decreases in isotopically heavy sources (e.g., biomass burning), or increases in both microbial and fossil fuel emissions but with increases in microbial emissions stronger than those from fossil fuel sources (Nisbet et al., 2019). It is quite possible that, rather than the energy sector, the increases in the agriculture and waste sectors could be the largest contributors to the renewed

growth in methane. In that case, it is possible that the growth of agriculture and waste emissions could be underestimated in the optimized emissions, while the growth of energy emissions could be overestimated.

2365 The optimized emission totals estimated in this work represent temporal and spatial distribution of methane total sources reasonably well. However, the emission adjustments are either applied to anthropogenic (including biomass burning) sectors only (uniformly to all anthropogenic sectors) or wetland sector only. Uncertainties therefore exist on the distribution of the emission adjustments to individual sectors. Without accurate estimates of emissions from individual sources, it would be difficult to attribute the methane trend and variability to specific sectors. The application of methane isotopes and additional
2370 observational constraints (e.g., ethane and $\delta^{13}\text{CH}_4$) could potentially help better partition the emission adjustments to different sectors. In addition, the spatial distribution of optimized emissions depends on the spatial information in the initial emission inventories. Uncertainties in the spatial distribution from the initial emission inventories may remain in the optimized emissions. Our model evaluation suggests that the optimized inventory may overestimate tropical emissions. A process-based emission model (e.g., wetland emissions) coupled with AM4.1 may better represent the spatial and temporal patterns of the
2375 emissions than prescribed in the present work.

Author contribution

Jian He and Vaishali Naik designed the research. Jian He developed the model configuration, performed model simulations, analyzed model results, and prepared the manuscript with contributions from all co-authors. Vaishali Naik provided GFDL-model ready CMIP6 emissions. Larry Horowitz led the development of the base configuration of AM4.1 and provided
2380 meteorological data for nudging. Ed Dlugokencky provided surface observations. Kirk Thoning provided scripts to process observational data. All authors contributed to the discussion of results.

Acknowledgements

This work is supported by the Carbon Mitigation Initiative at Princeton University. Atmospheric methane dry air mole fractions are obtained from the NOAA ESRL Carbon Cycle Cooperative Global Air Sampling Network (Dlugokencky et al., 2018, ftp://aftp.cmdl.noaa.gov/data/trace_gases/ch4/flask/surface/). The globally averaged marine surface monthly mean data and annual mean growth rates are obtained from www.esrl.noaa.gov/gmd/ccgg/trends_ch4/. HIPPO data is obtained from Wofsy et al. (2012), Merged 10-second Meteorology, Atmospheric Chemistry, Aerosol Data (R_20121129). We are grateful to Prabir Patra for providing methane emissions for nearshore exchange and mud volcanoes. We also thank Fabien Paulot for processing sea surface temperatures and sea ice data and the GFDL model development team for developing the AM4.1.

1390 References

- Bândă, N., Krol, M., van Weele, M., van Noije, T., Le Sager, P., and Röckmann, T.: Can we explain the observed methane variability after the Mount Pinatubo eruption?, *Atmos. Chem. Phys.*, 16, 195–214, <https://doi.org/10.5194/acp-16-195-2016>, 2016.
- 1395 Bloom, A. A., Bowman, K. W., Lee, M., Turner, A. J., Schroeder, R., Worden, J. R., Weidner, R., McDonald, K. C., and Jacob, D. J.: A global wetland methane emissions and uncertainty dataset for atmospheric chemical transport models (WetCHARTs version 1.0), *Geosci. Model Dev.*, 10, 2141–2156, <https://doi.org/10.5194/gmd-10-2141-2017>, 2017.
- Bousquet, P., Ciais, P., Miller, J. B., Dlugokencky, E. J., Hauglustaine, D. A., Prigent, C., van der Werf, G. R., Peylin, P., Brunke, E.-G., Carouge, C., Langenfelds, R. L., Lathiere, J., Papa, F., Ramonet, M., Schmidt, M., Steele, L. P., Tyler, S. C., and White, J.: Contribution of anthropogenic and natural sources to atmospheric methane variability, *Nature*, 443, 439–443, 1400 [doi:10.1038/nature05132](https://doi.org/10.1038/nature05132), 2006.
- Bousquet, P., Ringeval, B., Pison, I., Dlugokencky, E. J., Brunke, E.-G., Carouge, C., Chevallier, F., Fortems-Cheiney, A., Frankenberg, C., Hauglustaine, D. A., Krummel, P. B., Langenfelds, R. L., Ramonet, M., Schmidt, M., Steele, L. P., Szopa, S., Yver, C., Viovy, N., and Ciais, P.: Source attribution of the changes in atmospheric methane for 2006–2008, *Atmos. Chem. Phys.*, 11, 3689–3700, [doi:10.5194/acp-11-3689-2011](https://doi.org/10.5194/acp-11-3689-2011), 2011.
- 1405 Brasseur, G. P., Hauglustaine, D. A., Walters, S., Rasch, P. J., Muller, J. F., Granier, C., and Tie, X. X.: MOZART, a global chemical transport model for ozone and related chemical tracers, 1. Model description, *J. Geophys. Res. A.*, 103(D21), 28 265–28 289, 1998.
- Dalsøren, S. B., Myhre, C. L., Myhre, G., Gomez-Pelaez, A. J., Søvde, O. A., Isaksen, I. S. A., Weiss, R. F., and Harth, C. M.: Atmospheric methane evolution the last 40 years, *Atmos. Chem. Phys.*, 16, 3099–3126, [https://doi.org/10.5194/acp16-3099-](https://doi.org/10.5194/acp16-3099-2016) 1410 2016, 2016.
- Dentener, F., Kinne, S., Bond, T., Boucher, O., Cofala, J., Generoso, S., Ginoux, P., Gong, S., Hoelzemann, J. J., Ito, A., Marelli, L., Penner, J. E., Putaud, J.-P., Textor, C., Schulz, M., van der Werf, G. R., and Wilson, J.: Emissions of primary aerosol and precursor gases in the years 2000 and 1750 prescribed data-sets for AeroCom, *Atmos. Chem. Phys.*, 6, 4321–4344, [doi:10.5194/acp-6-4321-2006](https://doi.org/10.5194/acp-6-4321-2006), 2006.
- 1415 Dlugokencky, E. J., Dutton, E. G., Novelli, P. C., and Masarie, K. A.: Changes in CH₄ and CO growth rates after the eruption of Mt. Pinatubo and their link with changes in tropical tropospheric UV flux, *Geophys. Res. Lett.*, 23, 2761–2764, 1996.
- Dlugokencky, E. J., Houweling, S., Bruhwiler, L., Masarie, K., Lang, P., Miller, J., and Tans, P.: Atmospheric methane levels off: Temporary pause or a new steady-state?, *Geophys. Res. Lett.*, 30, 19, [doi:10.1029/2003GL018126](https://doi.org/10.1029/2003GL018126), 2003.
- Dlugokencky, E. J., Myers, R., Lang, P., Masarie, K., Crotwell, A., Thoning, K., Hall, B., Elkins, J., and Steele, L.: Conversion of NOAA atmospheric dry air CH₄ mole fractions to a gravimetrically prepared standard scale, *J. Geophys. Res.*, 110, D18306, 1420 [doi:10.1029/2005JD006035](https://doi.org/10.1029/2005JD006035), 2005.

- Dlugokencky, E. J., Bruhwiler, L., White, J. W. C., Emmons, L. K., Novelli, P. C., Montzka, S. A., Masarie, K. A., Lang, P. M., Crotwell, A. M., Miller, J. B., and Gatti, L. V.: Observational constraints on recent increases in the atmospheric CH₄ burden, *Geophys. Res. Lett.*, 36, L18803, 10.1029/2009GL039780, 2009.
- 2425 Dlugokencky, E. J., Nisbet, E. G., Fisher, R., and Lowry, D.: Global atmospheric methane: budget, changes and dangers, *Philos. T. R. Soc. A*, 369, 2058–2072, 2011.
- Dlugokencky, E. J., Lang, P. M., Crotwell, A. M., Mund, J. W., Crotwell, M. J., and Thoning, K. W.: Atmospheric Methane Dry Air Mole Fractions from the NOAA ESRL Carbon Cycle Cooperative Global Air Sampling Network, 1983–2017, Version: 2018-08-01, Path: ftp://aftp.cmdl.noaa.gov/data/trace_gases/ch4/flask/surface/, 2018.
- 2430 Donner, L. J., Wyman, B. L., Hemler, R. S., Horowitz, L. W., Ming, Y., Zhao, M., Golaz, J.-C., Ginoux, P., Lin, S.-J., Schwarzkopf, M. D., Austin, J., Alaka, G., Cooke, W. F., Delworth, T. L., Freidenreich, S. M., Gordon, C. T., Griffies, S. M., Held, I. M., Hurlin, W. J., Klein, S. A., Knutson, T. R., Langenhorst, A. R., Lee, H.-C., Lin, Y., Magi, B. I., Malyshev, S. L., Milly, P. C. D., Naik, V., Nath, M. J., Pincus, R., Ploshay, J. J., Ramaswamy, V., Seman, C. J., Shevliakova, E., Sirutis, J. J., Stern, W. F., Stouffer, R. J., Wilson, R. J., Winton, M., Wittenberg, A. T., and Zeng, F.: The Dynamical Core, Physical
2435 Parameterizations, and Basic Simulation Characteristics of the Atmospheric Component AM3 of the GFDL Global Coupled Model CM3, *J. Clim.*, 24, 3484–3519, doi:10.1175/2011JCLI3955.1, 2011.
- Etheridge, D. M., Steele, L. P., Francy, R. J., and Langenfelds, R. L.: Atmospheric methane between 1000 A. D. and present: Evidence of anthropogenic emissions and climatic variability, *J. Geophys. Res.*, 103, 15 979–15 993, 1998.
- Etiopie, G. and Milkov, A. V.: A new estimate of global methane flux from onshore and shallow submarine mud volcanoes to
2440 the atmosphere, *Environ. Geol.*, 46, 997–1002, doi:10.1007/s00254-004-1085-1, 2004.
- Fiore, A. M., Dentener, F. J., Wild, O., Cuvelier, C., Schultz, M. G., Hess, P., Textor, C., Schulz, M., Doherty, R. M., Horowitz, L. W., MacKenzie, I. A., Sanderson, M. G., Shindell, D. T., Stevenson, D. S., Szopa, S., van Dingenen, R., Zeng, G., Atherton, C. S., Bergmann, D. J., Bey, I., Carmichael, G. R., Collins, W. J., Duncan, B. N., Faluvegi, G., Folberth, G. A., Gauss, M., Gong, S., Hauglustaine, D., Holloway, T., Isaksen, I. S. A., Jacob, D. J., Jonson, J. E., Kaminski, J. W., Keating, T. J., Lupu,
2445 A., Marmer, E., Montanaro, V., Park, R. J., Pitari, G., Pringle, K. J., Pyle, J. A., Schroeder, S., Vivanco, M. G., Wind, P., Wojcik, G., Wu, S., and Zuber, A.: Multimodel estimates of intercontinental source-receptor relationships for ozone pollution, *J. Geophys. Res.*, 114, D04301, doi:10.1029/2008JD010816, 2009.
- Fiore, A. M., Horowitz, L. W., Dlugokencky, E. J., and West, J. J.: Impact of meteorology and emissions on methane trends, 1990–2004, *Geophys. Res. Lett.*, 33, L12809, doi:10.1029/2006GL026199, 2006.
- 2450 Fiore, A. M., Jacob, D. J., Field, B. D., Streets, D. G., Fernandes, S. D., and Jang, C.: Linking ozone pollution and climate change: The case for controlling methane, *Geophys. Res. Lett.* 29(19), 1919, doi:10.1029/2002GL015601, 2002.
- Fung, I., John, J., Lerner, J., Matthews, E., Prather, M., Steele, L. P., and Fraser, P. J.: Three-dimensional model synthesis of the global methane cycle, *J. Geophys. Res.*, 96, 13033–13065, 1991.
- Ghosh, A., Patra, P. K., Ishijima, K., Umezawa, T., Ito, A., Etheridge, D. M., Sugawara, S., Kawamura, K., Miller, J. B.,
2455 Dlugokencky, E. J., Krummel, P. B., Fraser, P. J., Steele, L. P., Langenfelds, R. L., Trudinger, C. M., White, J. W. C., Vaughn,

- B., Saeki, T., Aoki, S., and Nakazawa, T.: Variations in global methane sources and sinks during 1910–2010, *Atmos. Chem. Phys.*, 15, 2595–2612, <https://doi.org/10.5194/acp-15-2595-2015>, 2015.
- Gidden, M. J., Riahi, K., Smith, S. J., Fujimori, S., Luderer, G., Kriegler, E., van Vuuren, D. P., van den Berg, M., Feng, L., Klein, D., Calvin, K., Doelman, J. C., Frank, S., Fricko, O., Harmsen, M., Hasegawa, T., Havlik, P., Hilaire, J., Hoesly, R.,
2460 Horing, J., Popp, A., Stehfest, E., and Takahashi, K.: Global emissions pathways under different socioeconomic scenarios for use in CMIP6: a dataset of harmonized emissions trajectories through the end of the century, *Geosci. Model Dev.*, 12, 1443–1475, <https://doi.org/10.5194/gmd-12-1443-2019>, 2019.
- Gromov, S., Brenninkmeijer, C. A. M., and Jöckel, P.: A very limited role of tropospheric chlorine as a sink of the greenhouse gas methane, *Atmos. Chem. Phys.*, 18, 9831–9843, <https://doi.org/10.5194/acp-18-9831-2018>, 2018.
- 2465 Guenther, A., Karl, T., Harley, P., Wiedinmyer, C., Palmer, P. I., and Geron, C.: Estimates of global terrestrial isoprene emissions using MEGAN (Model of Emissions of Gases and Aerosols from Nature), *Atmos. Chem. Phys.*, 6, 3181–3210, <https://doi.org/10.5194/acp-6-3181-2006>, 2006.
- Hausmann, P., Sussmann, R., and Smale, D.: Contribution of oil and natural gas production to renewed increase in atmospheric methane (2007–2014): top–down estimate from ethane and methane column observations, *Atmos. Chem. Phys.*, 16, 3227–
2470 3244, <https://doi.org/10.5194/acp-16-3227-2016>, 2016.
- Hess, P. G., Flocke, S., Lamarque, J.-F., Barth, M. C., and Madronich, S.: Episodic modeling of the chemical structure of the troposphere as revealed during the spring MLOPEX intensive, *J. Geophys. Res.*, 105(D22), 26 809–26 839, 2000.
- Hoesly, R. M., Smith, S. J., Feng, L., Klimont, Z., Janssens-Maenhout, G., Pitkanen, T., Seibert, J. J., Vu, L., Andres, R. J., Bolt, R. M., Bond, T. C., Dawidowski, L., Kholod, N., Kurokawa, J.-I., Li, M., Liu, L., Lu, Z., Moura, M. C. P., O'Rourke, P.
2475 R., and Zhang, Q.: Historical (1750–2014) anthropogenic emissions of reactive gases and aerosols from the Community Emissions Data System (CEDS), *Geosci. Model Dev.*, 11, 369–408, <https://doi.org/10.5194/gmd-11-369-2018>, 2018.
- Holmes, C. D.: Methane Feedback on Atmospheric Chemistry: Methods, models, and mechanisms, *Journal of Advances in Modeling Earth Systems*, 10, 1087–1099, <https://doi.org/10.1002/2017MS001196>, 2018.
- Hossaini, R., Chipperfield, M. P., Saiz-Lopez, A., Fernandez, R., Monks, S., Feng, W., Brauer, P., and von Glasow, R.: A
2480 global model of tropospheric chlorine chemistry: Organic versus inorganic sources and impact on methane oxidation, *J. Geophys. Res.-Atmos.*, 121, 14271–14297, <https://doi.org/10.1002/2016JD025756>, 2016.
- Horowitz, L. W., Walters, S., Mauzerall, D. L., Emmons, L. K., Rasch, P. J., Granier, C., Tie, X., Lamarque, J.-F., Schultz, M. G., Tyndall, G. S., Orlando, J. J., and Brasseur, G. P.: A global simulation of tropospheric ozone and related tracers: Description and evaluation of MOZART, version 2, *J. Geophys. Res.-Atmos.*, 108, doi:10.1029/2002JD002853, 2003.
- 2485 Houweling, S., Bergamaschi, P., Chevallier, F., Heimann, M., Kaminski, T., Krol, M., Michalak, A. M., and Patra, P.: Global inverse modeling of CH₄ sources and sinks: an overview of methods, *Atmos. Chem. Phys.*, 17, 235–256, <https://doi.org/10.5194/acp-17-235-2017>, 2017.
- Houweling, S., Krol, M., Bergamaschi, P., Frankenberg, C., Dlugokencky, E. J., Morino, I., Notholt, J., Sherlock, V., Wunch, D., Beck, V., Gerbig, C., Chen, H., Kort, E. A., Röckmann, T., and Aben, I.: A multi-year methane inversion using

- 2490 SCIAMACHY, accounting for systematic errors using TCCON measurements, *Atmos. Chem. Phys.*, 14, 3991–4012, <https://doi.org/10.5194/acp-14-3991-2014>, 2014.
- Kai, F. M., Tyler, S. C., Randerson, J. T., and Blake, D. R.: Reduced methane growth rate explained by decreased Northern Hemisphere microbial sources, *Nature*, 476, 194–197, 2011.
- Kaylnay, E., Kanamitsu, M., Kistler, R., Collins, W., Deaven, D., Gandin, L., Iredell, M., Saha, S., White, G., Woollen, J.,
2495 Zhu, Y., Chelliah, M., Ebisuzaki, W., Higgins, W., Janowiak, J., Mo, K. C., Ropelewski, C., Wang, J., Leetmaa, A., Reynolds, R., Jenne, R., and Joseph, D.: The NCEP/NCAR 40-year reanalysis project, *Bull. Amer. Meteorol. Soc.* 77: 437–471, [https://doi.org/10.1175/1520-0477\(1996\)077<0437:TNYRP>2.0.CO;2](https://doi.org/10.1175/1520-0477(1996)077<0437:TNYRP>2.0.CO;2), 1996.
- Kirschke, S., Bousquet, P., Ciais, P., Saunio, M., Canadell, J. G., Dlugokencky, E. J., Bergamaschi, P., Bergmann, D., Blake, D. R., Bruhwiler, L., Cameron-Smith, P., Castaldi, S., Chevallier, F., Feng, L., Fraser, A., Heimann, M., Hodson, E. L.,
2500 Houweling, S., Josse, B., Fraser, P. J., Krummel, P. B., Lamarque, J.-F., Langenfelds, R. L., Le Quere, C., Naik, V., O’Doherty, S., Palmer, P. I., Pison, I., Plummer, D., Poulter, B., Prinn, R. G., Rigby, M., Ringeval, B., Santini, M., Schmidt, M., Shindell, D. T., Simpson, I. J., Spahni, R., Steele, L. P., Strode, S. A., Sudo, K., Szopa, S., van der Werf, G. R., Voulgarakis, A., van Weele, M., Weiss, R. F., Williams, J. E., and Zeng, G.: Three decades of global methane sources and sinks, *Nat. Geosci.*, 6, 813–823, doi:10.1038/ngeo1955, 2013.
- 2505 Knox, S. H., Matthes, J. H., Sturtevant, C., Oikawa, P. Y., Verfaillie, J., and Baldocchi, D.: Biophysical controls on interannual variability in ecosystem-scale CO₂ and CH₄ exchange in a California rice paddy, *J. Geophys. Res. Biogeosci.*, 121, 978–1001, doi:10.1002/2015JG003247, 2016.
- Lambert, G. and Schmidt, S.: Reevaluation of the oceanic flux of methane: uncertainties and long term variations, *Chemosph. Global Change Sci.*, 26, 579–589, doi:10.1016/0045-6535(93)90443-9, 1993.
- 2510 Levin, I., Veidt, C., Vaughn, B. H., Brailsford, G., Bromley, T., Lowe, R. H. D., Miller, J. B., Poß, C., and White, J. W. C.: No inter-hemispheric $\delta^{13}\text{C}_{\text{CH}_4}$ trend observed, *Nature*, 486, E3–E4, doi:10.1038/nature11175, 2012.
- Lin, M., Fiore, A. M., Horowitz, L. W., Cooper, O. R., Naik, V., Holloway, J., Johnson, B. J., Middlebrook, A. M., Oltmans, S. J., Pollack, I. B., Ryerson, T. B., Warner, J. X., Wiedinmyer, C., Wilson, J., and Wyman, B.: Transport of Asian ozone pollution into surface air over the western United States in spring, *J. Geophys. Res.-Atmos.*, 117, D00V07,
2515 doi:10.1029/2011JD016961, 2012.
- Maasackers, J. D., Jacob, D. J., Sulprizio, M. P., Scarpelli, T. R., Nesser, H., Sheng, J.-X., Zhang, Y., Hersher, M., Bloom, A. A., Bowman, K. W., Worden, J. R., Janssens-Maenhout, G., and Parker, R. J.: Global distribution of methane emissions, emission trends, and OH concentrations and trends inferred from an inversion of GOSAT satellite data for 2010–2015, *Atmos. Chem. Phys.*, 19, 7859–7881, <https://doi.org/10.5194/acp-19-7859-2019>, 2019.
- 2520 Mao, J., Fan, S., Jacob, D. J., and Travis, K. R.: Radical loss in the atmosphere from Cu-Fe redox coupling in aerosols, *Atmos. Chem. Phys.*, 13, 509–519, doi:10.5194/acp-13-509-2013, 2013a.
- Mao, J., Horowitz, L. W., Naik, V., Fan, S., Liu, J., and Fiore, A. M.: Sensitivity of tropospheric oxidants to biomass burning emissions: implications for radiative forcing, *Geophys. Res. Lett.*, 40, 1241–1246, doi:10.1002/grl.50210, 2013b.

- Monteil, G., Houweling, S., Dlugokenky, E. J., Maenhout, G., Vaughn, B. H., White, J. W. C., and Rockmann, T.: Interpreting methane variations in the past two decades using measurements of CH₄ mixing ratio and isotopic composition, *Atmos. Chem. Phys.*, 11, 9141–9153, doi:10.5194/acp-11-9141-2011, 2011.
- Montzka, S. A., Krol, M., Dlugokenky, E., Hall, B., Jockel, P., and Lelieveld, J.: Small interannual variability of global atmospheric hydroxyl, *Science*, 331, 67–69, doi:10.1126/science.1197640, 2011.
- Murray, L. T., Logan, J. A., and Jacob, D. J.: Interannual variability in tropical tropospheric ozone and OH: the role of lightning, *J. Geophys. Res.*, 118, 1–13, doi:10.1002/jgrd.50857, 2013.
- Myhre, G., Shindell, D., Bréon, F.-M., Collins, W. Fuglestedt, J., Huang, J., Koch, D. Lamarque, J.-F., Lee, D., Mendoza, B., Nakajima, T., Robock, A., Stephens, G. Takemura, T., and Zhang, H.: Anthropogenic and natural radiative forcing, in: *Climate Change 2013: The Physical Science Basis, Fifth Assessment Report of the Intergovernmental Panel on Climate Change*, edited by: Stocker, T. F. et al., Cambridge University Press, Cambridge, UK, New York, NY, USA, 659–740, 2013.
- Naik, V., Horowitz, L. W., Fiore, A. M., Ginoux, P., Mao, J., Aghedo, A. M., and Levy, H.: Impact of preindustrial to present-day changes in short-lived pollutant emissions on atmospheric composition and climate forcing, *J. Geophys. Res.-Atmos.*, 118, 8086–8110, doi:10.1002/jgrd.50608, 2013a.
- Naik, V., Voulgarakis, A., Fiore, A. M., Horowitz, L. W., Lamarque, J.-F., Lin, M., Prather, M. J., Young, P. J., Bergmann, D., Cameron-Smith, P. J., Cionni, I., Collins, W. J., Dalsøren, S. B., Doherty, R., Eyring, V., Faluvegi, G., Folberth, G. A., Josse, B., Lee, Y. H., MacKenzie, I. A., Nagashima, T., van Noije, T. P. C., Plummer, D. A., Righi, M., Rumbold, S. T., Skeie, R., Shindell, D. T., Stevenson, D. S., Strode, S., Sudo, K., Szopa, S., and Zeng, G.: Preindustrial to present-day changes in tropospheric hydroxyl radical and methane lifetime from the Atmospheric Chemistry and Climate Model Intercomparison Project (ACCMIP), *Atmos. Chem. Phys.*, 13, 5277–5298, doi:10.5194/acp-13-5277-2013, 2013b.
- Naus, S., Montzka, S. A., Pandey, S., Basu, S., Dlugokenky, E. J., and Krol, M.: Constraints and biases in a tropospheric two-box model of OH, *Atmos. Chem. Phys.*, 19, 407–424, <https://doi.org/10.5194/acp-19-407-2019>, 2019.
- Nisbet, E. G., Dlugokenky, E. J., and Bousquet, P.: Methane on the Rise – Again, *Science*, 343, 493–495, doi:10.1126/science.1247828, 2014.
- Nisbet, E. G., Manning, M. R., Dlugokenky, E. J., Fisher, R. E., Lowry, D., Michel, S. E., Myhre, C. Lund, Platt, S. M., Allen, G., Bousquet, P., Brownlow, R., Cain, M., France, J. L., Hermansen, O., Hossaini, R., Jones, A. E., Levin, I., Manning, A. C., Myhre, G., Pyle, J. A., Vaughn, B., Warwick, N. J., White, J. W. C.: Very strong atmospheric methane growth in the four years 2014–2017: Implications for the Paris Agreement, *Global Biogeochem. Cy.*, <https://doi.org/10.1029/2018GB006009>, 2019.
- Nisbet, E. G., Dlugokenky, E. J., Manning, M. R., Lowry, D., Fisher, R. E., France, J. L., Michel, S. E., Miller, J. B., White, J. W. C., Vaughn, B., Bousquet, P., Pyle, J. A., Warwick, N. J., Cain, M., Brownlow, R., Zazzeri, G., Lanoisellé, M., Manning, A. C., Gloor, E., Worthy, D. E. J., Brunke, E.-G., Labuschagne, C., Wolff, E. W., and Ganesan, A. L.: Rising atmospheric methane: 2007–2014 growth and isotopic shift, *Global Biogeochem. Cy.*, 30, 1356–1370, <https://doi.org/10.1002/2016GB005406>, 2016.

- Patra, P. K., Houweling, S., Krol, M., Bousquet, P., Belikov, D., Bergmann, D., Bian, H., Cameron-Smith, P., Chipperfield, M. P., Corbin, K., Fortems-Cheiney, A., Fraser, A., Gloor, E., Hess, P., Ito, A., Kawa, S. R., Law, R. M., Loh, Z., Maksyutov, S., Meng, L., Palmer, P. I., Prinn, R. G., Rigby, M., Saito, R., and Wilson, C.: TransCom model simulations of CH₄ and related species: linking transport, surface flux and chemical loss with CH₄ variability in the troposphere and lower stratosphere, *Atmos. Chem. Phys.*, 11, 12813–12837, <https://doi.org/10.5194/acp-11-12813-2011>, 2011.
- Patra, P. K., Saeki, T., Dlugokencky, E. J., Ishijima, K., Umezawa, T., Ito, A., Aoki, S., Morimoto, S., Kort, E. A., Crotwell, A., Ravi Kumar, K., and Nakazawa, T.: Regional Methane Emission Estimation Based on Observed Atmospheric Concentrations (2002–2012), *J. Met. Soc. Jap.*, 94, 91–112, doi:10.2151/jmsj.2016-006, 2016.
- Paulot, F., Ginoux, P., Cooke, W. F., Donner, L. J., Fan, S., Lin, M.-Y., Mao, J., Naik, V., and Horowitz, L. W.: Sensitivity of nitrate aerosols to ammonia emissions and to nitrate chemistry: implications for present and future nitrate optical depth, *Atmos. Chem. Phys.*, 16, 1459–1477, <https://doi.org/10.5194/acp-16-1459-2016>, 2016.
- Prather, M. J., Holmes, C. D., and Hsu, J.: Reactive greenhouse gas scenarios: Systematic exploration of uncertainties and the role of atmospheric chemistry, *Geophys. Res. Lett.*, 39, L09803, doi:10.1029/2012gl051440, 2012.
- Rice, A. L., Butenhoff, C. L., Teama, D. G., Röger, F. H., Khalil, M. A. K., and Rasmussen, R. A.: Atmospheric methane isotopic record favors fossil sources flat in 1980s and 1990s with recent increase, *Proceedings of the National Academy of Sciences*, 113, 10791–10796, 10.1073/pnas.1522923113, 2016.
- Rigby, M., Prinn, R. G., Fraser, P. J., Simmonds, P. G., Langenfelds, R. L., Huang, J., Cunnold, D. M., Steele, L. P., Krummel, P. B., Weiss, R. F., O'Doherty, S., Salameh, P. K., Wang, H. J., Harth, C. M., Mühle, J., and Porter, L. W.: Renewed growth of atmospheric methane, *Geophys. Res. Lett.*, 35, L22805, doi:10.1029/2008GL036037, 2008.
- Rigby, M., Manning, A. J., and Prinn, R. G.: The value of high frequency, high-precision methane isotopologue measurements for source and sink estimation, *J. Geophys. Res.-Atmos.*, 117, D12312, doi:10.1029/2011jd017384, 2012.
- Rigby, M., Montzka, S. A., Prinn, R. G., White, J. W. C., Young, D., O'Doherty, S., Lunt, M. F., Ganesan, A. L., Manning, A. J., Simmonds, P. G., Salameh, P. K., Harth, C. M., Mühle, J., Weiss, R. F., Fraser, P. J., Steele, L. P., Krummel, P. B., McCulloch, A., and Park, S.: Role of atmospheric oxidation in recent methane growth, *P. Natl. Acad. Sci.*, 114, 5373–5377, <https://doi.org/10.1073/pnas.1616426114>, 2017.
- Saeki, T., and Patra, P. K.: Implications of overestimated anthropogenic CO₂ emissions on East Asian and global land CO₂ flux inversion, *Geoscience Letters*, 4:9, <https://doi.org/10.1186/s40562-017-0074-7>, 2017.
- Saunois, M., Bousquet, P., Poulter, B., Peregon, A., Ciais, P., Canadell, J. G., Dlugokencky, E. J., Etiope, G., Bastviken, D., Houweling, S., Janssens-Maenhout, G., Tubiello, F. N., Castaldi, S., Jackson, R. B., Alexe, M., Arora, V. K., Beerling, D. J., Bergamaschi, P., Blake, D. R., Brailsford, G., Brovkin, V., Bruhwiler, L., Crevoisier, C., Crill, P., Covey, K., Curry, C., Frankenberg, C., Gedney, N., Höglund-Isaksson, L., Ishizawa, M., Ito, A., Joos, F., Kim, H.-S., Kleinen, T., Krummel, P., Lamarque, J.-F., Langenfelds, R., Locatelli, R., Machida, T., Maksyutov, S., McDonald, K. C., Marshall, J., Melton, J. R., Morino, I., Naik, V., O'Doherty, S., Parmentier, F.-J. W., Patra, P. K., Peng, C., Peng, S., Peters, G. P., Pison, I., Prigent, C., Prinn, R., Ramonet, M., Riley, W. J., Saito, M., Santini, M., Schroeder, R., Simpson, I. J., Spahni, R., Steele, P., Takizawa,

- A., Thornton, B. F., Tian, H., Tohjima, Y., Viovy, N., Voulgarakis, A., van Weele, M., van der Werf, G. R., Weiss, R., Wiedinmyer, C., Wilton, D. J., Wiltshire, A., Worthy, D., Wunch, D., Xu, X., Yoshida, Y., Zhang, B., Zhang, Z., and Zhu, Q.: The global methane budget 2000–2012, *Earth Syst. Sci. Data*, 8, 697–751, <https://doi.org/10.5194/essd-8-697-2016>, 2016.
- 2595 Saunio, M., Bousquet, P., Poulter, B., Peregon, A., Ciais, P., Canadell, J. G., Dlugokencky, E. J., Etiope, G., Bastviken, D., Houweling, S., Janssens-Maenhout, G., Tubiello, F. N., Castaldi, S., Jackson, R. B., Alexe, M., Arora, V. K., Beerling, D. J., Bergamaschi, P., Blake, D. R., Brailsford, G., Bruhwiler, L., Crevoisier, C., Crill, P., Covey, K., Frankenberg, C., Gedney, N., Höglund-Isaksson, L., Ishizawa, M., Ito, A., Joos, F., Kim, H.-S., Kleinen, T., Krummel, P., Lamarque, J.-F., Langenfelds, R., Locatelli, R., Machida, T., Maksyutov, S., Melton, J. R., Morino, I., Naik, V., O'Doherty, S., Parmentier, F.-J. W., Patra, P.
- 2600 K., Peng, C., Peng, S., Peters, G. P., Pison, I., Prinn, R., Ramonet, M., Riley, W. J., Saito, M., Santini, M., Schroeder, R., Simpson, I. J., Spahni, R., Takizawa, A., Thornton, B. F., Tian, H., Tohjima, Y., Viovy, N., Voulgarakis, A., Weiss, R., Wilton, D. J., Wiltshire, A., Worthy, D., Wunch, D., Xu, X., Yoshida, Y., Zhang, B., Zhang, Z., and Zhu, Q.: Variability and quasi-decadal changes in the methane budget over the period 2000–2012, *Atmos. Chem. Phys.*, 17, 11135–11161, <https://doi.org/10.5194/acp-17-11135-2017>, 2017.
- 2605 Saunio, M., Stavert, A. R., Poulter, B., Bousquet, P., Canadell, J. G., Jackson, R. B., Raymond, P. A., Dlugokencky, E. J., Houweling, S., Patra, P. K., Ciais, P., Arora, V. K., Bastviken, D., Bergamaschi, P., Blake, D. R., Brailsford, G., Bruhwiler, L., Carlson, K. M., Carrol, M., Castaldi, S., Chandra, N., Crevoisier, C., Crill, P. M., Covey, K., Curry, C. L., Etiope, G., Frankenberg, C., Gedney, N., Hegglin, M. I., Höglund-Isakson, L., Hugelius, G., Ishizawa, M., Ito, A., Janssens-Maenhout, G., Jensen, K. M., Joos, F., Kleinen, T., Krummel, P. B., Langenfelds, R. L., Laruelle, G. G., Liu, L., Machida, T., Maksyutov, S., McDonald, K. C., McNorton, J., Miller, P. A., Melton, J. R., Morino, I., Müller, J., Murgia-Flores, F., Naik, V., Niwa, Y., Noce, S., O'Doherty, S., Parker, R. J., Peng, C., Peng, S., Peters, G. P., Prigent, C., Prinn, R., Ramonet, M., Regnier, P., Riley, W. J., Rosentreter, J. A., Segers, A., Simpson, I. J., Shi, H., Smith, S. J., Steele, P. L., Thornton, B. F., Tian, H., Tohjima, Y., Tubiello, F. N., Tsuruta, A., Viovy, N., Voulgarakis, A., Weber, T. S., van Weele, M., van der Werf, G. R., Weiss, R. F., Worthy, D., Wunch, D., Yin, Y., Yoshida, Y., Zhang, W., Zhang, Z., Zhao, Y., Zheng, B., Zhu, Q., Zhu, Q., and Zhuang, Q.:
- 2615 The Global Methane Budget 2000–2017, *Earth Syst. Sci. Data Discuss.*, <https://doi.org/10.5194/essd-2019-128>, in review, 2019.
- Schaefer, H., Fletcher, S. E. M., Veidt, C., Lassey, K. R., Brailsford, G. W., Bromley, T. M., Dlugokencky, E. J., Michel, S. E., Miller, J. B., Levin, I., Lowe, D. C., Martin, R. J., Vaughn, B. H., and White, J. W. C.: A 21st century shift from fossil-fuel to biogenic methane emissions indicated by $^{13}\text{CH}_4$, *Science*, 352, 80–84, <https://doi.org/10.1126/science.aad2705>, 2016.
- 2620 Schnell, J. L., Naik, V., Horowitz, L. W., Paulot, F., Mao, J., Ginoux, P., Zhao, M., and Ram, K.: Exploring the relationship between surface $\text{PM}_{2.5}$ and meteorology in Northern India, *Atmos. Chem. Phys.*, 18, 10157–10175, <https://doi.org/10.5194/acp-18-10157-2018>, 2018.
- Schumann, U. and Huntrieser, H.: The global lightning-induced nitrogen oxides source, *Atmos. Chem. Phys.*, 7, 3823–3907, <https://doi.org/10.5194/acp-7-3823-2007>, 2007.

- 2625 Schwietzke, S, Sherwood, O. A., Bruhwiler, L. M. P., Miller, J. B., Etiope, G., Dlugokencky, E. J., Michel, S. E., Arline, V.A.,
vaughn, B. H., White, J. W. C., and Tans, P. P.: Upward revision of global fossil fuel methane emissions based on isotope
database, *Nature*, 538, 88–91, <https://doi.org/10.1038/nature19797>, 2016.
- Shindell, D., Kuylenstierna, J. C. I., Vignati, E., van Dingenen, R., Amann, M., Klimont, Z., Anenberg, S. C., Muller, N.,
JanssensMaenhout, G., Raes, F., Schwartz, J., Faluvegi, G., Pozzoli, L., Kupiainen, K., Höglund-Isaksson, L., Emberson, L.,
2630 Streets, D., Ramanathan, V., Hicks, K., Oanh, N. T. K., Milly, G., Williams, M., Demkine, V., and Fowler, D.: Simultaneously
mitigating near-term climate change and improving human health and food security, *Science*, 335, 183–189, 2012.
- Simpson, I. J., Sulbaek Andersen, M. P., Meinardi, S., Bruhwiler, L., Blake, N. J., Helmig, D., Rowland, F. S., and Blake, D.
R.: Long-term decline of global atmospheric ethane concentrations and implications for methane, *Nature*, 488, 490–494, 2012.
- Tans, P. P., Conway, T. J., and Nakazawa, T.: Latitudinal distribution of the sources and sinks of atmospheric carbon dioxide
2635 derived from surface observations and an atmospheric transport model, *J. Geophys. Res.*, 94, 5151–5172,
doi:10.1029/JD094iD04p05151, 1989.
- Taylor, K. E., Williamson, D., and Zwiers, F.: The sea surface temperature and sea-ice concentration boundary conditions of
AMIP II simulations, PCMDI Rep. 60, 20 pp, 2000.
- Thoning, K. W.: Curve Fitting Methods Applied to Time Series in NOAA/ESRL/GMD, path:
2640 <https://www.esrl.noaa.gov/gmd/ccgg/mbl/crvfit/crvfit.html>, 2019.
- Thoning, K.W., Tans, P. P., and Komhyr, W. D.: Atmospheric carbon dioxide at Mauna Loa Observatory, 2. Analysis of the
NOAA/GMCC data, 1974–1985, *J. Geophys. Res.*, 94, 8549–8565, 1989.
- Thompson, R. L., Stohl, A., Zhou, L. X., Dlugokencky, E., Fukuyama, Y., Tohjima, Y., Kim, S. Y., Lee, H., Nisbet, E. G.,
Fisher, R. E., Lowry, D., Weiss, R. F., Prinn, R. G., O’Doherty, S., Young, D., and White, J. W. C.: Methane emissions in East
2645 Asia for 2000–2011 estimated using an atmospheric Bayesian inversion, *J. Geophys. Res.-Atmos.*, 120, 4352–4369,
doi:10.1002/2014JD022394, 2015.
- Tsuruta, A., Aalto, T., Backman, L., Hakkarainen, J., van der Laan-Luijkx, I. T., Krol, M. C., Spahni, R., Houweling, S., Laine,
M., Dlugokencky, E., Gomez-Pelaez, A. J., van der Schoot, M., Langenfelds, R., Ellul, R., Arduini, J., Apadula, F., Gerbig,
C., Feist, D. G., Kivi, R., Yoshida, Y., and Peters, W.: Global methane emission estimates for 2000–2012 from CarbonTracker
2650 Europe-CH4 v1.0, *Geosci. Model Dev.*, 10, 1261–1289, <https://doi.org/10.5194/gmd-10-1261-2017>, 2017.
- Turner, A. J., Frankenberg, C., Wennberg, P. O., and Jacob, D. J.: Ambiguity in the causes for decadal trends in atmospheric
methane and hydroxyl, *P. Natl. Acad. Sci. USA*, 114, 5367–5372, <https://doi.org/10.1073/pnas.1616020114>, 2017.
- van Marle, M. J. E., Kloster, S., Magi, B. I., Marlon, J. R., Daniau, A.-L., Field, R. D., Arneeth, A., Forrest, M., Hantson, S.,
Kehrwald, N. M., Knorr, W., Lasslop, G., Li, F., Mangeon, S., Yue, C., Kaiser, J. W., and van der Werf, G. R.: Historic global
2655 biomass burning emissions for CMIP6 (BB4CMIP) based on merging satellite observations with proxies and fire models
(1750–2015), *Geosci. Model Dev.*, 10, 3329–3357, <https://doi.org/10.5194/gmd-10-3329-2017>, 2017.
- Voulgarakis, A., Naik, V., Lamarque, J. F., Shindell, D. T., Young, P. J., Prather, M. J., Wild, O., Field, R. D., Bergmann, D.,
Cameron-Smith, P., Cionni, I., Collins, W. J., Dalsøren, S. B., Doherty, R. M., Eyring, V., Faluvegi, G., Folberth, G. A.,

- Horowitz, L. W., Josse, B., MacKenzie, I. A., Nagashima, T., Plummer, D. A., Righi, M., Rumbold, S. T., Stevenson, D. S.,
2660 Strode, S. A., Sudo, K., Szopa, S., and Zeng, G.: Analysis of present day and future OH and methane lifetime in the ACCMIP
simulations, *Atmos. Chem. Phys.*, 13, 2563–2587, <https://doi.org/10.5194/acp13-2563-2013>, 2013.
- Wang, X., Jacob, D. J., Eastham, S. D., Sulprizio, M. P., Zhu, L., Chen, Q., Alexander, B., Sherwen, T., Evans, M. J., Lee, B.
H., Haskins, J. D., Lopez-Hilfiker, F. D., Thornton, J. A., Huey, G. L., and Liao, H.: The role of chlorine in global tropospheric
chemistry, *Atmos. Chem. Phys.*, 19, 3981–4003, <https://doi.org/10.5194/acp-19-3981-2019>, 2019.
- 2665 Wofsy, S. C., Daube, B., Jimenez, R., Kort, E., Pittman, J., Park, S., Commane, R., Xiang, B., Santoni, G. and Jacob, D., Fisher,
J., Pickett-Heaps, C., Wang, H., Wecht, K., Wang, Q.-Q., Stephens, B., Shertz, S., Romashkin, P., Campos, T., Haggerty, J.,
Cooper, W., Rogers, D., Beaton, S., Hendershot, R., Elkins, J. W., Fahey, D. W., Gao, F. R. S., Moore, F., Montzka, S. A.,
Schwarz, D. J. P., Miller, Hurst, B., Sweeney, C., Oltmans, S. J., Nance, D., Hints, E., Dutton, G., Watts, L. A., Spackman,
J. R., Rosenlof, K. H., Ray, E. A., Zondlo, M., Diao, M., Keeling, R., Bent, J., Atlas, E., Lueb, R., Mahoney, M., Chahine, M.,
2670 Olson, E., Patra, P., Ishijima, K., Engelen, R., Flemming, J., Nassar, R., Jones, D. B. A., and Mikaloff Fletcher, S. E.: HIAPER
Pole-to-Pole Observations (HIPPO): fine-grained, global-scale measurements of climatically important atmospheric gases and
aerosols, *Philos. T. R. Soc. A*, 369, 2073–2086, doi:10.1098/rsta.2010.0313, 2011.
- Worden, J. R., Bloom, A. A., Pandey, S., Jiang, Z., Worden, H. M., Walker, T. W., Houweling, S., and Röckmann, T.: Reduced
biomass burning emissions reconcile conflicting estimates of the post-2006 atmospheric methane budget, *Nature Commun.*,
2675 8, 2227, <https://doi.org/10.1038/s41467-017-02246-0>, 2017.
- Wesely, M. L.: Parameterization of surface resistances to gaseous dry deposition in regional-scale numerical models, *Atmos.
Environ.*, 23, 1293–1304, 1989.
- Zhao, M., Golaz, J.-C., Held, I. M., Guo, H., Balaji, V., Renson, R., Chen, J.-H., Chen, X., Donner, L. J., Dunne, J. P., Dunne,
K., Durachta, J., Fan, S.-M., Freidenreich, S. M., Garner, S. T., Ginoux, P., Harris, L. M., Horowitz, L. W., Krasting, J. P.,
2680 Langenhorst, A. R., Liang, Z., Lin, P., Lin, S.-J., Malyshev, S. L., Mason, E., Milly, P. C. D., Ming, Y., Naik, V., Paulot, F.,
Paynter, D., Phillipps, P., Radhakrishnan, A., Ramaswamy, V., Robinson, T., Schwarzkopf, D., Seman, C. J., Shevliakova, E.,
Shen, Z., Shin, H., Silvers, L. G., Wilson, J. R., Winton, M., Wittenberg, A. T., Wyman, B., and Xian, B.: The GFDL global
atmosphere and land model AM4.0/LM4.0: 1. Simulation characteristics with prescribed SSTs. *J. Adv. Model. Earth Syst.*,
10, 691–734, <https://doi.org/10.1002/2017MS001208>, 2018a.
- 2685 Zhao, M., Golaz, J.-C., Held, I. M., Guo, H., Balaji, V., Renson, R., Chen, J.-H., Chen, X., Donner, L. J., Dunne, J. P., Dunne,
K., Durachta, J., Fan, S.-M., Freidenreich, S. M., Garner, S. T., Ginoux, P., Harris, L. M., Horowitz, L. W., Krasting, J. P.,
Langenhorst, A. R., Liang, Z., Lin, P., Lin, S.-J., Malyshev, S. L., Mason, E., Milly, P. C. D., Ming, Y., Naik, V., Paulot, F.,
Paynter, D., Phillipps, P., Radhakrishnan, A., Ramaswamy, V., Robinson, T., Schwarzkopf, D., Seman, C. J., Shevliakova, E.,
Shen, Z., Shin, H., Silvers, L. G., Wilson, J. R., Winton, M., Wittenberg, A. T., Wyman, B., and Xian, B.: The GFDL global
2690 atmosphere and land model AM4.0/LM4.0: 2. Model description, sensitivity studies, and tuning strategies. *J. Adv. Model.
Earth Syst.*, 10, 735–769, <https://doi.org/10.1002/2017MS001209>, 2018b.

2695 Zhao, Y., Sauniois, M., Bousquet, P., Lin, X., Hegglin, M. I., Canadell, J. G., Jackson, R. B., Hauglustaine, D. A., Szopa, S., Stavert, A. R., Abraham, N. L., Archibald, A. T., Bekki, S., Deushi, M., Jöckel, P., Josse, B., Kinnison, D., Kirner, O., Marécal, V., O'Connor, F. M., Plummer, D. A., Revell, L. E., Rozanov, E., Stenke, A., Strode, S., Tilmes, S., Dlugokencky, E. J., and Zheng, B.: Inter-model comparison of global hydroxyl radical (OH) distributions and their impact on atmospheric methane over the 2000–2016 period, *Atmos. Chem. Phys. Discuss.*, <https://doi.org/10.5194/acp-2019-281>, in review, 2019.

Table 1. Emission inventories used in this study

Source Category	Database	Temporal Variability	References
Anthropogenic	CEDS v2017-05-18	1980-2014 monthly data	Hosely et al. (2018)
	SSP2-4.5	2015-2017 monthly data	Gidden et al. (2019)
Biomass Burning	BB4MIP	1980-2014 monthly data	van Marle et al. (2017)
	SSP2-4.5	2015-2017 monthly data	Gidden et al. (2019)
Wetlands	WetChart v1.0	Climatological monthly mean (with seasonal variability) for 1980-2017	Bloom et al. (2017)
Ocean	MOZART	Climatological monthly mean (with seasonal variability) for 1980-2017	Brasseur et al. (1998)
Near-shore	TransCom-CH4	Climatological annual mean (no seasonal variability) for 1980-2017	Lambert and Schmidt (1993), Patra et al. (2011)
Termites	NASA-GISS	Climatological annual mean (no seasonal variability) for 1980-2017	Fung et al. (1991)
Mud volcanoes	TransCom-CH4	Climatological annual mean (no seasonal variability) for 1980-2017	Etiopie and Milkov (2004), Patra et al. (2011)

Table 2. List of simulations conducted using GFDL-AM4.1 to explore trends and variability in methane

Simulations	Description
S0Aopt	Standard AM4.1 configuration, but with optimized anthropogenic emissions for 1980-2017
S0Wopt	Standard AM4.1 configuration, but with optimized wetland emissions for 1980-2017
S0A06	S0Aopt emissions for 1980-2005, with repeating 2006 S0Aopt anthropogenic emissions for 2006-2014 and adjusting wetland emissions for 2006-2014 to ensure the total emissions are same as optimized totals
S0Comb	S0Aopt emissions for 1980-2005 and S0Wopt emissions for 2006-2014
S1Wopt	AM4.1 configuration with low OH levels (LNO _x emissions scaled by a factor of 0.5), and optimized wetland emissions for 1980-2017
S2Wopt	AM4.1 configuration with high OH levels (LNO _x emissions scaled by a factor of 2), and optimized wetland emissions for 1980-2017

Table 3. Comparisons of simulated methane growth rates (annual mean \pm standard deviation) with observed methane growth rates (ppb yr⁻¹)

	1984-1991	1992-1998	1999-2006	2007-2017
Observed	11.7 \pm 1.4	5.5 \pm 3.5	0.7 \pm 3.1	7.0 \pm 2.7
S0Aopt	13.7 \pm 3.2	5.4 \pm 3.4	1.3 \pm 4.1	6.1 \pm 2.7
S0Wopt	13.6 \pm 3.4	5.4 \pm 3.6	1.3 \pm 4.4	6.1 \pm 2.6

Table 4. Global methane budget (Tg CH₄ yr⁻¹) during 1980-2017

Period of time	1980-1989	1990-1999	2000-2009	2008-2017	1999-2006	2007-2017
Sources^a						
Natural sources	203 [203-282] 203 [150-267] ^b 355 [244-466] ^c	203 [203-297] 182 [167-197] ^b 336 [230-465] ^c	203 [203-288] 218 [179-273] ^b 347 [238-484] ^c 214 [176-243] ^d 369 [245-485] ^e	203 [203-277] 215 [176-248] ^d 371 [245-488] ^e	203 [203-297]	203 [203-277]
Natural wetlands	166 [166-245] 167 [115-231] ^b 225 [183-266] ^c	166 [166-260] 150 [144-160] ^b 206 [169-265] ^c	166 [166-251] 175 [142-208] ^b 217 [177-284] ^c 180 [153-196] ^d 147 [102-179] ^e	166 [166-240] 178 [155-200] ^d 149 [102-182] ^e	166 [166-260]	166 [166-240]
Other natural sources	37	37	37 35 [21-47] ^d 222 [143-306] ^e	37 37 [21-50] ^d 222 [143-306] ^e	37	37
Oceans	9.5	9.5	9.5 18 [2-40] ^c 13 [9-22] ^e	9.5	9.5	9.5
Termites	20	20	20	20	20	20
Mud volcanoes	7.5	7.5	7.5	7.5	7.5	7.5
Anthropogenic sources	289 [289-368] 348 [305-383] ^b 308 [292-323] ^c	311 [311-405] 372 [290-453] ^b 313 [281-347] ^c	340 [340-425] 335 [273-409] ^b 331 [304-368] ^c 331 [310-346] ^d 334 [325-357] ^e	379 [379-452] 357 [334-375] ^d 366 [348-392] ^e	328 [328-422]	377 [377-450]
Agriculture and waste	159 [159-203] 208 [187-220] ^b 185 [172-197] ^c	172 [172-224] 239 [180-301] ^b 188 [177-196] ^c	185 [185-232] 209 [180-241] ^b 200 [187-224] ^c 202 [173-219] ^d 192 [178-206] ^e	201 [201-240] 219 [175-239] ^d 206 [191-223] ^e	181 [181-233]	200 [200-239]
Biomass burning	13 [13-16]	18 [18-24]	15 [15-18] 19 [15-32] ^e	14 [14-17] 17 [14-26] ^e	15 [15-20]	14 [14-17]
Fossil fuels	104 [104-132] 94 [75-108] ^b 89 [89-89] ^c	107 [107-139] 95 [84-107] ^b 84 [66-96] ^c	127 [127-159] 96 [77-123] ^b 96 [85-105] ^c 100 [70-149] ^d 110 [93-129] ^e	151 [151-180] 109 [79-168] ^d 127 [111-154] ^e	120 [120-153]	150 [150-179]
Other anthropogenic sources	14 [14-17]	14 [14-18]	13 [13-16]	13 [13-16]	12 [12-16]	13 [13-16]
$\Delta E^{f,g}$	47 [23-79]	60 [36-94]	52 [29-85]	39 [16-73]	57 [34-93]	40 [17-73]
Sinks^g						
Total chemical loss	486 [462-519] 490 [450-533] ^b 539 [411-671] ^c	540 [516-573] 525 [491-554] ^b 571 [521-621] ^c	577 [553-610] 518 [510-538] ^b 604 [483-738] ^c 505 [459-516] ^d	592 [569-626] 518 [474-532] ^d	570 [546-603]	592 [568-625]

			595 [489-749] ^e			
OH loss	442 [419-476] 468 [382-567] ^c	486 [462-519] 479 [457-501] ^c	526 [502-559] 528 [454-617] ^c 553 [476-677] ^e	543 [519-576]	519 [495-552]	542 [519-576]
OD loss	38 46 [16-67] ^c	47 67 [51-83] ^c	43 51 [16-84] ^c 31 [12-37] ^e	42	44	42
Cl loss	5 25 [13-37] ^c	7 25 [13-37] ^c	7 25 [13-37] ^c 11 [1-35] ^e	7	8	7
Soils	13 21 [10-27] ^b 28 [9-47] ^c	14 27 [27-27] ^b 28 [9-47] ^c	14 32 [26-42] ^b 28 [9-47] ^c 34 [27-41] ^d 30 [11-49] ^e	14 38 [27-45] ^d	14	14
Totals^g						
Sum of sources	539 [515-571] 551 [500-592] ^b 663 [536-789] ^c	574 [549-608] 554 [529-596] ^b 649 [511-812] ^c	595 [572-628] 548 [526-569] ^b 678 [542-852] ^c 545 [522-559] ^d 703 [570-842] ^e	621 [598-655] 572 [538-593] ^d 737 [593-880] ^e	589 [565-625]	620 [597-653]
Sum of sinks	499 [475-532] 511 [460-559] ^b 539 [420-718] ^c	554 [530-586] 542 [518-579] ^b 596 [530-668] ^c	591 [567-624] 540 [514-560] ^b 632 [592-785] ^c 540 [486-556] ^d 625 [600-798] ^e	606 [583-640] 556 [501-574] ^d	584 [560-617]	606 [582-639]
Imbalance	40 [39-40] 30 [16-40] ^b	20 [19-22] 12 [7-17] ^b	4 [4-5] 8 [-4-19] ^b 4 [-11-36] ^d	15 [15-15] 16 [0-47] ^d	5 [5-8]	14 [15-14]
Atmospheric growth	36 34 ^b 32 ^h	19 17 ^{b,h}	4.8 6 ^{b,h}	16.7 18.7±2.7 ^h	3.5 1.9±1.6 ^h	16.6-17.2 18.9±1.7 ^h

^aThe decadal mean values are based on initial emission inventories. The lower and upper limits of the ranges are based on the minimum and maximum among all the optimized emission scenarios (i.e., S0Aopt, S0Wopt, S1Aopt, S1Wopt, S2Aopt, and S2Wopt) conducted in this work.

^bValues are based on Kirschke et al. (2013) top-down approach.

715 ^cValues are based on Kirschke et al. (2013) bottom-up approach.

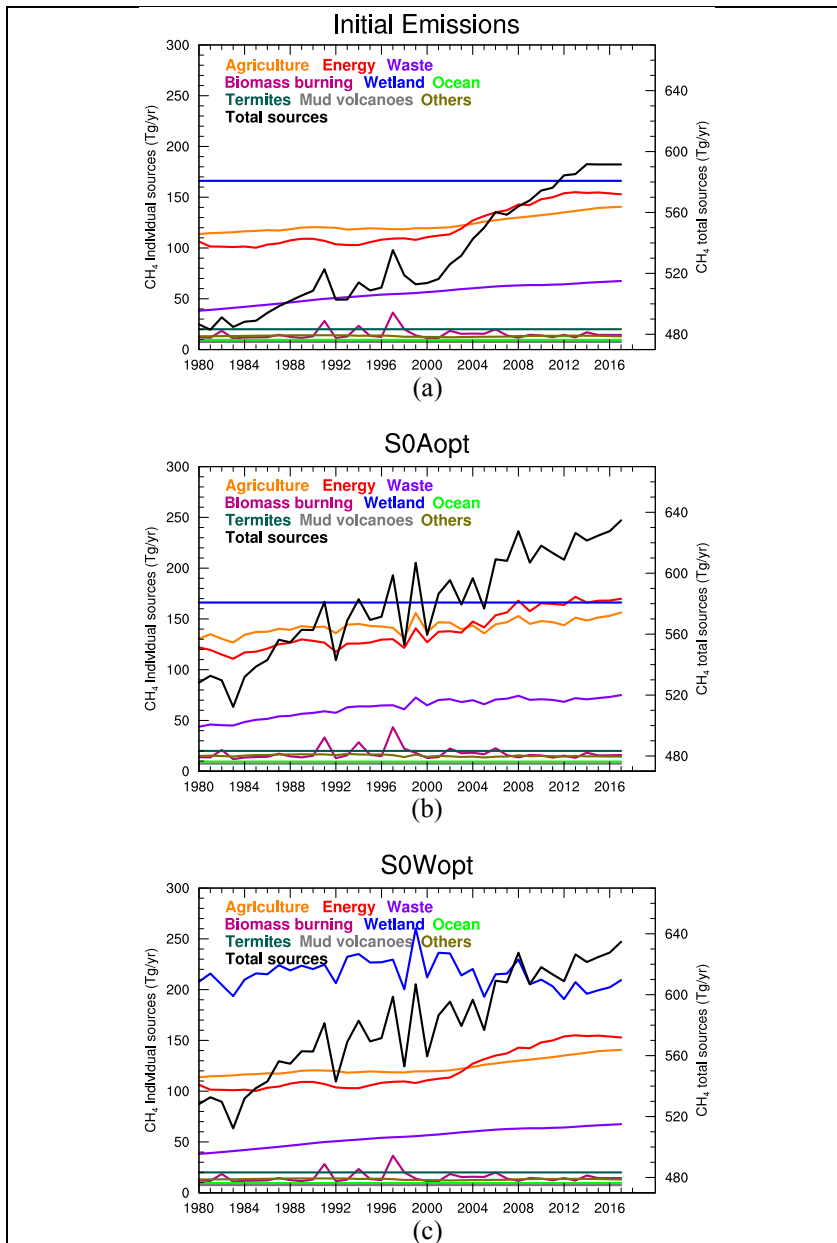
^dValues are based on Saunio et al. (2019) top-down approach.

^eValues are based on Saunio et al. (2019) bottom-up approach.

^fΔE is calculated based on the methodology of Ghosh et al. (2015).

720 ^gThe ranges are based on the low OH (S1Wopt) and high OH cases (S2Wopt) and the decadal mean values shown in the table are based on the default OH (S0Wopt).

^hThe observed atmospheric growth rates (Tg yr⁻¹) are estimated based on a few MBL sites (Dlugokencky et al., 2018), which are not the same as the Imbalance Row (based on the entire globe).



2725 **Figure 1. Time series of methane emissions from the initial methane inventories (a), optimized methane emissions on**
anthropogenic sectors (S0Aopt, b) and wetland sector (S0Wopt, c) for the period of 1980-2017. The emissions for major
major sectors are shown on the left y axis, including agriculture sector, energy production sector, waste sector, biomass
burning sector, wetland sector, ocean and near-shore fluxes, termites, mud volcanoes, and other sources (i.e., industrial
processes, surface transportation, international shipping, residential, commercial, and others). The total methane
 2730 **emissions from the initial emission inventories (black line) are shown on the right y axis.**

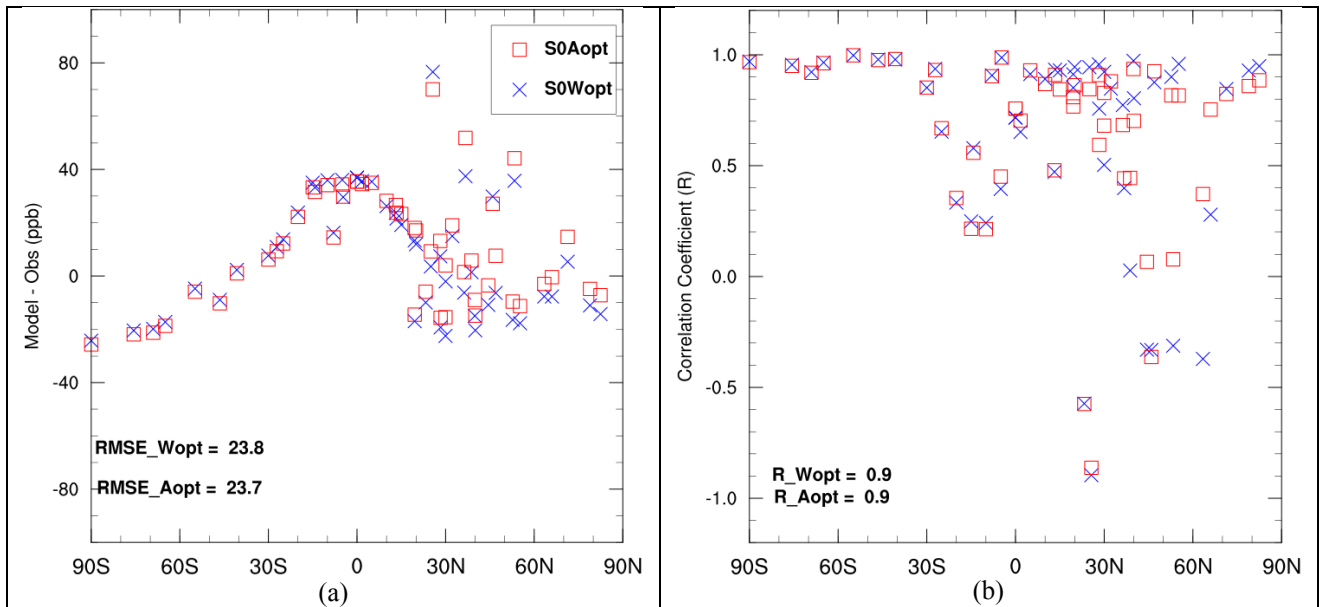


Figure 2. Model bias (a) and correlation coefficient (b) of simulated climatological mean surface methane concentrations against NOAA GMD observations for the 1983-2017 time period. GMD sites with at least 20-year observations are selected for model climatological evaluation. In Fig.2a, each red square or blue cross represents model mean bias by S0Aopt or S0Wopt at the corresponding GMD site. Root-mean-square-error (RMSE) is shown for all the GMD sites in Fig.2a. In Fig.2b, each red square or blue cross represents correlation of climatological seasonal variability by S0Aopt or S0Wopt at the corresponding GMD site. Spatial correlation (R) is shown for all the GMD sites in Fig.2b.

2735

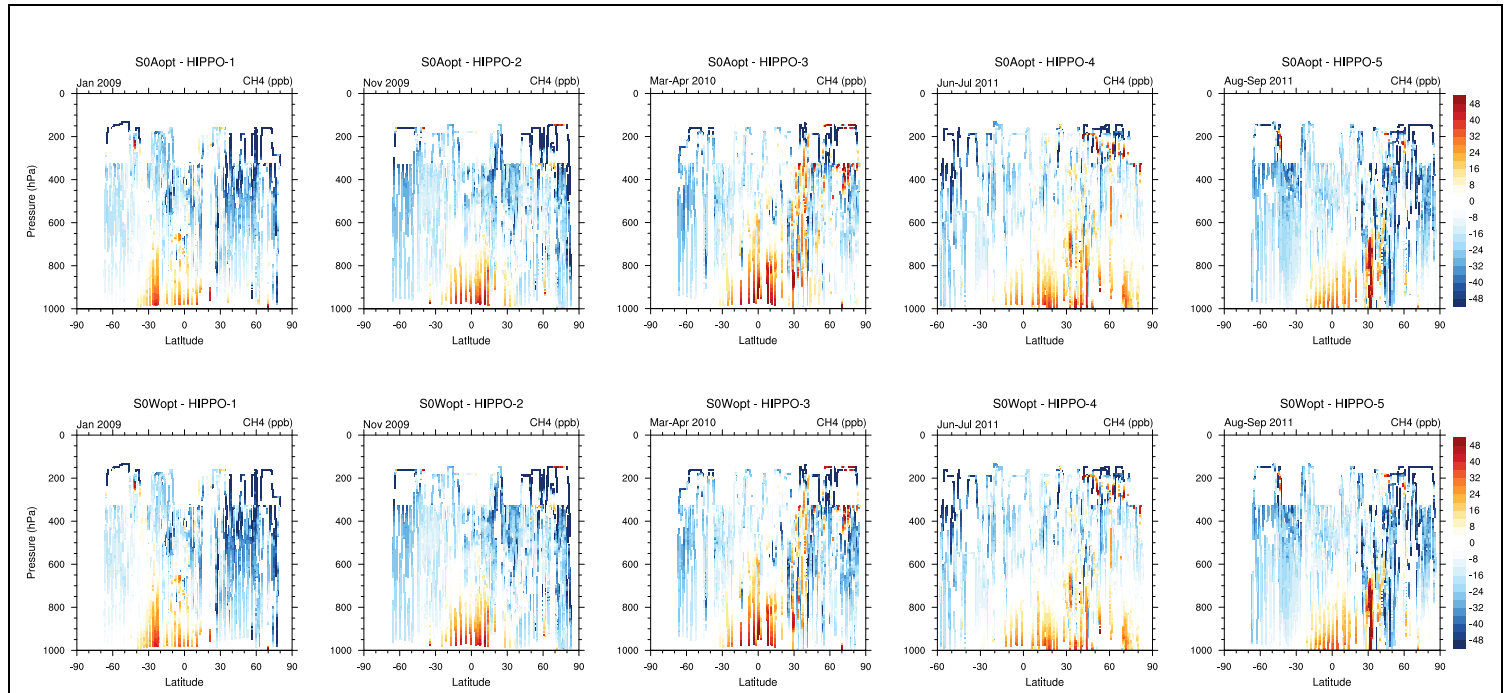


Figure 3. Comparison of vertical distribution of methane from S0Aopt and S0Wopt simulations with measurements from individual HIPPO campaigns. Months of campaign are given at the top left of the individual plots.

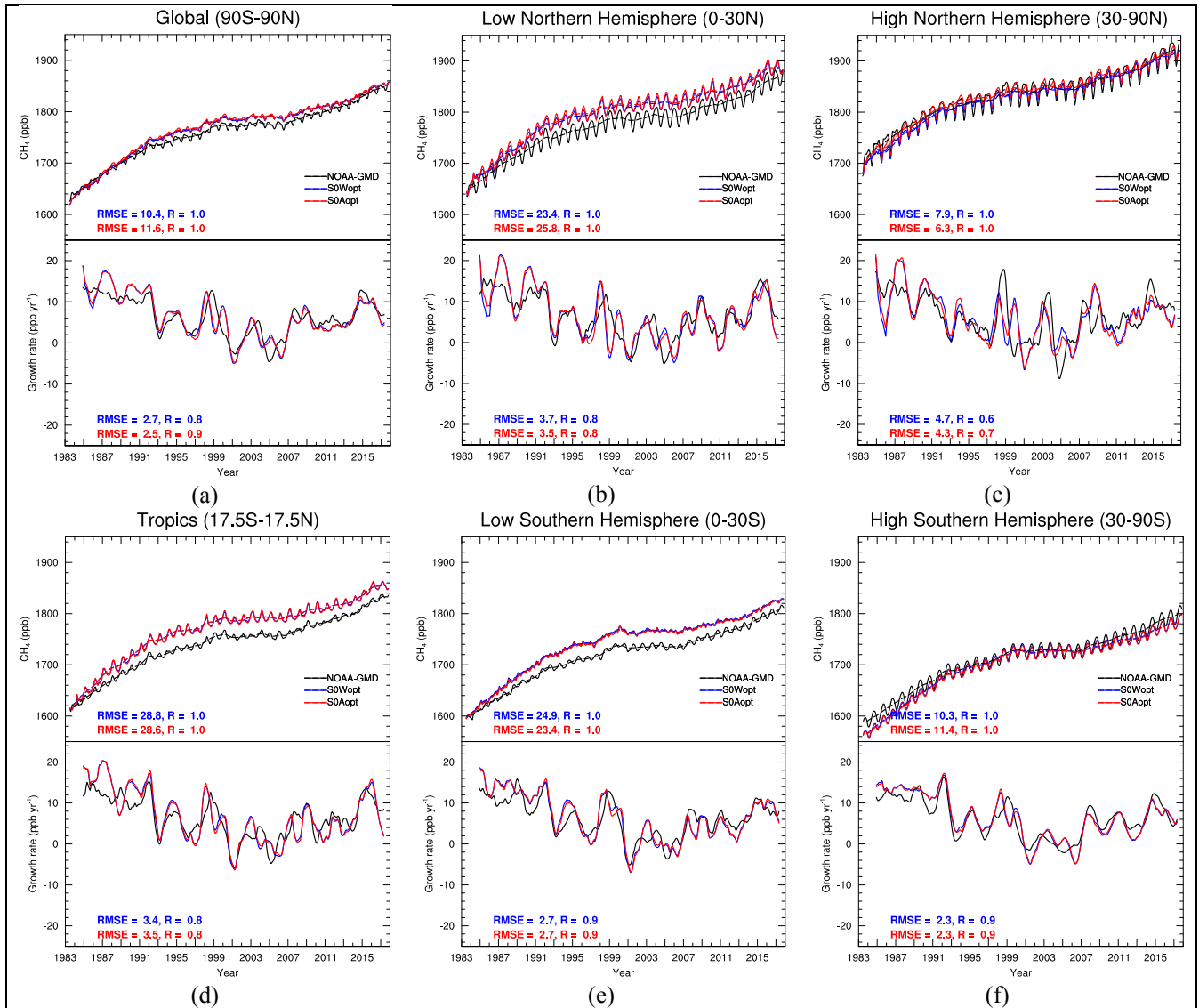


Figure 4. Comparison of GFDL-AM4.1 simulated methane concentrations and growth rates with NOAA-GMD surface observations. For the upper plot in each panel, dash line represents smoothed trends (i.e., 12-month running mean) from deseasonalized monthly data. A meridional curve (Tans et al., 1989) was fitted through NOAA-GMD site observations to get the latitudinal distribution of methane. A function fit consisting of yearly harmonics and a polynomial trend, with fast fourier transform and low pass filtering of the residuals are applied to the monthly mean methane DMF (Thoning et al., 1989; Thoning, 2019) to approximate the long-term trend. For the lower plot in each panel, the growth rates are calculated from the time derivative of the dash line in the corresponding upper plot.

2745

2750

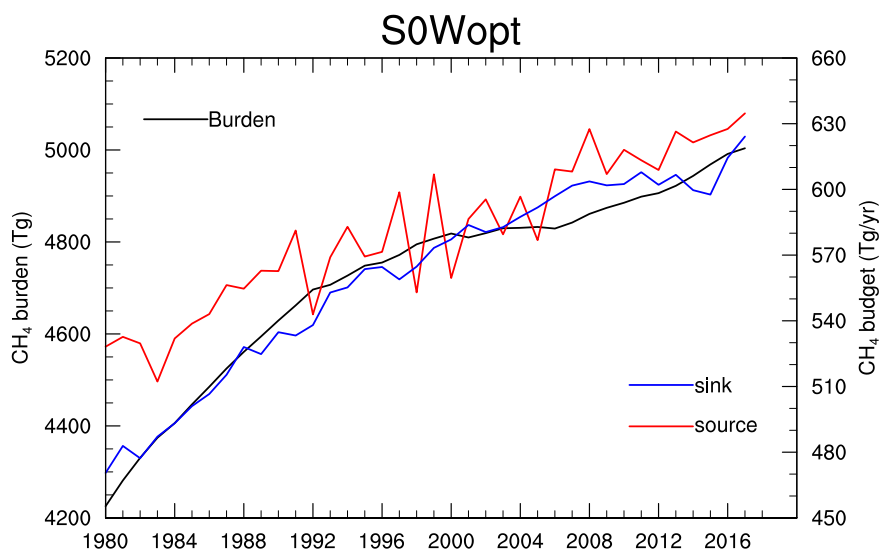
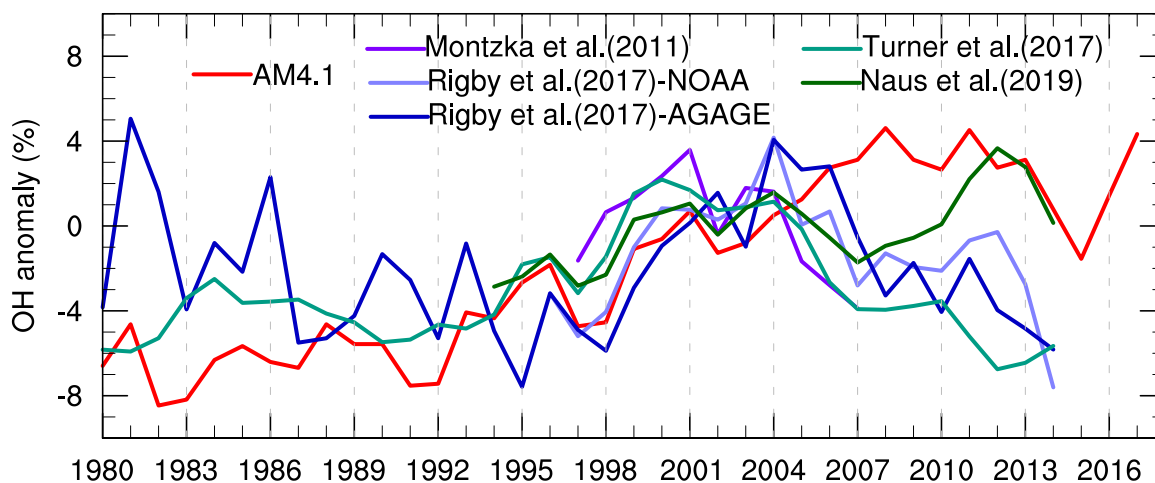


Figure 5. Time series of global methane burden (black line, left Y axis), methane sources (red line, right Y axis), and methane sinks (blue line, right Y axis) by S0Wopt.



2755

Figure 6. Time series of global tropospheric OH anomalies with respect to 1998-2007. Results of Montzka et al. (2011) are shown in dark purple (with the mean interannual variability of OH as $\pm 2.3\%$ for the period of 1998-2007). Results of Rigby et al. (2017) derived from NOAA observations are shown in light blue (with the mean interannual variability of OH as $\pm 2.3\%$ for the period of 1998-2007 and $\pm 2.6\%$ for the period of 1980-2014), and derived from AGAGE observations are shown in dark blue (with the mean interannual variability of OH as $\pm 3.0\%$ for the period of 1998-2007 and $\pm 3.1\%$ for the period of 1980-2014). Results from Turner et al. (2017) are shown in green (with the mean interannual variability of OH as $\pm 2.0\%$ for the period of 1998-2007 and $\pm 2.5\%$ for the period of 1980-2014). Results from Naus et al. (2019) are shown in dark green (with the mean interannual variability of OH as $\pm 1.2\%$ for the period of 1998-2007 and $\pm 1.8\%$ for the period of 1994-2014). OH anomalies in this work are shown in red (with the mean interannual variability of OH as $\pm 2.2\%$ for the period of 1998-2007 and $\pm 4.1\%$ for the period of 1980-2014).

2760

2765

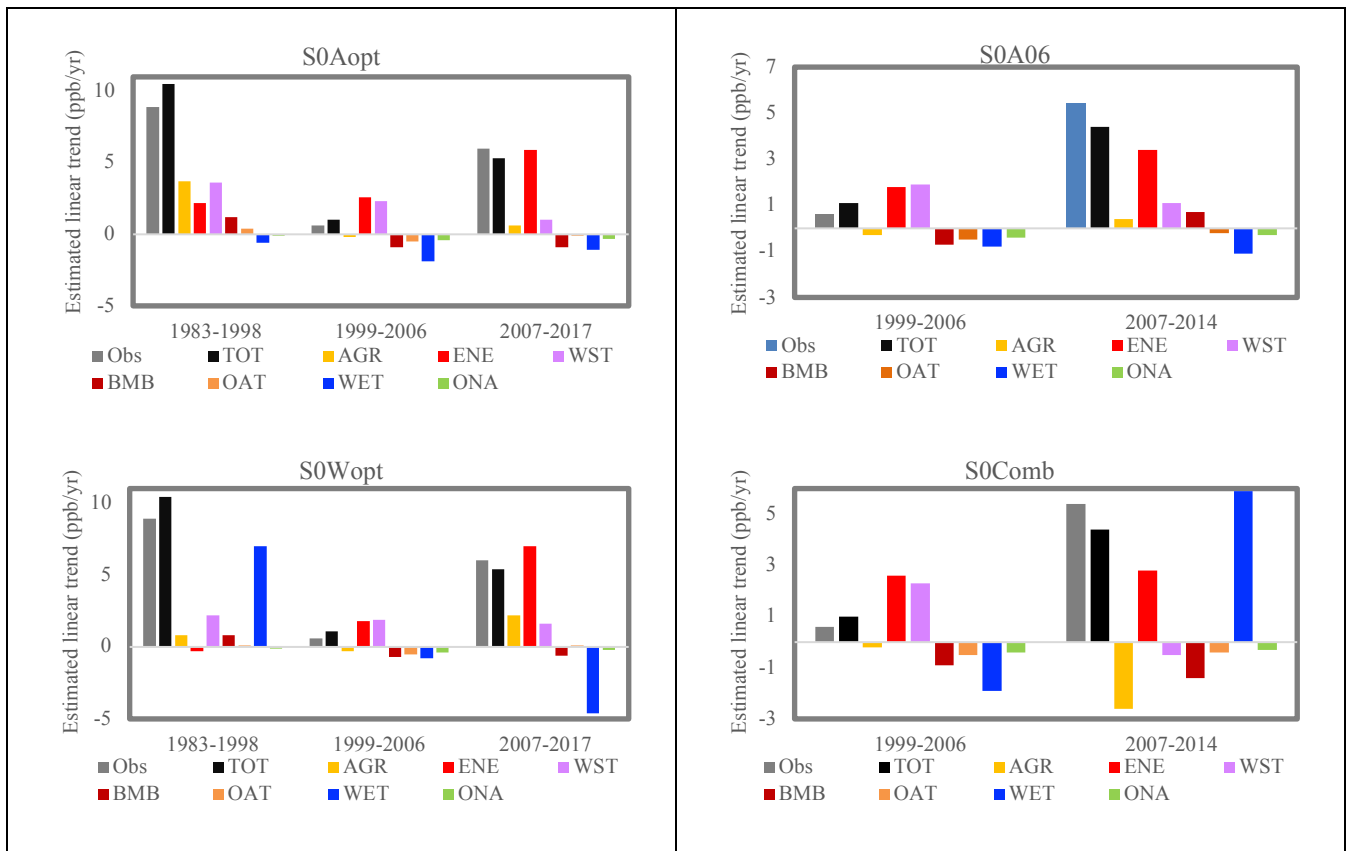
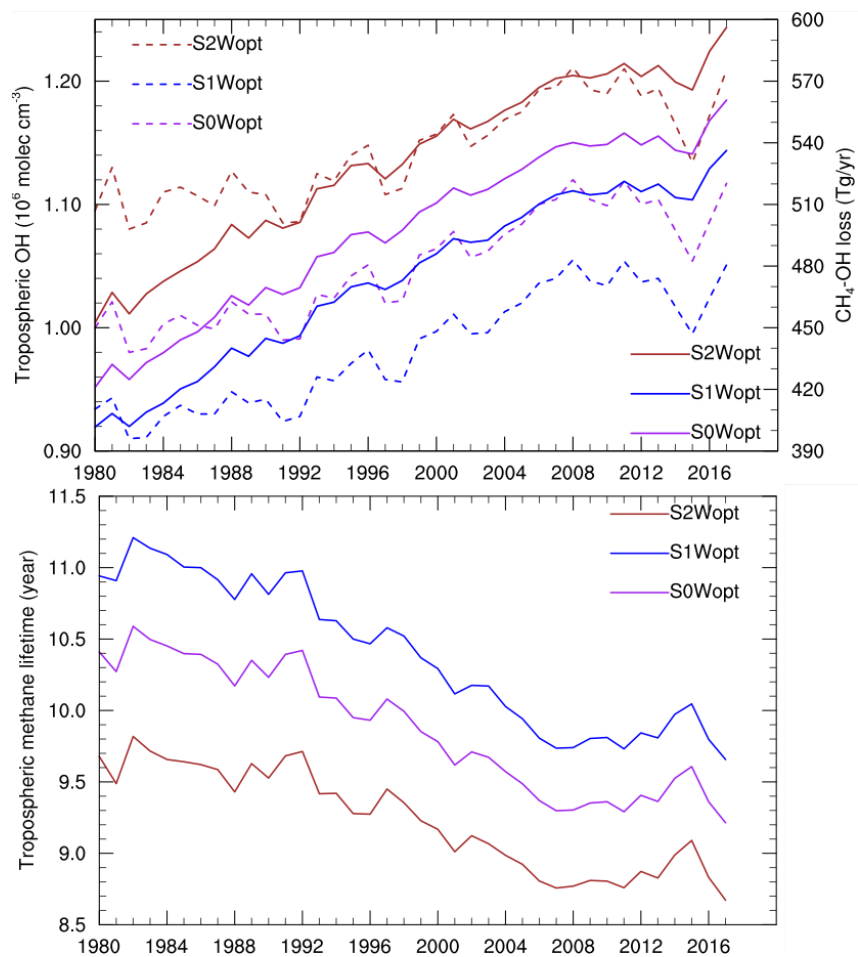


Figure 7. Estimated global linear trends for source tagged tracers and total methane (TOT). The source tagged tracers include tracer for agriculture sector (AGR), energy sector, (ENE), waste sector (WST), biomass burning sector (BMB), other anthropogenic sectors (OAT), wetland sector (WET), and other natural sectors (ONA). The grey bar represents total methane trend from NOAA-GMD observations. In the left panel (i.e., S0Aopt and S0Wopt), the trends are estimated for the periods of 1983-1998, 1999-2006, and 2007-2017. In the right panel (i.e., S0A06 and S0Comb), the trends are estimated for the period of 2007-2014, with 1999-2006 trends from S0Wopt and S0Aopt respectively.

2770



2775

Figure 8. Time series of global tropospheric OH levels (left Y axis, dash line) and methane OH loss (right Y axis, solid line) from S0Wopt (purple), S1Wopt (blue), and S2Wopt (brown) in the upper panel and time series of methane tropospheric lifetime from S0Wopt (purple), S1Wopt (blue), and S2Wopt (brown) in the lower panel.

2780